Title
The Duality of ARF: Enhanced Tumor Suppression at the Expense of Cellular Plasticity and Regenerative Ability

Author
Hesse, Robert Gerrie

Publication Date
2015

Peer reviewed|Thesis/dissertation

The Duality of ARF: Enhanced Tumor Suppression at the Expense of Cellular Plasticity and Regenerative Ability

by

Robert G. Hesse

DISSERTATION

Submitted in partial satisfaction of the requirements for the degree of

DOCTOR OF PHILOSOPHY

in

Biomedical Sciences

in the

GRADUATE DIVISION

Dedication and Acknowledgements

I dedicate this dissertation to my family and friends for all their support over the years, especially my love, Annie Lindseth.

I would like to acknowledge and thank David Staudt, and Hua Tian for their guidance and insightful conversations, Kimberly Evason for guidance and Tg(*fabp10a*:pt-β-cat) transgenic zebrafish and *tp53*$^{M214K/M214K}$ mutant zebrafish, Karl Murphy, Macrina Francisco, and Ma Valdez for fish colony care, Hilde Schjerven for equipment usage, Vagan Tapaltsyan and Alison May for vibratome sectioning help, Gordon Peters for *ARF* luciferase reporter constructs, Peter Jones for *ARF* promoter constructs, David Traver for Tg(*bactin2*:loxP-STOP-loxP-DsRed-express)^{sd5} transgenic zebrafish, Shannon Fisher for Tg(*runx2*:GFP) transgenic zebrafish, and Nadav Ahituv and Ophir Klein and the members of their respective labs for helpful advice and discussion and for helping get the work included in this dissertation started. Nadav and his lab members provided the original zebrafish from which all transgenic lines that I created originated as well as the knowledge to care for the fish. Ophir and his lab members provided invaluable advice and assistance over the years.

I would like to especially acknowledge and thank Matthias Hebrok, Jeremy Reiter, and my thesis advisor, Jason Pomerantz, for serving on my thesis committee and providing guidance and constructive criticism over the years.

Abstract

The control of proliferation and differentiation by tumor suppressor genes suggests that evolution of divergent tumor suppressor repertoires could influence species' regenerative capacity. To directly test that premise we humanized the zebrafish p53 pathway by introducing regulatory and coding sequences of the human tumor suppressor *ARF* into the zebrafish genome. *ARF* was dormant during development, in uninjured adult fins, and during wound healing, but was highly expressed in the blastema during epimorphic fin regeneration after amputation. Regenerative, but not developmental signals resulted in binding of zebrafish E2f to the human *ARF* promoter and activated conserved ARF-dependent Tp53 functions. The context-dependent activation of ARF did not affect growth and development but prevented regeneration, an unexpected distinct tumor suppressor response to regenerative versus developmental environments. To test the effect of loss of *Arf* on regeneration, we used *Arf* deficient mice to investigate digit tip regeneration, a mammalian model of epimorphic regeneration. Regardless of *Arf* dosage, regeneration was only observed with amputation made in the nail bed. To investigate other tumor suppressors that may influence regeneration, we examined the role of Rb1, a well conserved tumor suppressor, in zebrafish fin regeneration. We identified a differentiation promoting role for the Rb pathway, the pathway surveilled by *Arf* in mammals, during the redifferentiation phase of epimorphic zebrafish fin regeneration. Finally, in an effort to explore the basis for the divergence of *Arf*, we performed an evolutionary analysis comparing regenerative capacity, thermal regulation, and *Arf* expression to discover that ectotherms usually lack Arf and are highly regeneration while endotherms express Arf and not poorly regenerative. We also discovered a role for oxidative stress in zebrafish fin regeneration and *ARF* activation. Oxidative stress is observed in regeneration but not development and may represent the boost in

signaling required for *ARF* activation during regeneration. These findings highlight the importance of tumor suppressors in regeneration, especially the Rb and p53 pathways. They display the antagonistic pleiotropic characteristics of *ARF* as both tumor and regeneration suppressor, and they imply that inducing epimorphic regeneration clinically would require modulation of ARF-p53 axis activation.

Table of Contents

Table of Tables

Table of Figures

Introduction

Ever since Spallanzani published his work on regeneration in 1768 (Manzini et al., Tsonis, 1996), biologists have been fascinated with the phenomenon of regeneration. Urodele amphibians and teleost fish are unique among vertebrates in that they possess the innate ability to regenerate lost structures perfectly throughout their lives. Notable examples include regeneration of the heart (Oberpriller and Oberpriller, 1974), lens of the eye (Tsonis et al., 2004), and limbs and fins (Tanaka and Reddien, 2011, Poss et al., 2003). Mammals, on the other hand, have a limited ability to regenerate solid organs, and the mechanisms underlying regenerative responses in mammals are generally thought to be very different from those that underlie regenerative responses in urodeles and teleosts.

Two distinct types of regeneration can be distinguished in vertebrates as a means of replacing damaged or lost tissue: tissue regeneration and epimorphic regeneration, a term coined by T.H. Morgan (Dinsmore and American Society of Zoologists., 1991). During tissue regeneration, uninjured regions of an organ become activated and grow and/or proliferate to replace the lost tissue; an example of this occurs when hepatocytes replicate without progenitor cell activation after a partial hepatectomy. Another example of tissue regeneration is the restoration of skeletal muscle by satellite cells, a pool of resident, poised progenitor cells (Stoick-Cooper et al., 2007). However, during tissue regeneration, the original structure and architecture of the uninjured tissue is not reestablished in the regenerate. Epimorphic regeneration occurs via the formation of a blastema, a pool of undifferentiated cells that give rise to the regenerate. During epimorphic regeneration, multiple tissues types can be reestablished with the same structure and patterning as the uninjured organ. It is best exemplified by limb regeneration.

In axolotl limb regeneration, the regenerative process proceeds through several defined steps. First, the wound is closed by migrating epidermal cells. These cells form the wound epithelium that covers the site of injury and subsequent regeneration. Simultaneously, matrix metalloproteinases are activated, which degrade the extracellular matrix surrounding mesenchymal cells in a process termed histolysis. Mesenchymal-like cells subjacent to the wound epithelium are then replaced by relatively undifferentiated cells, by a process that has not been fully characterized, to form the blastema. Multiple investigators have termed this process of shedding differentiated characteristics for more progenitor-like ones to populate the blastema as dedifferentiation (Tsonis, 1996, Brockes and Kumar, 2002, Nacu and Tanaka, 2011). Whether the relatively undifferentiated cells arise from existing cells in the immediate wound area or are replaced by migratory cells from other regions remains an open question in the field. The wound epithelium then matures into a structure termed the apical epithelial cap, which is assumed to be analogous to the apical ectoderm ridge present during limb development. Via proposed epithelial-mesenchymal interactions, the blastema elongates and is subsequently patterned into a perfect, functional copy of the lost tissue. The outgrowth and patterning of the regenerate is in part controlled by pathways and processes deployed during development (Nacu and Tanaka, 2011). The cellular source of blastema cells is being actively investigated. Mechanisms and cellular sources have been shown in different contexts and are not mutually exclusive; both classically defined stem cells and dedifferentiated, proliferative, lineage-committed cells may contribute to the blastema (Stocum and Cameron, 2011, Hyun et al., 2012). While an extensive understanding of limb development currently exists, less is known regarding the processes of dedifferentiation and blastema formation.

Though the field of limb regeneration has existed since the 18th century (Tsonis, 1996), many of the mechanisms and pathways involved have remained elusive until recently. As a result of this, the historical literature of the field has been mainly descriptive in nature and many of the terms associated with these studies were vaguely defined mostly because of the technology of the day. These terms have since been adapted independently to define processes and characteristics that can be more rigorously observed due to the availability of modern tools and methods. The independent evolution of a particular term, dedifferentiation, which was originally introduced in 1902 by Driesch (Tsonis, 1996), has led to confusion and thus controversy in the field. I define dedifferentiation as the process by which a cell loses its terminally differentiated state to adopt a more progenitor-like one. Evidence of this transition would include the downregulation of terminally differentiated cell markers and upregulation of markers present during development, which would signify a less mature state of the tissue. While the cells that participate in limb and fin regeneration are highly proliferative, it is unclear how interrelated the processes of dedifferentiation and cell cycle re-entry are.

Some cell types are known to have cell cycle regulators intimately tied to the genetic programs that establish or maintain their terminally differentiated state. The role of the retinoblastoma protein Rb1 in terminal differentiation of multiple tissues including muscle is one example (Jacks et al., 1992). If Rb1 is inactivated in urodele cells, genes essential for the maintenance of the post-mitotic, terminally differentiated state of muscle cells called muscle regulatory factors including myogenin (Walsh and Perlman, 1997, Charge and Rudnicki, 2004) are downregulated and the terminally differentiated state is lost in a process of dedifferentiation thought to be important for regeneration (Tanaka et al., 1997). However, in species that possess the *Cdnk2a* locus such as mammals, the effect of the absence of Rb1 is reversed and the

terminally differentiated state is maintained as a result of upregulation of the alternative reading frame protein (ARF), one of two proteins encoded by the *Cdkn2a* locus (Pajcini et al., 2010, Huh et al., 2004). These two proteins, p16Ink4a and Arf (p14ARF in humans and p19Arf in mice), are translated via alternate reading frames. While there are many species with orthologues of p16Ink4a, a cyclin-dependent kinase inhibitor (CKI), chicken is the earliest species in which an ancestor of Arf (p7Arf) is found (Kim et al., 2003). This chicken protein is a highly truncated form, encoded in a single exon (Moulin et al., 2008).

Arf serves as a bridge between the Rb and p53 pathways. When induced, Arf stabilizes and activates Tp53 by binding and sequestering Mdm2, an E3 ubiquitin ligase and negative regulator of Tp53 (Pomerantz et al., 1998, Weber et al., 1999). Depending on the context, stabilized Tp53 either promotes cell cycle arrest or apoptosis.

In addition to canonical Tp53-dependent functions, Arf has other important functions including controlling ribosome biogenesis and responding to oxidative stress (Sherr, 2006, Weber et al., 2000, Damalas et al., 2011, Menendez et al., 2003). With regards to oxidative stress, reactive oxygen species (ROS) have been reported to not only be present during zebrafish fin regeneration (Gauron et al., 2013) and *Xenopus* tadpole tail regeneration (Love et al., 2013), but also necessary for successful regeneration. If not tightly controlled and properly balanced by antioxidants, ROS can cause oxidative stress and even DNA damage and tumorigenesis (Maddocks and Vousden, 2011). Since ARF can respond to oxidative stress by causing cell death (Damalas et al., 2011), ROS production during zebrafish fin regeneration may contribute to ARF-Tp53 axis activation.

The risk of DNA damage and tumorigenesis as a consequence of unchecked mitochondrial ROS production and oxidative stress is a potential pressure that drove the

evolution of *Arf*. It is known that the mitochondria of endothermic species are more active than those of ectothermic species (Hulbert and Else, 1989); therefore, without properly evolved controls, endothermic species would be at a higher risk of developing tumors spontaneously due to oxidative stress-induced DNA damage. An additional hypothesis that has arisen during the course of this work is that cellular metabolic changes associated with the transition of vertebrates from ectothermic to endothermic regulation over the course of evolutionary history play a large role in the evolution of the *Cdkn2a* locus. A logical question that arises from the previously described observations is whether the evolution of *Arf* as a tumor suppressor occurred at the expense of regenerative ability. A high degree of regenerative ability seems to require a high degree of cellular plasticity, which is not possible if cellular plasticity is tightly regulated by complex, sensitive tumor suppressor mechanisms that function to prevent tumorigenesis.

In the following chapters, I describe and interpret my investigations of the role of Arf in zebrafish epimorphic fin regeneration, the role of Arf in a mammalian model of epimorphic regeneration, the role of the Rb pathway in the maintenance of the differentiated state in the context of zebrafish epimorphic fin regeneration, and finally potential evolutionary pressures driving the evolution of *Arf*.

Chapter 1. *ARF* is a regeneration suppressor and a tumor suppressor

Introduction

Urodele amphibians and teleost fish are unique among vertebrates in that they possess the ability to regenerate injured complex structures such as limbs, fins, jaws, and heart by epimorphic regeneration (Morgan, 1901, Brockes and Kumar, 2008, Poss, 2010). For example, zebrafish fin regeneration proceeds through steps that include wound healing, blastema formation, and regenerative outgrowth to faithfully restore preinjury structures and size of the fin (Poss et al., 2003). In such highly regenerative species, the blastema consists of a heterogeneous pool of highly proliferative mesenchymal cells that gives rise to the large amount of new tissue in the regenerate (Knopf et al., 2011, Tu and Johnson, 2011). In contrast, absence of a proliferative blastema is a prominent feature of most mammalian solid tissue injury responses (Muneoka et al., 2008, Straube and Tanaka, 2006). An open question in biology is how cellular mechanisms controlling proliferation affect the blastema and whether they have evolved to contribute to divergent regenerative capacities among vertebrate species.

Tumor suppressor genes control the proliferative and differentiated state of cells, and many are also developmental regulators critical for normal formation of tissues (Jacks et al., 1992, Berman et al., 2008). The complex and precisely controlled proliferation and differentiation that occurs during epimorphic regeneration likely requires similar machinery, and as a group, tumor suppressors are probably necessary for well-orchestrated regeneration to occur (Pomerantz and Blau, 2013). For example, in eukaryotes the retinoblastoma gene *Rb1* regulates the G1/S transition by sequestering E2f transcription factors, and it controls cellular differentiation by associating with chromatin modifiers to regulate activity of tissue-specific transcription factors. Therefore, the role of *Rb1* in tumor suppression is likely less important

from an evolutionary standpoint than its ancient broad functions in regulating cellular differentiation and tissue formation. In contrast, the mammalian gene *Cdkn2a* is an essential tumor suppressor in mice and humans, but it is dispensable for mammalian development and tissue formation (Serrano et al., 1996). In mammals, *Cdkn2a* encodes two structurally unrelated proteins translated via alternate reading frames, p16Ink4a and Arf, each of which is a tumor suppressor (Chin et al., 1998, Sherr, 2006). While p16Ink4a is a cyclin-dependent kinase inhibitor (CKI) that functions upstream of Rb1, Arf exerts its tumor suppressor function by responding to inappropriate Rb pathway signaling above a presumed threshold (Lowe and Sherr, 2003). When induced, it stabilizes and activates Tp53 by binding and sequestering Mdm2, an E3 ubiquitin ligase and negative regulator of Tp53 (Pomerantz et al., 1998, Weber et al., 1999). Depending on the context, stabilized Tp53 either promotes cell cycle arrest or apoptosis. In addition to canonical Tp53-dependent functions, Arf has other important functions including controlling ribosome biogenesis and responding to oxidative stress (Sherr, 2006, Weber et al., 2000, Damalas et al., 2011, Menendez et al., 2003). The resulting general function of Arf is to maintain the postmitotic state, and our group has previously shown that suppression of Arf in the context of compromise of the Rb pathway results in dedifferentiation and proliferation of mammalian muscle cells in culture (Pajcini et al., 2010). Unlike in development or in regeneration of epithelial and hematopoietic tissues, reversal of the postmitotic state and dedifferentiation also occur in lower vertebrate epimorphic regeneration scenarios that involve a blastema. Regulation of Tp53 has recently been shown to be important during epimorphic regeneration, where it is downregulated during blastema formation (Yun et al., 2013). Although cell cycle reentry of postmitotic cells and dedifferentiation are characteristics of malignant transformation which tumor suppressor mechanisms oppose, why these two processes are

permitted to occur in the context of intact tumor suppressor mechanisms during epimorphic regeneration is unknown.

How evolution of the central cellular growth and tumor suppressor pathways impacts regenerative capacity is poorly understood. The advent of somatic stem cells in metazoans is thought to have enabled the formation of new types of cancer, thus requiring advanced tumor suppressor mechanisms (Belyi et al., 2010, Pearson and Sanchez Alvarado, 2008). Among metazoan species, including vertebrates, selective pressures such as different physiologies and environmental exposures undoubtedly continue to apply pressure to generate species-specific tumor suppressor repertoires. For some tumor suppressor genes such as *Tp53*, multiple family members have evolved to carry out certain differentiation functions separately from tumor suppression. For others, such as *Arf*, a single member has evolved and exists in a limited number of species. Whether such differences in turn relate to distinct regenerative capacities remains unknown.

Although tumor suppressors are generally highly conserved in eukaryotes, *Arf* is unusual in that it is poorly conserved in non-mammalian lineages (Figure 1A). The *Cdkn2a/b* locus of teleost fish, including zebrafish (*Danio rerio*) and fugu (*Takifugu rubripes*) (Gilley and Fried, 2001), exists as a single protein producing unit that only encodes for a CKI. During evolution, *Cdkn2a* and *Cdkn2b* developed into two separate but related genes encoding for biochemically related CKIs. Arf is not a CKI and is not closely related to either Cdkn2a or Cdkn2b. Arf is thought to be the product of a genetic duplication caused by either an insertion or transposition into the *Cdkn2a/b* locus (Gil and Peters, 2006). Of the highly regenerative species for which genomes have been completely sequenced, none possess an orthologue of *Arf* (Figure 1A) (Flicek et al., 2014, Karolchik et al., 2014). The earliest documented orthologue of *Arf* exists in

the chicken genome (Kim et al., 2003). This restricted representation coupled with *ARF* functions of responding to a high threshold of proliferative signaling and inhibiting dedifferentiation (Pajcini et al., 2010, Sherr, 2006) is compatible with a hypothesis that the presence of *Arf* could impact regenerative capacity.

In this chapter, I used transgenesis to examine the activity of human *ARF* in the context of zebrafish fin regeneration. I show that *ARF* can activate zebrafish Tp53 functions to restrict cellular proliferation and induce apoptosis, which causes a marked suppression of fin regeneration after injury. Remarkably, the human *ARF* regulatory sequences are dormant throughout zebrafish development but induce ARF expression specifically during regeneration after injury. These findings provide experimental evidence that species-specific tumor suppressors can impact tissue regeneration potential.

Method and Materials

Zebrafish

Zebrafish maintenance at 28-30°C and all experiments were approved by the Institutional Animal Care and Use Committee (IACUC) of the University of California, San Francisco (UCSF). 3-6 month old wild-type or transgenic AB zebrafish were used for all experiments. The Tg(*hsp70l*:ARF), Tg(*ARF*:ARF), and Tg(*ARF*:GFP) constructs were created by either subcloning the cDNA of human ARF (exons 1β, 2, and 3 of *CDKN2A*) or an EGFP cassette downstream of either the promoter sequences of zebrafish *hsp70l* (Halloran et al., 2000) or the human *CDKN2A* promoter (Robertson and Jones, 1998), respectively. Tol2-mediated transgenesis was used to generate transgenic animals (Kwan et al., 2007). Transgenic animals were detected based on their GFP-positive hearts, due to the transgenes containing a *cmlc2*:GFP cassette. All transgenic strains were analyzed as hemizygotes. For drug treatment experiments, zebrafish were treated with 5 μM Pifithrin-α (PTFα, Sigma, St. Louis, MO) in DMSO (5mM stock) or 5 μM (-)-Nutlin-3 (Nutlin-3, Cayman, Ann Arbor, MI) in EtOH (5mM stock). Water was exchanged daily. For EdU pulse-chase experiments, 5 μL of 5 mg/mL of EdU (Life Technologies, Carlsbad, CA) in saline was injected intraperitoneally into anesthetized fish 30 minutes before tissue harvest.

Immunostaining

Zebrafish fin immunostaining was performed on whole-mounted fins as previously described (Sousa et al., 2011). Briefly, fin tissue was fixed flat in 4% PFA 1 hour, and then incubated in 80% MeOH, 20% DMSO overnight 4°C. Tissue was rehydrated in 75%, 50%, and finally 25% MeOH in PBS 5 minutes each, permeabilized in acetone 20 minutes -20°C, PBS 5 minutes 2X, 0.5% Triton X-100 in PBS (PBTx) 30 minutes, PBS 5 minutes 3X, serum-free protein block

(Dako, Carpinteria, CA) 1 hour, primary antibodies in antibody diluent (Dako) overnight 4°C. Tissue was washed multiple times throughout the day, secondary antibodies in antibody diluent overnight 4°C, PBS 5 minutes 3X, mounted with Vectashield mounting medium with DAPI (Vector Laboratories, Burlingame, CA). For coronal views, whole mount stained fins were embedded in 5% agarose, and 200 μm sections were cut with a vibratome. Imaging was performed with a confocal microscope.

Zebrafish embryo immunostaining was performed on whole-mounted, 1-phenyl 2-thiourea (PTU; Sigma)-treated embryos as previously described (Macdonald, 1999). Briefly, embryos were fixed in 4% PFA overnight 4°C, washed in PBS 5 minutes 3X, and then storage in MeOH -20°C. Embryos were rehydrated in 75%, 50%, and finally 25% MeOH in PBS 5 minutes each, 0.1% Tween-20 in PBS (PBT) 5 minutes 2X. Only 48 hpf and 72 hpf embryos were washed in ddH_2O 5 minutes, acetone 7 minutes -20°C, rinsed in ddH_2O and then PBT 2X. All embryos were blocked in 10% goat serum in PBT 1-2 hours, primary antibodies in 10% goat serum in PBT overnight 4°C. Tissue was washed in PBT 15 minutes 5X throughout the day, secondary antibodies in 10% goat serum in PBT overnight 4°C, PBT 15 minutes 3X, Hoechst stain in PBS 15 minutes, PBS 5 minutes 2X, mounted in methyl cellulose and then imaged.

Zebrafish cell and liver immunostaining: 4% PFA 10 minutes (if not already fixed), PBS 5 minutes 3X, 0.3% PBTx 15 minutes, PBS 5 minutes 3X, serum-free protein block (Dako) 1 hour, primary antibodies in antibody diluent (Dako) overnight 4°C, PBS 5 minutes 3X, secondary antibodies in antibody diluent 1 hour, PBS 5 minutes 3X, mounted with Vectashield mounting medium with DAPI (Vector Laboratories, Burlingame, CA).

EdU incorporation was detected using the Click-iT EdU imaging kit per the manufacturer's instructions (Life Technologies). Briefly, fin tissue was fixed flat in 4% PFA 1 hour, and then

incubated in 80% MeOH, 20% DMSO overnight 4°C. Tissue was rehydrated in 75%, 50%, and finally 25% MeOH in PBS 5 minutes each, permeabilized in acetone 20 minutes -20°C, PBS 5 minutes 2X, 0.5% PBTx 30 minutes, PBS 5 minutes 2X. The Click-iT cocktail was prepared fresh and 50 μL was applied per fin, incubated 30 minutes dark, PBS 5 minutes, 3X, mounted with Vectashield mounting medium with DAPI (Vector Laboratories).

TUNEL detection was performed using the In Situ Cell Death Detection Kit (Roche, Basel, Switzerland) per the manufacturer's instructions. Briefly, fin tissue was fixed flat in 4% PFA 1 hour, and then incubated in 80% MeOH, 20% DMSO overnight 4°C. Tissue was rehydrated in 75%, 50%, and finally 25% MeOH in PBS 5 minutes each, permeabilized in acetone 20 minutes -20°C, PBS 5 minutes 2X, 0.5% PBTx 30 minutes, PBS 5 minutes 2X. The labeling/enzyme mix was prepared fresh and 50 μL was applied per fin, incubated 30 minutes dark and humid, PBS 5 minutes, 3X, mounted with Vectashield mounting medium with DAPI (Vector Laboratories).

Images were quantified in ImageJ. The percent of EdU- or TUNEL-positive cells was quantified by first counting the number of positive cells in the regenerate and then dividing that count by the number of nuclei in the field counted.

In Situ Hybridization

Zebrafish embryo mRNA *in situ* hybridization was performed on whole-mounted, PTU-treated embryos as previously described (Chitramuthu and Bennett, 2013). Briefly, embryos were fixed in 4% PFA overnight 4°C, washed in PBS 5 minutes 3X, and then storage in MeOH -20°C. Embryos were rehydrated in 75%, 50%, and finally 25% MeOH in PBS 5 minutes each, 0.1% PBT 5 minutes 3X, incubated in 10 μg/mL proteinase K in PBS 15 minutes (24 hpf), 30 minutes (48 hpf), or 40 minutes (72 hpf). Embryos were fixed in 4% PFA 20 minutes, PBT 5 minutes 3X,

incubated in acetylation mixture (125 uL triethanolamine, 27 uL acetic anhydride in 10 mL DEPC H_2O) 10 minutes 2X, PBT 10 minutes, 2X, prehybridized in 200 mL hybridization buffer (50% formamide, 5X SSC, 0.1% Tween-20, 50 ug/mL heparin, 500 ug yeast RNA; pH 6.0 with citric acid) 2-4 hours 70°C. Extra embryos were used to preadsorb the anti-digoxygenin-AP antibody (1:500) in blocking buffer (2% calf serum, 2 mg/mL BSA in PBT) 2-4 hours, and then stored overnight 4°C. After 2-4 hours at 70°C, approximately 200ng probe was added and allowed to hybridize overnight 70°C. Embryos were washed in 100% hybridization buffer, 75%, 50%, 25% with 2x SSC 15 minutes 70°C, 2x SSC 15 minutes 2X 70°C, 0.2x SSC 30 minutes 2X 65°C, 100% 0.2x SSC, 75%, 50%, 25% with PBT 5 minutes, PBT 5 minutes 2X, preincubated in blocking buffer 3-4 hours, incubated with 1:5000 anti-digoxygenin-AP antibody in blocking buffer (1:10 preadsorbed) overnight 4°C. Embryos were washed PBT 15 minutes 6X, NTM (0.1M Tris-HCl pH 9.5, 50mM MgCl2, 0.1M NaCl, 0.1% Tween-20) 15 minutes 2X, incubated with BM Purple supernatant for 0.25-16 hrs (check every 30 min) dark. The reaction was stopped with stop solution (1 mM EDTA PBT, pH 5.5) 10 minutes 2X, mounted in methyl cellulose and then imaged. The antisense GFP probe was labeled with digoxygenin-11-UTP (Roche) and generated using the following primers: 5'- AAG GGC GAG GAG CTG TTC AC-3' and 5'- GAA CTC CAG CAG GAC CAT GT-3' (MacDonald et al., 2010).

Western Blot

50-60 μg of total protein isolated from adult zebrafish fin tissue was loaded per lane, electrophoresed on NuPAGE Novex 4-12% Bis-Tris protein gels (Life Technologies), and transferred to PVDF membranes. The Novex system (Life Technologies) was used exclusively. Protein was isolated using the following protocol. Individual zebrafish fins were homogenized

and incubated in 200 μL RIPA buffer containing protease and phosphatase inhibitors (Roche), 1 mM PMSF, and 1 mM DTT for 20 minutes 4°C with trituration every 5 minutes. Tissue was then centrifuged at maximum speed for 10 minutes 4°C, and the supernatant was then aliquoted and storage at -80°C. Protein concentration was assessed using a Pierce BCA protein assay kit with a standard curve (Life Technologies). Protein was visualized using ECL Prime (GE Healthcare Bio-Sciences, Pittsburgh, PA) and an ImageQuant LAS 4000 (GE Healthcare Bio-Sciences). Band quantification was performed using ImageQuantTL software. For each condition, Rb1 and p-Rb1 bands were normalized to β-actin, and the ratio of p-Rb1:Rb1 was calculated and made relative to uninjured tissue.

Primary Antibodies

Host Species	Antigen	Company	Cat. No.	Dilution	Application
Mouse	Tp53	Abcam	ab77813	1:50	IHC
Rabbit	Mdm2	Santa Cruz	C-18	1:50	IHC
Rabbit	GFP	Torrey Pines	TP401	1:3000	IHC
Chicken	GFP	Abcam	ab13970	1:3000	IHC
Mouse	Msxb	DSHC	4G1-c	1:50	IHC
Rabbit	PCNA	Abcam	ab2426	1:500	IHC
Mouse	p14ARF	Cell Signaling	2407	1:100/1:500	IHC/WB
Rabbit	Rb1	AnaSpec	55432	1:500	WB
Rabbit	p-Rb1 (S780)	Abcam	ab47763	1:500	WB
Rabbit	Beta-actin	Millipore	EP1123Y	1:1000	WB
Rabbit	E2f1	Abcam	ab14769	1:1000	WB

Fin Regeneration & Wounding

Caudal fin amputations were performed with a razor blade on fish anesthetized with 0.016% tricaine in aquarium water; only the distal halves of fins were amputated. Heat shocks were delivered by housing fish in a water bath set to 37°C with bidiurnal (every other day) water exchanges. The water bath achieved 37°C within 15 minutes, maintained that temperature for 1

hour, and then passively cooled to fish room temperature (26-28°C). An automatic digital timer (Intermatic, Spring Grove, IL) was used to turn on and off the water bath. For heat shock experiments, an initial heat shock was delivered and then fins were amputated 3 hours later. Heat shocks were subsequently delivered every 6 hours for the duration of the experiment. Quantification of fin regenerate length, area, and GFP intensity was performed in ImageJ. Fin regenerate length was calculated by averaging the length of the longest dorsal and ventral fin ray. Caudal fin wounding experiments were performed as previously described (Gauron et al., 2013). Briefly, fish were anesthetized with 0.016% tricaine in aquarium water and fins were cut (2 to 3 segments long) between rays 2 and 3 at the level of the first ray bifurcation.

Chromatin Immunoprecipitation (ChIP)

Chromatin immunoprecipitation of zebrafish fin tissue was performed as previously described (Wehner et al., 2014). Briefly, embryos were dechorionated, and Protein G Dynabeads (Life Technologes) were pre-blocked with blocking buffer (0.2 mg/mL BSA, 0.2 mg/mL yeast tRNA (Life Technologies) in ChIP dilution buffer (Millipore, Billerica, MA)) overnight 4°C the day before the ChIP assay was performed. On the next day, 30-50 72 hpf embryos or 30 adult fin regenerates were collected, rinsed in PBS, transferred to 1 mL ice-cold PBS, 67 μL 16% PFA was added and tissue was incubated 20 minutes 37°C. 125 μL 1M glycine was added and tissues was incubated 5 minutes rotating. Tissue was centrifuged at 1300 rpm 4 minutes 4°C, PBS 5 minutes 2X, incubated in 500 uL Nuclear Isolation Buffer (85 mM KCl. 0.5% NP40, 5 mM PIPES, pH 8 with protease and phosphatase inhibitors (Roche)) 10 minutes 4°C, centrifuged at 6000 rpm 10 minutes 4°C, dissolved in 320 uL Lysis Buffer (1.5 mM EDTA, 10% glycerol, 50 mM HEPES, 150 mM NaCl, 0.1% Triton X-100, pH 7.5 with protease and phosphatase

inhibitors (Roche)) 10 minutes 4°C, sonicated with a Bioruptor UCD-200 (Diagenode, Denville, NJ) at high power for 6 5-minutes cycles of 30 seconds ON, 30 seconds OFF; water was changed after each cycle. Tissue was then centrifuged at 13,000 rpm 10 minutes 4°C. 40 μL of the supernatant was removed as Input (stored at 4°C). The remainder was diluted 1:10 in ChIP dilution buffer (Millipore) containing protease and phosphatase inhibitors (Roche), precleared with 150 uL pre-blocked beads (resuspended in 150 uL ChIP dilution buffer (Millipore) containing protease and phosphatase inhibitors (Roche) per sample) 1-2 hours 4°C rotating, diluted if necessary in ChIP dilution buffer (Millipore) containing protease and phosphatase inhibitors (Roche) to 900 μL. 5 μg of rabbit anti-E2f1 antibody or rabbit IgG (Vector Laboratories) was added and incubated overnight 4°C rotating. 50 μL Protein G Dynabeads (Life Technologies) per sample were pre-blocked in blocking buffer overnight 4°C. On the next day, samples were immunoprecipitated with 50 μL pre-blocked beads (resuspended in 50 uL ChIP dilution buffer (Millipore) containing protease and phosphatase inhibitors (Roche) per sample) 4 hours 4°C rotating. Samples were then washed in High Salt Buffer (2.5% NaCl, 0.1% SDS, 1% Triton X-100) 30 minutes 4°C rotating, Low Salt Buffer (0.5% NaCl, 0.1% SDS, 1% Triton X-100) 30 minutes 4°C rotating, TE Buffer 15 minutes 4°C rotating 2X. Beads were then incubated in 200 μL (add 160 μL to Input) Elution Buffer (20 mM EDTA, 0.2 M NaCl, 0.1 M $NaHCO_3$, 1% SDS, 0.5 M Tris-HCl (pH 7.5), 0.2 mg/mL Proteinase K) 2 hours 68°C. DNA was purified using the QIAquick PCR purification kit (Qiagen, Venlo, The Netherlands).

Primers were designed to amplify a 200-300 bp fragment of genomic DNA containing immediate upstream sequences of the transcriptional start site (TSS) of the gene of interest. TSS was identified using EST and RNASeq data displayed by the Ensembl genome browser. Control primers (*tk1*-) were designed to amplify a 200-300 bp fragment of genomic DNA 2 kbp upstream

of the TSS, which did not contain consensus E2f1 binding motifs. Primer were tested on serial dilutions of genomic zebrafish DNA to determine amplification efficiencies (AE). qPCR was performed on 2 μL diluted DNA (1:2) derived from ChIP experiments using 1 μL of each primer (10 pmol/μL) and iTaq Universal SYBR Green Supermix (Bio-rad, Hercules, CA) in a 12 μL total reaction volume. The PCR was performed for 45 cycles with annealing temperature of 60°C and 30 second elongation time. For each immunoprecipitated sample the fraction of precipitated input was calculated using the formula $AE^{Ct(input)-Ct(sample)}$. Next, the rabbit anti-E2f1 antibody/input ratio was normalized to the rabbit IgG antibody/input ratio (rabbit IgG antibody/input ratio was set to 1) to determine the fold enrichment of target sequence over background.

ChIP Primers

Gene	Ensembl ID	Target Site	Forward Primer	Reverse Primer
CDKN2A	ENSG00000147889	TSS	5'- GCT GAG GGT GGG AAG ATG-3'	5'-CCT TAA CTG CAG ACT GGG A-3'
tk1	ENSDARG00000086561	TSS	5'-AGT CAC TGT GCC GGT TTA TT-3'	5'-GTC GTC TGC TTG TTG TCT TTA TTT-3'
tk1-	ENSDARG00000086561	2kbp 5' of TSS	5'-CAG GCT TAC GGA GAC AGC AA-3'	5'-AGT GTT TGC TGC TGG ATC AC-3'

ARF Genotyping Primers

Gene	RefSeq ID	Forward Primer	Reverse Primer
CDKN2A	NM_058195.3	5'-ATG GTG CGC AGG TTC TTG GTG A-3'	5'-CAC CAC CAG CGT GTC CAG GAA G-3'
actb2	NM_181601.4	5'-CGA GCA GGA GAT GGG AAC C-3'	5'-CAA CGG AAA CGC TCA TTG C-3'

Cell Culture

Zebrafish cells were cultured at 32°C, 5% CO_2 in DMEM:F-12 medium (ATCC, Manassas, VA) with 10% FBS, 1% Pen/Strep (ZF4) or 50% L-15, 35% DMEM, 15% Ham's F-12 medium with 1.8 mM $NaHCO_3$, 15 mM HEPES, 1% Pen/Strep, 10% FBS, 1% L-glutamine, 0.2% Gentamincin Sulfate (ZKS). HeLa cells were grown at 37°C, 5% CO_2 in DMEM with 10% FBS, 1% Pen/Strep. The pcDNA-ARF construct was created by subcloning the cDNA of human ARF (exons 1β, 2, and 3 of *CDKN2A*) into the multiple cloning site of pcDNA3.1(+). Cells were transfected with either pcDNA-ARF or an empty vector (pcDNA). Transient transfections were performed using the FuGENE 6 transfection reagent (Roche) according to the manufacturer's instructions. Cells were analyzed 2 days post transfection. Luciferase assays were performed with pGL3-ARF-736bp and pGL3-ARF-3.4kb as previously described (del Arroyo et al., 2007). Briefly, promoter assays were performed in a 96 well format with each well containing 10,000 cells. Approximately 24 hour after plating, the cells were transfected as previously described with a total of 175 ng of DNA comprising 150 ng of the relevant reporter plasmid and 25 ng of a Renilla TK plasmid (RL‑TK, Promega, Madison, WI) as an internal control for transfection efficiency. Reporter activity was measured using the Dual‑Glo Luciferase Assay System (Promega) according to the manufacturer's protocols.

Statistical Analysis

Data are presented as mean ± SD. Statistical analyses were performed by using SPSS Statistics Desktop, version 22.0 (IBM, Armonk, NY). Statistical differences were analyzed by using a Student's *t*-test. A p-value <0.05 was set as the threshold for statistical significance.

Tumor Model Analysis

Both Tg(*fabp10a*:pt-β-cat) and Tg(ARF:ARF; *fabp10a*:pt-β-cat) transgenic zebrafish were assessed daily for survival and level of health. Fish were sacrificed and their livers processed at 6 months of age, a time point at which 80% of Tg(*fabp10a*:pt-β-cat) transgenic zebrafish displayed hepatocellular carcinoma (HCC)-like changes (Evason et al., 2015). Whole fish were massed (dry) as well as individual livers (dry) to quantify changes in liver mass relative to total body mass. Livers were divided in 2 and fixed in 4% PFA for either 2 hours (frozen) or overnight (paraffin) at 4°C. Following fixation, frozen samples were incubated in 30% sucrose in 1X PBS overnight at room temperature and then embedded and frozen in OCT (Sakura Finetek, Alphen aan den Rijn, The Netherlands). 6 μm sections were cut and stained. Following paraffin processing, samples were embedded, and 10 μm sections were cut and stained with hematoxylin and eosin (H&E) for pathological analysis by a board certified pathologist. Quantification and graphical representation of liver mass and mitotic figures was performed using SPSS Statistics Desktop, version 22.0 (IBM).

Results

Survey of *ARF* orthologues in highly and poorly regenerative vertebrate genomes

Using the Ensembl Genome Brower (Flicek et al., 2014), the UCSC Genome Browser (Karolchik et al., 2014), and Sal-Site (Smith et al., 2005), I analyzed the Ink4b-Arf-Ink4a locus in the genomes of 6 different vertebrate species including highly regenerative (teleost fish and urodele amphibians) and poorly-regenerative (avians and mammals) vertebrates (Monaghan and Maden, 2013). My analysis confirms prior reports (Kim et al., 2003) that an ARF ancestor exists in chickens. I found that in contrast to Ink4 orthologues, which are pervasive throughout vertebrate genomes, ARF orthologues are not present in the genomes of highly-regenerative vertebrates (Figure 1A). The results of this analysis, while not directly demonstrating an association of ARF with regeneration, support the hypothesis and prompted my investigation.

Context specific activation of *ARF* by regenerative signals in the zebrafish blastema

To investigate how the *ARF* gene responds to environmental cues, I generated reporter fish in which GFP is expressed under the control of the human *ARF* promoter (Tg(*ARF*:GFP) or *ARF*:GFP) (Figure 1B, top). In mammals, ARF expression is regulated by a promoter that contains several putative E2F binding sites, but *ARF* is unusual in that its expression pattern implies that a threshold exists at which E2F levels register as aberrant (Gil and Peters, 2006). The ARF promoter has previously been empirically defined (del Arroyo et al., 2007) and no other regulatory sequences or enhancers have been described to date. I first confirmed that the human *ARF* promoter can function in zebrafish cells *in vitro* in transfection experiments using previously described firefly luciferase reporter constructs (del Arroyo et al., 2007). Experiments

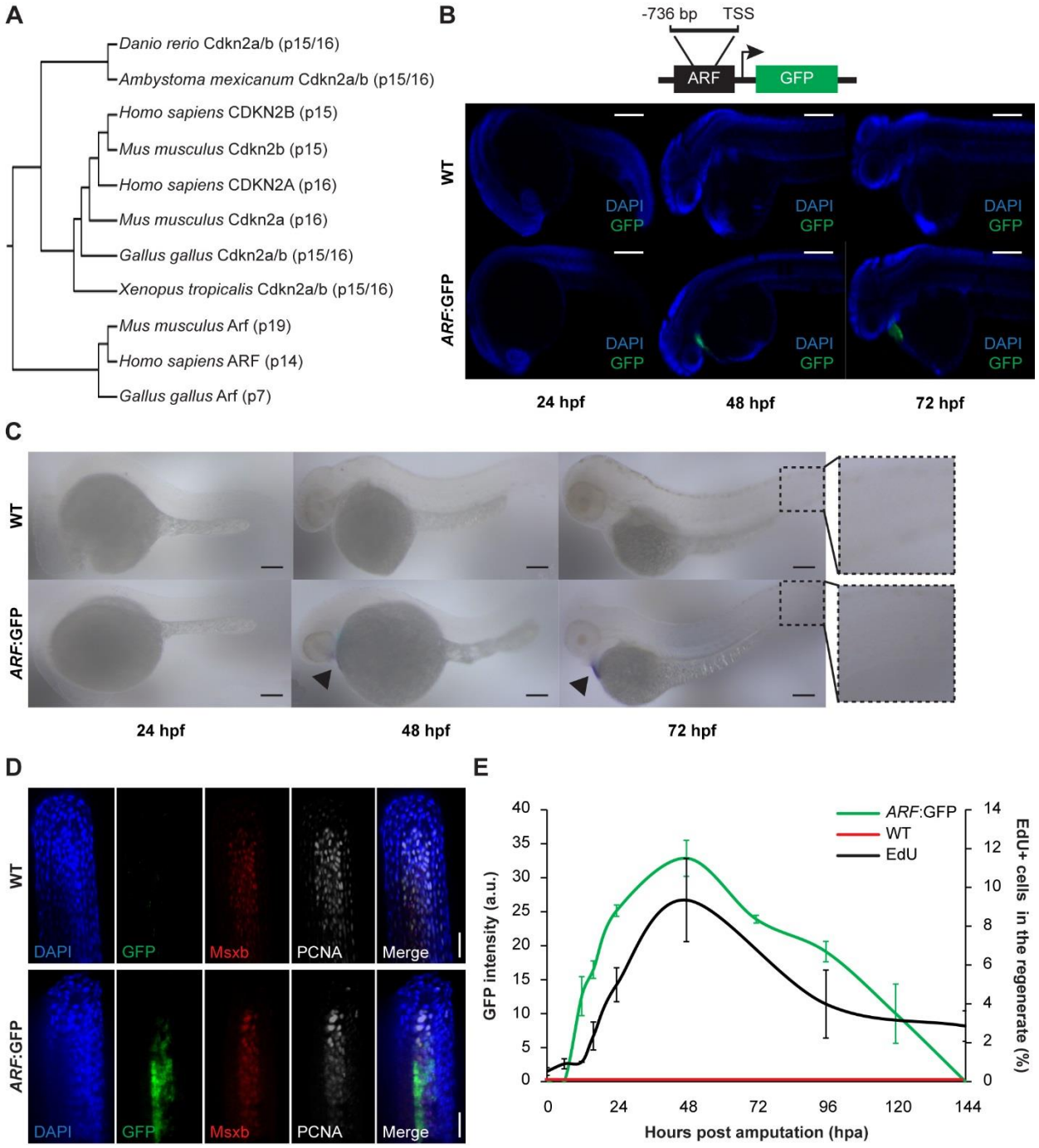

Figure 1. *ARF*, not normally present in highly regenerative vertebrates, is specifically activated in blastemas of ARF transgenic zebrafish. (A) Comparison of amino acid sequences of proteins produced by the Cdkn2a/b loci of zebrafish (*Danio rerio*), amphibians including the axolotl (*Ambystoma mexicanum*) and western clawed frog (*Xenopus tropicalis*), chickens (*Gallus gallus*), and mammals including the mouse (*Mus musculus*) and human (*Homo sapiens*). While Cdkn2a and Cdkn2b are conserved and encode Ink4 orthologues, Arf evolved recently and orthologues do not exist in highly regenerative vertebrates including teleost fish and urodele amphibians. (B) Schematic of transgene expressing GFP under the control of the human *ARF* promoter (top). The promoter consists of human regulatory sequences 736 base pairs upstream of the transcriptional state site (TSS) of *ARF*. Figure supplement 1 shows *in vitro ARF* promoter assays. Immunostaining (sagittal confocal images) for GFP at 24 hpf, 48 hpf, and 72 hpf in WT and *ARF*:GFP embryos (bottom). Scale bars: 200 μm. GFP expression is restricted to the hearts of transgenic fish due to presence of a separate transgene used for selection (*cmlc2*:GFP). (C) Whole-mount *in situ* hybridization for GFP at 24 hpf, 48 hpf, and 72 hpf in WT and *ARF*:GFP embryos. Scale bars: 100 μm. Alkaline phosphatase staining is restricted to the hearts of transgenic fish (arrow heads). No signal was detected in the larval fin fold (inset). (D) Confocal images of coronal vibratome sections immunostained for GFP, Msxb, and PCNA at 2 dpa in WT and *ARF*:GFP fins. Scale bars: 50 μm. GFP expression is induced in the proliferative blastema of the regenerate, but it is not expressed in the surrounding epithelium. (E) GFP intensity in the regenerates of *ARF*:GFP transgenic fish (green line) and WT fish (red line) after amputation. The black line represents the percentage of EdU+ cells in the regenerates of WT fish after amputation (N=3; secondary axis). Figure supplement 2 shows wound healing in WT and *ARF*:GFP fins. Results are shown as mean ± SD.

were performed with ZF4 and ZKS (Stachura et al., 2009) cells with HeLa cells used as a positive control since they express high levels of endogenous ARF (Figure 1–figure supplement 1). These assays confirmed that the 736 base pair (bp) promoter is active in HeLa cells and in zebrafish lines. Therefore, I chose the 736bp genomic fragment encompassing the human *ARF* promoter to generate *ARF* transgenics that mimic regulation of the human *ARF* gene. Tol2-mediated transgenesis (Kwan et al., 2007) was used to generate *ARF*:GFP fish, and transgenic fish were detected using cardiac GFP expression driven by a separate *cmlc2*:GFP cassette on the transgene.

I monitored expression of GFP driven by the human *ARF* promoter during normal development and in adult fish after injury and during regeneration. To determine if *ARF*:GFP is active during organogenesis in the zebrafish embryo, I assayed GFP expression at three developmental time points, 24, 48, and 72 hours post fertilization (hpf). I was unable to detect *ARF*:GFP expression in the embryo head, body or tail by confocal immunofluorescence indicating that the *ARF* promoter is silent at these developmental stages (Figure 1B). GFP expression in the heart driven by the *cmlc2* promoter serves as an internal control. To confirm that my analysis was not significantly compromised by limits of detection, I also performed *in situ* hybridization for GFP transcripts (Figure 1C). The *in situ* hybridization results confirmed the immunofluorescence analysis and indicate that *ARF* is silent or minimally expressed during development, including the developing tail fin region.

To investigate *ARF* activation during regeneration, *ARF*:GFP regenerates were assessed before amputation and then at time points during which wound healing, blastema formation, and outgrowth of regenerating fins occurs (Poss et al., 2003). *ARF*:GFP transgenic fish regenerated their fins normally. In stark contrast to development, *ARF*:GFP was induced and highly

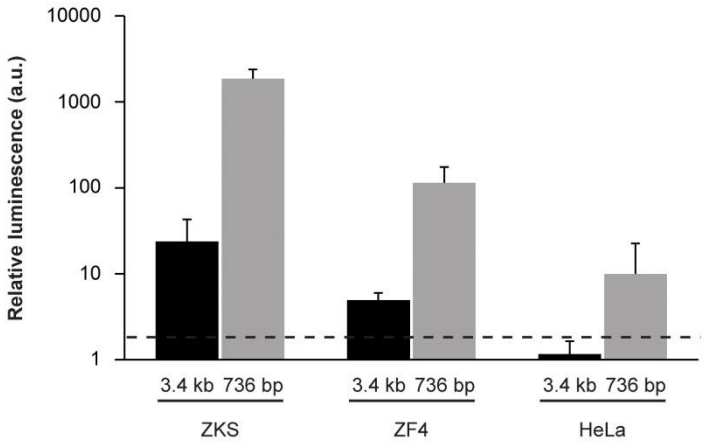

Figure 1-figure supplement 1. *In vitro* analysis of *ARF* promoter constructs in zebrafish and human cells. Representative luciferase reporter data of 3 replicates; relative luminescence generated by *ARF* promoter-firefly luciferase reporter constructs transfected into zebrafish (ZKS, ZF4) and human (HeLa) cells. Two *ARF* promoter-reporter constructs were tested; one contained sequences up to 3.4 kb upstream of the TSS of *ARF* (3.4 kb) while the other contained sequences up to 736 bp upstream of the TSS of *ARF* (736 bp). Relative luminescence was measured by normalizing firefly luciferase values to those detected from a Renilla luciferase construct used as a transfection efficiency control. The relative luminescence values were then normalized to those of the negative control construct, pcDNA. Any values above 2 (black dashed line) are considered significant (N=3; pcDNA=1; $p<0.05$). Results are shown as mean ± SD.

expressed in the blastema of regenerating adult fins. GFP was specifically detected in *ARF*:GFP fins after amputation, and GFP colocalized with Msxb and PCNA expressing cells (Figure 1D). GFP was not detected in the surrounding epithelium. This observation indicates that the *ARF* promoter is active in at least a subset of Msxb-positive blastema cells. GFP signal in the regenerate was first detected at 12 hours post amputation (hpa), peaked at 48 hpa, and then declined to undetectable levels within 6 days (Figure 1E). To correlate GFP expression with proliferation in *ARF*:GFP fins, I assessed EdU incorporation in regenerates at the above time points. There is a low level of proliferation in uninjured fins (0 hpa), but proliferation quickly increases to maximal levels within 48 hpa and then decreases (Figure 1E). GFP expression mirrored proliferative changes, suggesting that *ARF* detects and responds to high proliferative signaling in the regenerate.

To further examine the specificity of *ARF* regulation, I examined the response to the creation of an epithelial laceration wound. In this interray wound model, healing occurs without regeneration or blastema formation (Gauron et al., 2013). An epithelial wound was created in the dorsal fin lobe (Figure 1–figure supplement 2A) and the ventral fin lobe of the same fish was amputated. GFP expression was evaluated 1 day post injury (dpi) (Figure 1–figure supplement 2B). As expected, GFP was detected in the forming ventral blastema. However, GFP was undetectable in the healing wound. These distinct *ARF* responses to development and to the two different forms of injury indicate that *ARF* specifically senses and responds to signals particular to the regeneration environment that differ significantly from those present during wound healing or in the highly proliferative environment of developmental organogenesis.

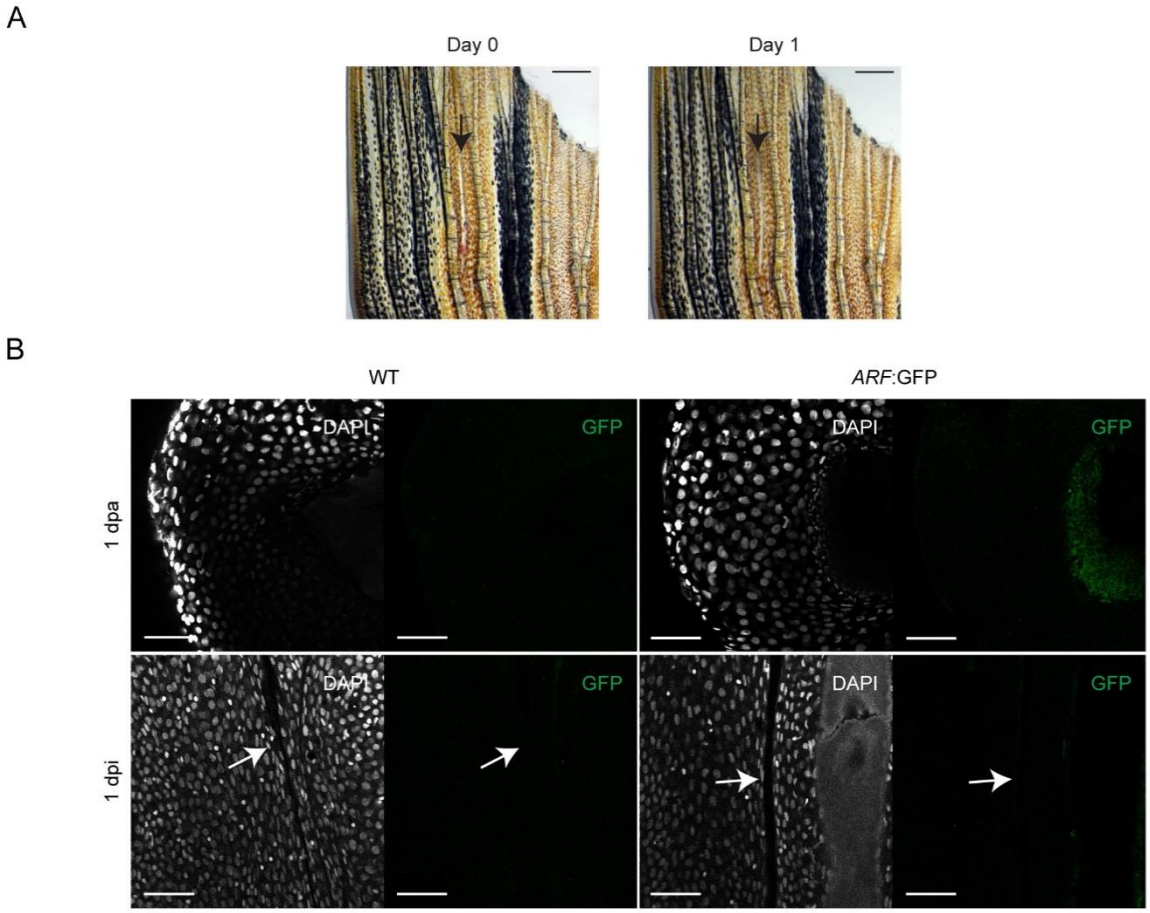

Figure 1-figure supplement 2. *ARF* is not activated during wound healing in the absence of a blastema. (A) At Day 0, dorsal fin lobes were wounded (interray laceration, 0 dpi) while ventral fin lobes were amputated (0 dpa). At Day 1, GFP expression was assayed in the healing (dorsal) and regenerating (ventral) fins. Scale bars: 0.5 mm. (B) Representative images (sagittal confocal images) of GFP expression in WT and *ARF*:GFP fins that were either amputated (1 dpa) or wounded (1 dpi). GFP is only detected in *ARF*:GFP fins that have been amputated (N=5). Scale bars: 50 μm. Arrows point to the interray wound.

Zebrafish E2f1 binds the human ARF promoter specifically in the context of Rb hyperphosphorylation during regeneration

In mammalian cells, *ARF* detects and responds to aberrant inhibition of the Rb pathway (Sharpless, 2005, Sherr, 2006). To investigate the specific factors that activate *ARF* during zebrafish fin regeneration, but not during development, I assessed Rb pathway inhibition by Western analysis of E2f1, Rb1, and hyperphosophorylated-Rb1 (p-Rb1) in developing embryos (72 hpf) and in adult uninjured fin tissue (uninj.) and at 2 days post amputation (dpa). Whereas p-Rb1 levels were relatively low in uninjured adult fins, a modest increase was detected in 72 hpf embryos. However, 2 dpa regenerates contained a dramatic increase in p-Rb1 levels despite stable levels of total Rb1 and total E2f1 (Figure 2). This reflects a high level of pro-proliferation signaling resulting in inactivation of Rb1 by phosphorylation, as occurs commonly in tumors. The hyperphosphorylation of Rb1 suggested that resulting elevated levels of free E2f could be sensed by *ARF* resulting in transcriptional activation. Moreover, since E2F can directly activate *ARF* in mammals (Gil and Peters, 2006), I evaluated the interaction of fish E2f1 with the mammalian *ARF* promoter by chromatin immunoprecipitation (ChIP) experiments using an anti-E2f1 antibody in developing *ARF*:GFP embryos and uninjured and 2 dpa *ARF*:GFP fins. I analyzed the precipitated DNA fragments by qPCR for three specific genomic regions, the *ARF* promoter, the *tk1* promoter (a known target gene of E2f1 (Wells et al., 2002)), and a region 2 kilobases (kb) upstream of the *tk1* promoter (*tk1*-) as a negative control. I found that in contrast to the state before amputation, *ARF* is bound by E2f1 specifically during regeneration as is *tk1* but not *tk1*- (Figure 2B). The ChIP assay showed that binding of the *ARF* promoter by E2f1 was enriched over 6-fold relative to non-amputated controls and the *tk1*- control. The *ARF* promoter was even more highly enriched than the *tk1* positive control. Despite the modestly increased p-

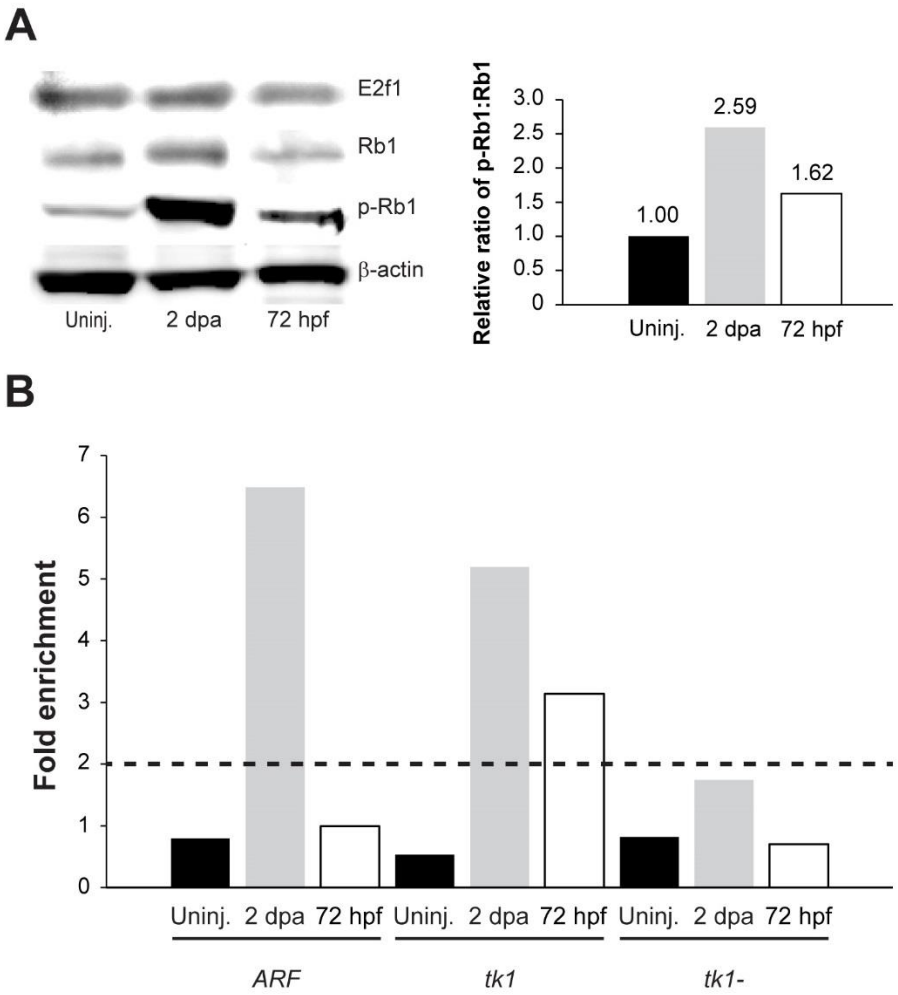

Figure 2. Rb1 hyperphosphorylation and E2f1 binding of the human *ARF* promoter in the blastema during regeneration. (A) Representative Western blot of 3 replicates of Rb pathway components, E2f1, Rb1, and hyperphosphorylated Rb1 (p-Rb1), before injury (uninj.), at 2 dpa, and during embryogenesis at 72 hpf (left). Quantification of Western blot bands normalized to β-actin and relative to uninjured tissue (right). The relative ratio of p-Rb1:Rb1 correlates with the relative amount of free E2f1 present in each condition. (B) Representative ChIP qPCR data of 3 replicates. Tissue was collected from *ARF*:GFP transgenic fish before injury (uninj.), at 2 dpa (regenerate only), and at 72 hpf. Fold enrichment of E2f1 binding was normalized to rabbit IgG. The zebrafish thymidine kinase 1 (*tk1*) promoter was used as a positive control for E2f1 binding. Sequences 2 kbp upstream of *tk1* were used as a negative control (*tk1*-). Values above 2 fold (black dashed line) are considered significant ($p<0.05$).

Rb1 levels in 72 hpf embryos, which correlated with enrichment of E2f1 at the tk1 promoter, no increase in E2f1 binding of the *ARF* promoter was observed. This finding suggests that the *ARF* promoter responds strongly and specifically to E2f1 suprathreshold levels present during regeneration as opposed to other physiological contexts. This result implies that proliferative signaling during fin regeneration has similarities to that during mammalian tumor formation which elicit the *ARF* tumor suppressor response.

Human ARF suppresses zebrafish fin regeneration

Since ARF is a human protein with no orthologues in zebrafish, I confirmed the expected subcellular localization of ARF and stabilization of Tp53 in zebrafish cells *in vitro* using the zebrafish cell lines, ZF4 and ZKS (Stachura et al., 2009). Cells were transfected with an ARF expression construct (human ARF cDNA subcloned into pcDNA3) to determine the subcellular localization of the protein as well as to confirm its interactions with orthologues of its mammalian partner, Mdm2 (Sherr, 2006, Sharpless, 2005). Confocal imaging showed that human ARF localized to the nucleolus and co-localized with Mdm2 in zebrafish cells (Figure 3–figure supplement 1A). Tp53 levels were examined in fish cells transfected with ARF expression or control constructs. Elevated Tp53 levels were readily observed in approximately 40% of ARF transfected cells (Figure 3–figure supplement 1A, B). The recapitulation of typical localization and Tp53 upregulation suggested conservation of human ARF functions in zebrafish cells and supported investigation of ARF transgenic fish. To investigate the phenotypic effects of ARF on regeneration *in vivo*, I first utilized the heat shock protein 70 inducible promoter to drive expression of ARF (Tg(*hsp70l*:ARF) or *hs*:ARF) (Figure 3). *hs*:ARF fish were subjected to multiple heat shock regimens to determine ARF expression and stability. Immunostaining

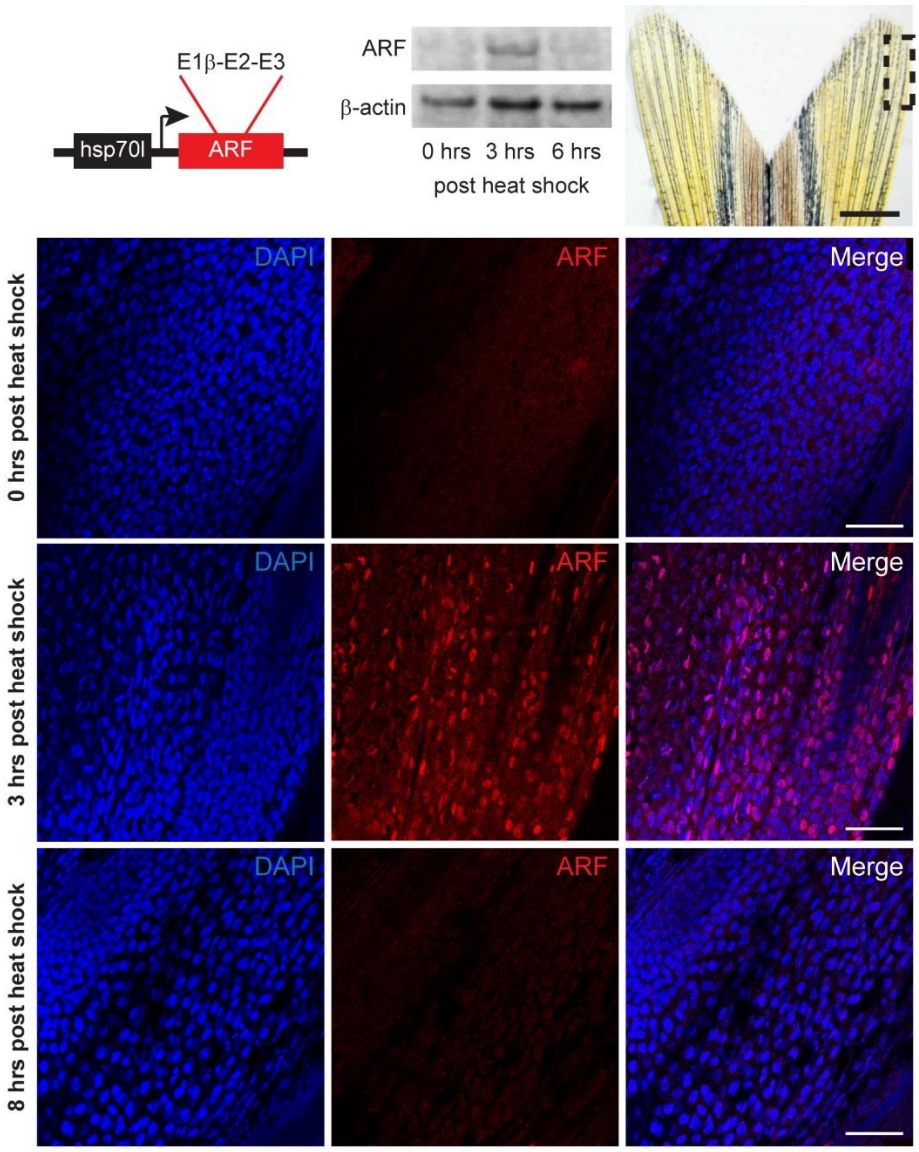

Figure 3. Expression of the mammalian tumor suppressor ARF in zebrafish driven by heat shock promoter. *In vivo* analysis of transgenic zebrafish expressing human ARF under the control of an inducible heat shock promoter, Tg(*hsp70l*:ARF) (*hs*:ARF). Schematic of the *hs*:ARF transgene (top left). The ARF cassette included in the transgene is a cDNA that consists of human exons 1β, 2, and 3 of CDKN2A. Figure supplement 1 shows *in vitro* assays. Representative Western blot of 3 replicates of ARF before (0 hours) and 3 and 6 hours post heat shock induction of ARF expression (top middle). Portion of fin shown below for analysis of expression *in vivo* (top right; dashed box). Scale bar: 1 mm. Immunostaining (sagittal confocal images) for ARF in adult hs:ARF zebrafish fins at 0, 3, and 8 hours after a single, hour long, 37°C heat shock (bottom). Scale bars: 50 μm. ARF expression is maximal at 3 hours post heat shock, and it is undetectable by 8 hours post heat shock.

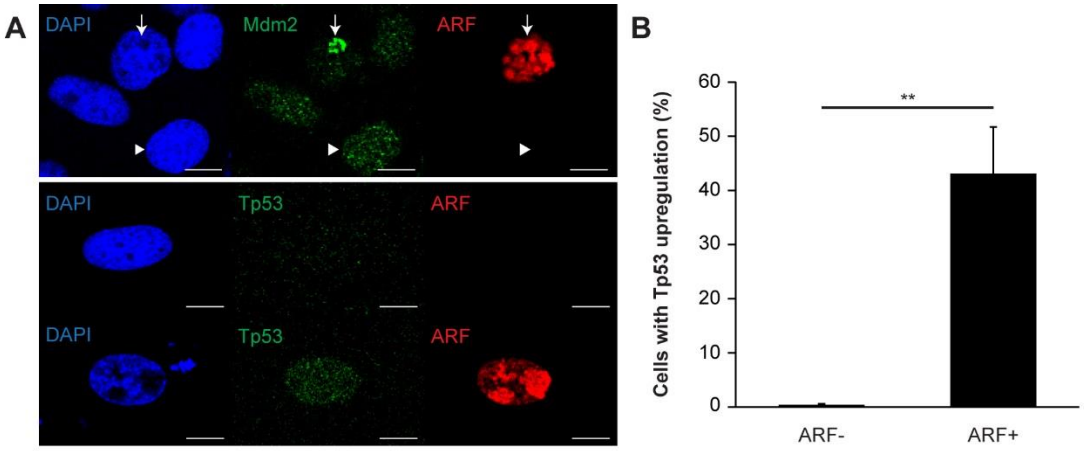

Figure 3-figure supplement 1. Analysis of ARF expression in zebrafish cells. (A) Immunofluorescence for Mdm2 and ARF (top) and Tp53 (bottom) in zebrafish cells (ZKS) transfected with pcDNA-ARF. ARF and Mdm2 co-localize in the nucleolus (arrow) when ARF is expressed; in cells without ARF, Mdm2 has a diffuse nuclear staining pattern (arrow head; top). Tp53 upregulation depends on ARF expression (bottom). Scale bars: 10 μm. (B) Quantification of Tp53 upregulation in zebrafish cells (ZKS) transfected with pcDNA-ARF (N=100, $p<0.01$). Results are shown as mean ± SD.

showed that when induced with an hour long, 37°C heat shock, ARF is robustly expressed in the fin three hours later (Figure 3). Western blot confirmed induction of ARF protein expression and also showed a rapid decrease almost to baseline at 6 hours (Figure 3), in accord with the known 6 hour half-life of the human protein (Sherr, 2006). I then examined the effects of inducible, transient ARF expression on fin regeneration. Using a regimen of one heat shock three hours prior to amputation and then subsequently every six hours up to 6 dpa (Figure 4A, top), fin regeneration in *hs*:ARF transgenic fish was compared to non-transgenic clutchmates (WT). *hs*:ARF and WT fish tolerated heat shock well without overt illness or mortality. ARF expression caused significant inhibition of fin regeneration as evidenced by reduced regenerate length and area; WT regenerates measured 1.2 mm ± 0.13 min length and 5.4 mm^2 ± 1.3 mm^2 in area compared to *hs*:ARF regenerates which measured 0.84 mm ± 0.13 mm in length and 3.0 mm^2 ± 0.76 mm^2 in area, a reduction of approximately 30% ($p<0.001$) and 45% ($p<0.001$), respectively (Figure 4B). After the heat shock regimen ended, fin regeneration resumed to reach full length by 14 dpa. Both *hs*:ARF transgenic fish maintained at 28-30°C and WT fish exposed to heat shock regenerated their fins normally. When previously heat-shocked *hs*:ARF fins were reamputated and allowed to regenerate in the absence of heat shock (Figure 4A, bottom), the fins regenerated equally as well as WT fins (Figure 4C). This indicates that ARF inhibits fin regeneration in a reversible manner and that its continued expression is required for regeneration suppression.

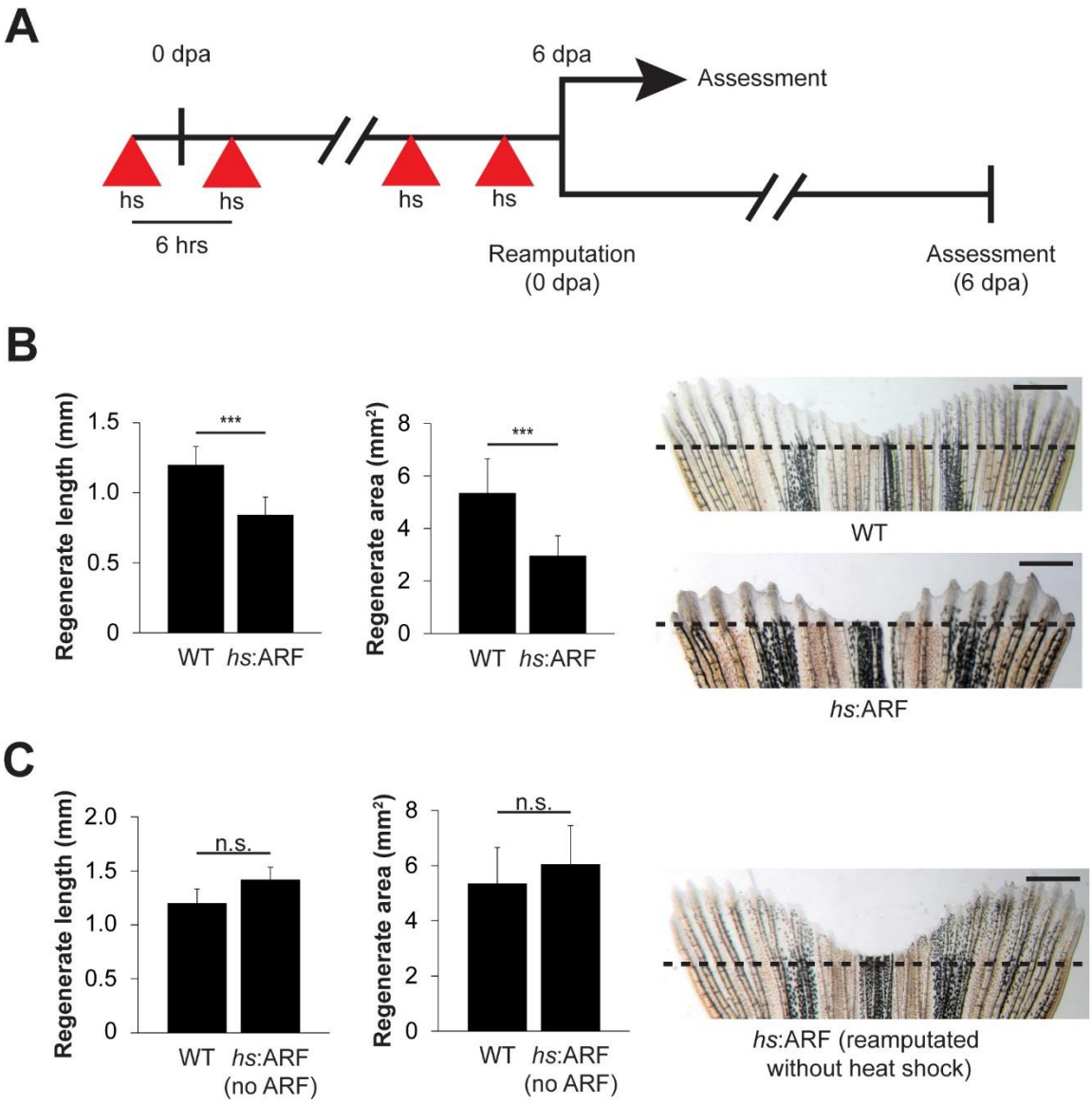

Figure 4. ARF suppresses fin regeneration. (A) Schematic of heat shock regimen. An initial hour long, 37°C heat shock is delivered 3 hours prior to amputation (0 dpa) and then every 6 hours thereafter for 6 days. Regenerates are then assessed (top) or fins are reamputated (0 dpa) and allowed to regenerate in the absence of heat shock for 6 days (bottom). (B) Quantification of regenerate length and area at 6 dpa in WT and *hs*:ARF fins exposed to the heat shock regimen (left; N=40 fins representing multiple different transgene insertions, $p<0.001$). Representative images of fin regeneration at 6 dpa in WT and *hs*:ARF fins exposed to the heat shock regimen (right). (C) Quantification of regenerate length and area at 6 dpa in reamputated *hs*:ARF fins not exposed to heat shock (left; N=40 fins, $p>0.05$). Representative image of fin regeneration at 6 dpa in a reamputated *hs*:ARF fin not exposed to heat shock (right). The dashed lines represent amputation planes. Scale bars: 1 mm. Results are shown as mean ± SD.

ARF suppresses fin regeneration in a p53-dependent manner by inducing apoptosis and causing cell-cycle arrest

To assess whether ARF functions through the p53 pathway to inhibit fin regeneration *in vivo*, I first crossed *hs*:ARF fish with *tp53*^{M214K} mutant fish to generate *hs*:ARF fish that are homozygous for the tp53^{M214K} allele (*hs*:ARF; *tp53*$^{M214K/M214K}$). The tp53^{M214K} mutation abrogates p53 transactivation functions (Berghmans et al., 2005). Using the same amputation and heat shock regimen, I analyzed fin regeneration and found no difference in regenerate length or area despite ARF expression in *tp53* mutant fish (Figure 5A). I also tested Tp53-dependence of ARF regeneration suppression by treating zebrafish with either pifithrin-α (PFTα), an inhibitor of Tp53 transactivation (Komarov et al., 1999), or nutlin3a, a molecule that disrupts the Mdm2-Tp53 interaction, thereby stabilizing Tp53 levels (Yun et al., 2013, Vassilev et al., 2004). Treatment of *hs*:ARF and WT fish with 5 μM pifithrin-α and heat shock increased *hs*:ARF regenerate length from 0.44 mm ± 0.04 mm to 0.66 mm ± 0.08 mm, an increase of 50% ($p<0.01$), and area from 1.8 mm^2 ± 0.7 mm^2 to 3.2 mm^2 ± 0.5 mm^2, an increase of approximately 75% ($p<0.05$), compared to carrier treated controls. Fin regeneration of WT fish was not affected by PFTα treatments (Figure 5B). Treatment of WT fish with 5 μM nutlin3a reduced fin regenerate length from approximately 0.65 mm ± 0.1 mm to 0.45 mm ± 0.1 mm, a decrease of 30% ($p<0.01$), and area from 4.7 mm^2 ± 1.2 mm^2 to 2.8 mm^2 ± 0.7 mm^2, a reduction of 40% ($p<0.05$) (Figure 5C, left), phenocopying the fin regeneration inhibition phenotype of induced *hs*:ARF fish (Figure 5C, right). Together, these experiments show that ARF functions through Tp53-dependent mechanisms to inhibit fin regeneration, and also demonstrate the importance of active suppression of Tp53 by Mdm2.

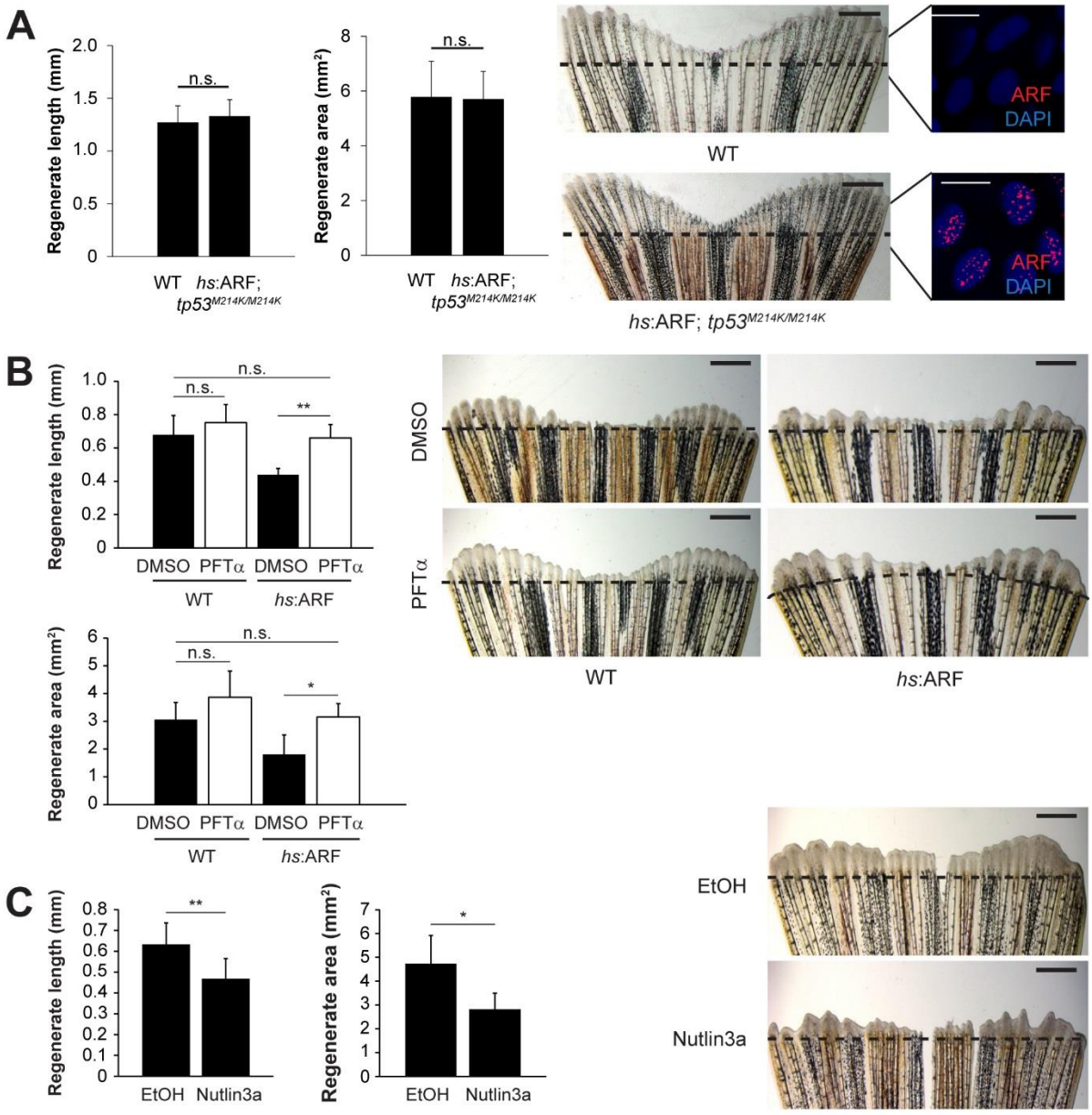

Figure 5. Human ARF functions through the Tp53 pathway in fish to suppress regeneration. (A) Quantification of regenerate length and area at 6 dpa in WT and *hs*:ARF; *tp53*$^{M214K/M214K}$ fins exposed to the heat shock regimen as in Figure 4 (left; N=30 fins). Representative images of fin regeneration at 6 dpa in WT and *hs*:ARF; *tp53*$^{M214K/M214K}$ fins exposed to heat shock (right). Scale bars: 1 mm. Immunostaining (sagittal confocal images) for ARF in WT and *hs*:ARF; *tp53*$^{M214K/M214K}$ fins 3 hours after a single heat shock (right inset). Scale bars: 10 μm. Fin regeneration proceeds equally well in WT and *hs*:ARF; *tp53*$^{M214K/M214K}$ fins exposed to heat shock. (B) Quantification of regenerate length and area at 4 dpa in WT and *hs*:ARF fins exposed to heat shock and 5 mM pifithrin-a (PFTa) or DMSO (vehicle) (left; N=8 fins, $p<0.01$). Representative images of fin regeneration at 4 dpa in WT and *hs*:ARF fins exposed to heat shock and 5 mM PFTa or DMSO (right). Scale bars: 0.5 mm. Inhibition of Tp53 activity with PFTa rescues regeneration suppression by ARF. (C) Quantification of regenerate length and area at 4 dpa in WT fins exposed to 5 mM nutlin3a or EtOH (vehicle) (left; N=8 fins, $p<0.01$). Representative images of fin regeneration at 4 dpa in WT fins exposed to 5 mM nutlin3a or EtOH (right). Scale bars: 0.5 mm. Inhibition of Mdm2 with nutlin3a phenocopies ARF expression by suppressing fin regeneration. Figure supplement 1 shows cell cycle (EdU incorporation) and apoptosis (TUNEL) assays. The dashed lines represent amputation planes. Results are shown as mean ± SD.

In order to understand the cellular effects of ARF that lead to inhibition of fin regeneration, I examined apoptosis and proliferation in blastema cells during regeneration with and without ARF expression. To estimate cell proliferation differences between WT and *hs*:ARF fins, EdU pulse-chase experiments were performed at 2, 4, and 6 dpa. EdU incorporation was significantly higher in WT fin regenerates compared to *hs*:ARF regenerates at all time points examined with the greatest difference occurring at 6 dpa (133%, $p<0.001$) (Figure 5–figure supplement 1A). Apoptotic cells in *hs*:ARF and WT regenerates were analyzed using TUNEL staining. When the percent of TUNEL-positive cells in WT and *hs*:ARF regenerates was compared, the incidence of apoptosis increased with ARF expression at all time points examined with the greatest difference occurring at 2 dpa (210%, $p<0.01$) (Figure 5–figure supplement 1B). To assess whether ARF directly affects proliferating blastema cells, I also measured EdU incorporation with different heat shock regimens starting at 4 dpa. The results showed that either a single heat shock or 24 hours of heat shocks at 4 dpa significantly reduced the number of cycling cells in the regenerate, demonstrating a direct effect of ARF on the regenerating cell population (Figure 5–figure supplement 1C).

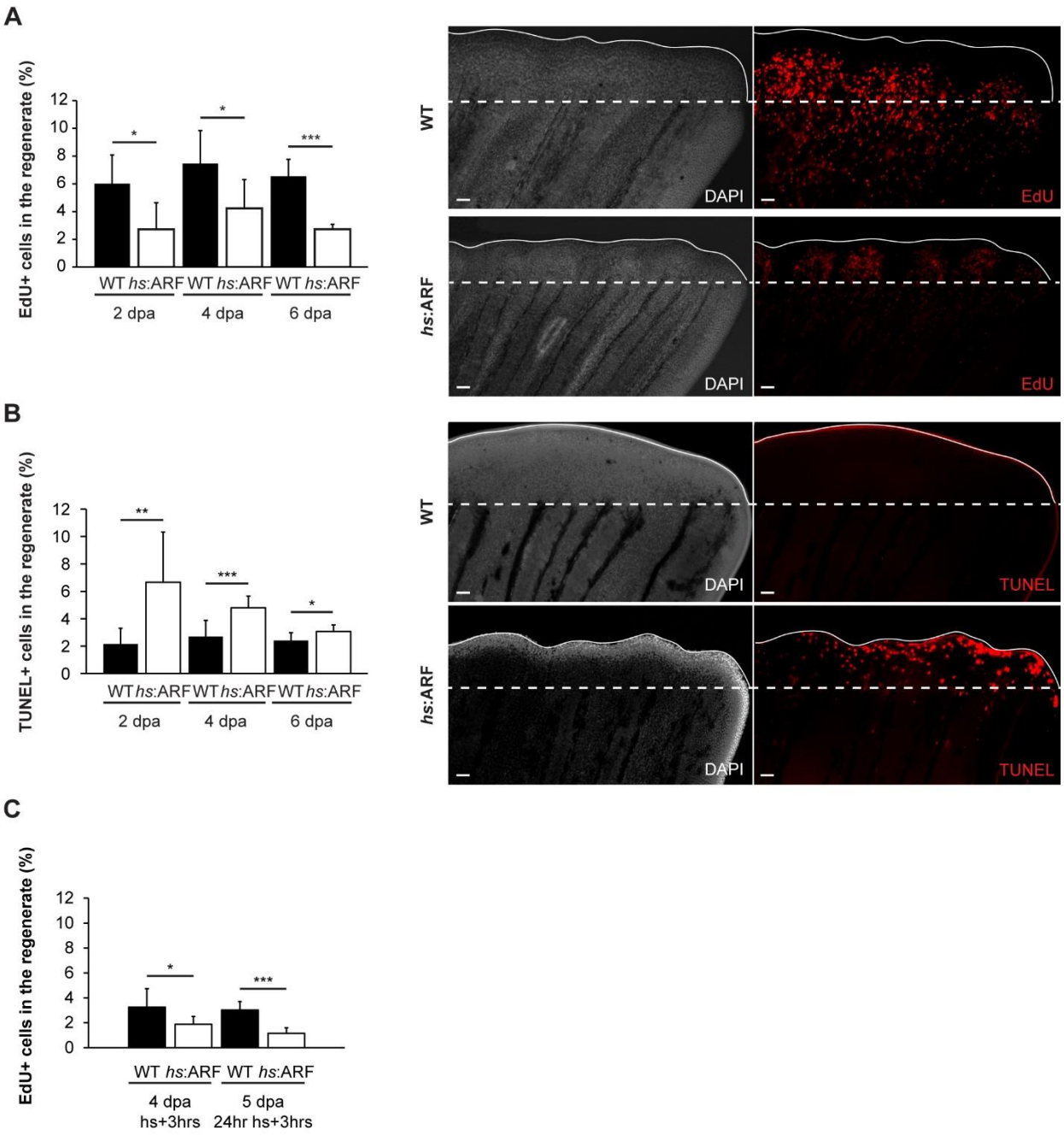

Figure 5-figure supplement 1. ARF suppresses fin regeneration by inducing apoptosis and cell-cycle arrest. (A) Quantification of EdU staining at 2, 4, and 6 dpa in WT and *hs*:ARF fins exposed to heat shock (left). At 2 dpa, 6.0% ± 2.1% of cells in WT regenerates were EdU-positive compared to approximately 2.7% ± 1.9% in *hs*:ARF regenerates. At 4 dpa, approximately 7.5% ± 2.4% of cells in WT regenerates were EdU-positive compared to 4.2% ± 2.1% in *hs*:ARF regenerates. At 6 dpa, approximately 6.5% ± 1.2% of cells in WT regenerates were EdU-positive compared to 2.7% ± 0.35% in *hs*:ARF regenerates. Significantly fewer cycling cells are detected with ARF expression (N=10 fins, $p<0.001$). Representative images (sagittal) of EdU staining at 2 dpa in WT and *hs*:ARF fins exposed to heat shock (right). (B) Quantification of TUNEL staining at 2, 4, and 6 dpa in WT and *hs*:ARF fins exposed to heat shock (left). At 2 dpa, 2.2% ± 1.2% of cells in WT regenerates were TUNEL-positive while 6.7% ± 3.7% of cells in *hs*:ARF regenerates were TUNEL-positive. At 4 dpa, only 2.7% ± 1.2% of cells in WT regenerates were TUNEL-positive compared to 4.8% ± 0.84% in *hs*:ARF regenerates. At 6 dpa, 2.4% ± 0.57% of cells in WT regenerates were TUNEL-positive while 3.1% ± 0.49% of cell in *hs*:ARF regenerates were TUNEL-positive. Significantly more apoptosis is detected with ARF expression (N=10 fins, $p<0.001$). Representative images (sagittal) of TUNEL staining at 2 dpa in WT and *hs*:ARF fins exposed to heat shock (right). Image quantification was performed on regenerates only. The dashed lines represent amputation planes. Scale bars: 50 μm. (C) Quantification of EdU staining in WT and *hs*:ARF fins 3 hours after a single heat shock or 24 hours of heat shock delivered at 4 dpa. After a single heat shock, 3.3% ± 1.5% of cells in WT regenerates were EdU-positive compared to 1.9% ± 0.62% in *hs*:ARF regenerates. After 24 hours of heat shock, 3.0% ± 0.69% of cells in WT regenerates were EdU-positive compared to 1.2% ± 0.44% in *hs*:ARF regenerates. Significantly fewer cycling cells are detected with ARF expression after blastema formation (N=10 fins, $p<0.001$). Results are shown as mean ± SD.

ARF does not affect development but suppresses fin regeneration in response to regeneration signals

Since the *ARF* promoter is activated specifically in the fin during regeneration, I tested how transgenic fish expressing ARF under control of the endogenous *ARF* promoter would develop and regenerate. To do so, I generated a line that utilizes the human *ARF* promoter to drive ARF expression (Tg(*ARF*:ARF) or *ARF*:ARF) (Figure 6A, left). ARF expression during development would be expected to adversely affect *ARF*:ARF fish. I observed, however, that *ARF*:ARF transgenic fish are viable, develop normally, and have no overt size or morphological differences when compared to age- and sex-matched WT counterparts (Figure 6A, right). Furthermore, examination of *ARF*:ARF embryos confirmed my findings in *ARF*:GFP transgenics. In agreement with the predictions of *ARF*:GFP experiments, there was no effect of the *ARF*:ARF transgene on survival during early embryogenesis compared to WT fish (Figure 6–figure supplement 1A). I also did not detect ARF expression in embryos, as expected given my findings with *ARF*:GFP fish (Figure 6–figure supplement 1A). To assess whether ARF, if expressed, would interfere with organogenesis or development, I evaluated the effects of induced ARF expression using *hs*:ARF fish. Upon heat shock, *hs*:ARF, but not WT clutches, exhibited drastically reduced survival that was associated with high levels of ARF expression throughout the embryo (Figure 6–figure supplement 1B). This finding indicates that ARF expression is very poorly tolerated by developing embryos and clearly implies that in *ARF*:ARF fish, ARF is not activated significantly during development to affect normal developmental growth and organogenesis.

I then performed fin regeneration experiments with *ARF*:ARF transgenic fish and WT fish. When *ARF*:ARF fins were injured, ARF was detected in the regenerate (Figure 6B), and the

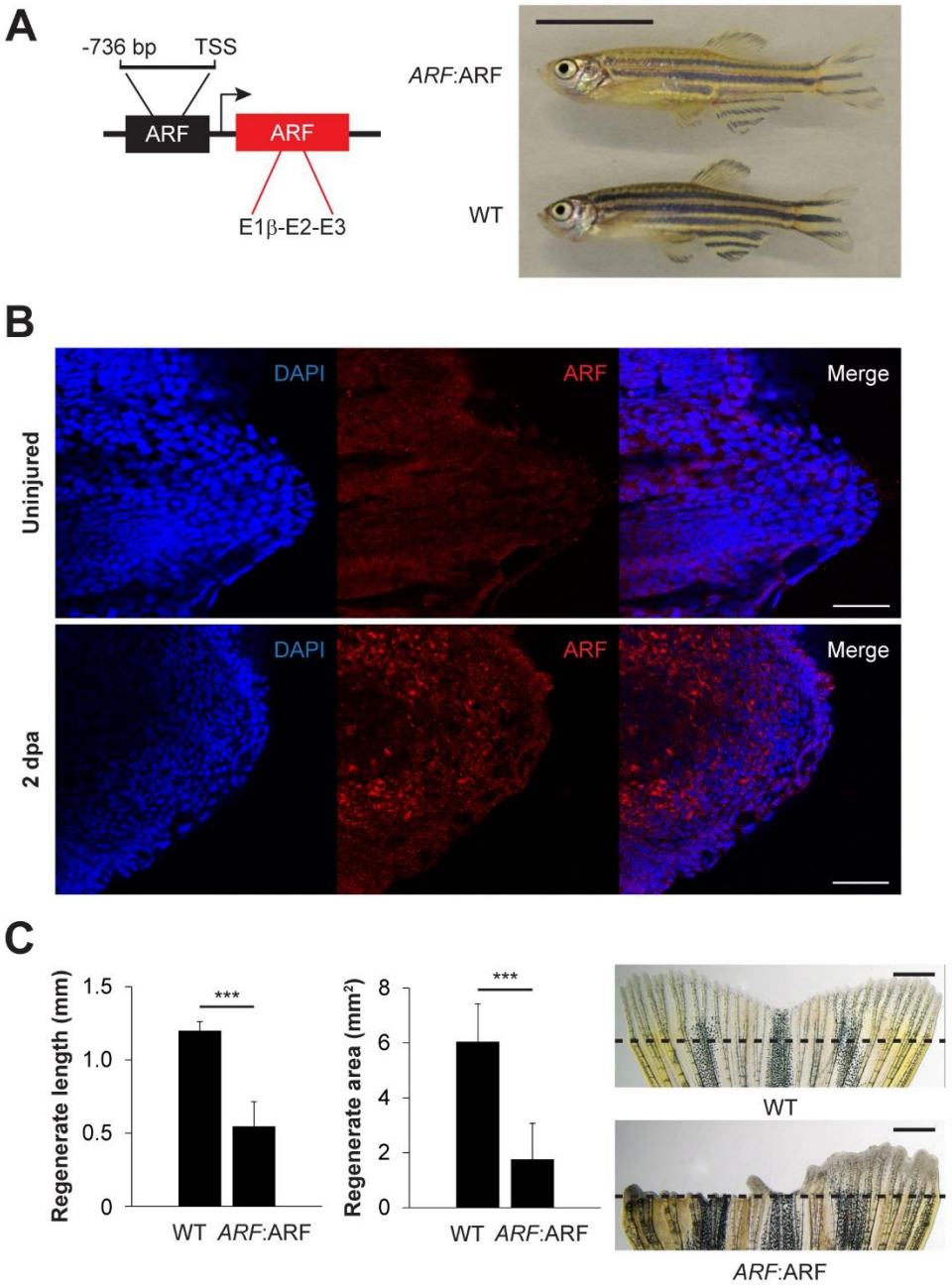

Figure 6. *ARF* senses regenerative signals and suppresses fin regeneration. (A) Schematic of transgene expressing human ARF under the control of the human *ARF* promoter (left). Representative images of age- and sex-matched *ARF*:ARF and WT zebrafish (right; 5 months post fertilization, male). Scale bar: 1 cm. *ARF*:ARF fish are viable, grow to adulthood and are of normal size and patterning. Figure supplement 1 shows the embryonic viability of ARF transgenic lines. (B) Immunostaining (sagittal confocal images) for ARF in *ARF*:ARF transgenic fish before injury (uninjured) and at 2 dpa. Scale bars: 50 μm. ARF is specifically expressed upon injury. (C) Quantification of regenerate length and area at 6 dpa in WT and *ARF*:ARF fins (left; N=10 fins, $p<0.001$). Representative images of fin regeneration at 6 dpa in WT and *ARF*:ARF fins (right). Scale bars: 1 mm. *ARF* causes marked inhibition of fin regeneration. The dashed lines represent amputation planes. Results are shown as mean ± SD.

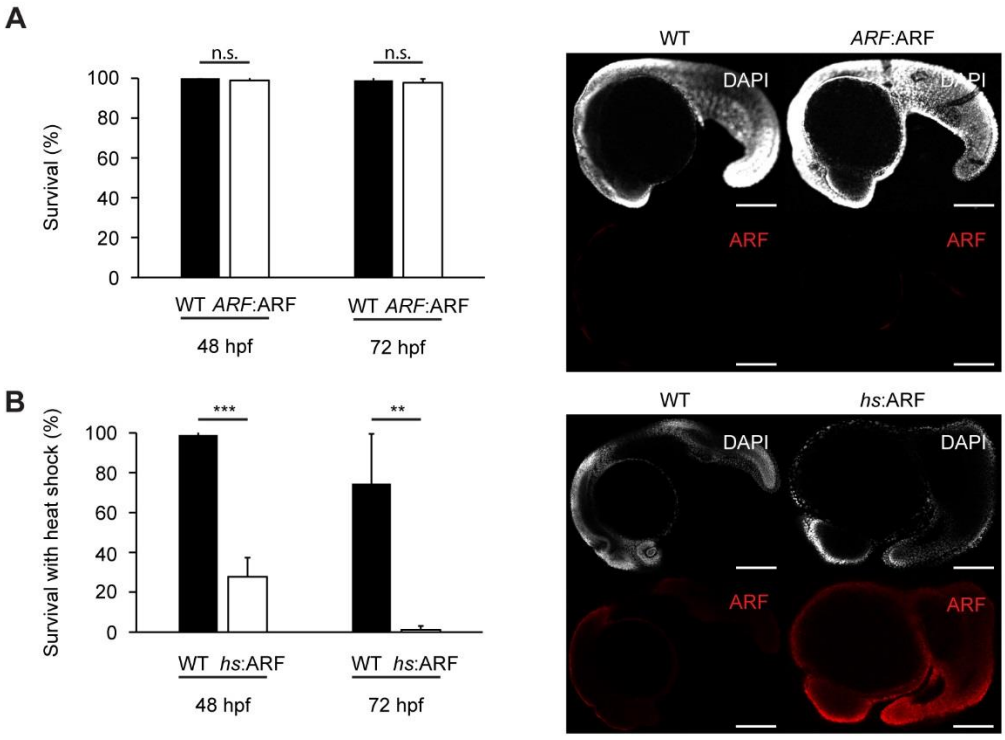

Figure 6-figure supplement 1. The *ARF*:ARF transgene does not interfere with development, whereas forced ARF expression causes embryonic lethality. (A) Quantification of embryonic mortality at 48 hpf and 72 hpf in WT and *ARF*:ARF embryos (left; N=90, $p>0.05$). Representative sagittal confocal images of ARF expression at 24 hpf in WT and *ARF*:ARF (right). (B) Quantification of embryonic mortality at 48 hpf and 72 hpf in WT and *hs*:ARF embryos exposed to heat shock (left; N=90, $p<0.001$). Representative sagittal confocal images of ARF expression at 27 hpf in WT and *hs*:ARF embryos 3 hours after a single heat shock (right). Scale bars: 200 μm. Results are shown as mean ± SD.

pattern of expression was similar to GFP expression in *ARF*:GFP regenerates at the same time point (Figure 1). When fin regeneration was compared between *ARF*:ARF transgenic fish and WT fish, *ARF*:ARF regenerates measured 0.55 mm ± 0.17 mm in length and 1.8 mm^2 ± 1.3 mm^2 in area while WT regenerates measured 1.2 mm ± 0.06 mm in length and 6.0 mm^2 ± 1.4 mm^2 in area. In all, *ARF*:ARF regenerates were 55% shorter ($p<0.001$) and 70% smaller in area ($p<0.001$) than WT regenerates, and never regenerated completely (Figure 6C). These results confirm that *ARF* activation is specific to regenerating tissue and show that the magnitude of activation is sufficient to inhibit regeneration. Thus, the presence of a functional human *ARF* gene in fish results in a diminished regenerative capacity, including absence of epimorphic regeneration, without significantly affecting other major physiological or developmental characteristics.

ARF acts as a tumor suppressor in a zebrafish model of hepatocellular carcinoma

While this chapter has focused on ARF in the context of regeneration, ARF is better known as a tumor suppressor (Sharpless, 2005, Sherr, 2006). Using a zebrafish model of hepatocellular carcinoma (HCC) (Evason et al., 2015) , I sought to investigate the ability of *ARF* to detect and respond to oncogenic signals. To do this I mated the Tg(*ARF*:ARF) transgenic line with a zebrafish model of HCC developed by Kimberley Evason that specifically expresses constitutively active β-catenin in the liver, Tg(*fabp10a*:pt-β-cat) or *fabp10a*:β-catenin (Evason et al., 2015), to create the Tg(*ARF*:ARF; *fabp10a*:pt-β-cat) or *ARF*:ARF; *fabp10a*:β-catenin transgenic line. It has been reported that by six months of age the Tg(*fabp10a*:pt-β-cat) transgenic line has a incidence of HCC-like changes of 80% (Evason et al., 2015). I used this same six month time point to assess the tumor burden of *fabp10a*:β-catenin and *ARF*:ARF;

fabp10a:β-catenin fish. First, I analyzed frozen liver sections for ARF staining. ARF expression was only detected with β-catenin overexpression (Figure 7A, left). Additionally, with the help of a board certified pathologist, we only observed pathological anomalies in paraffin sections of zebrafish livers lacking ARF expression (Figure 7A, right). Since liver size is correlated to tumor burden (Evason et al., 2015), I also dry massed individual fish and their livers to quantify liver size as a percent of total body mass. I discovered that the median liver mass of *fabp10a*:β-catenin zebrafish is 16.3% while the median liver mass of *ARF*:ARF; *fabp10a*:β-catenin zebrafish is 6.2%, a significant increase of 163% ($N=8$, $p<0.01$) (Figure 7B, left). Liver mass is between 5% and 10% of total body mass in wild-type zebrafish. In addition to liver mass, the number of mitotic figures present in H&E stained paraffin sections was assessed by a board certified pathologist. The median number of mitotic figures present in *fabp10a*:β-catenin livers was 10 while the median number of mitotic figures present in *ARF*:ARF; *fabp10a*:β-catenin livers was 2.5, a significant increase of 300% ($N=8$, $p<0.05$) (Figure 7B, right). Mitotic figures are not usually observed in wild-type livers. These results indicate that *ARF* acts as predicted in the context of tumorigenesis, as a potent tumor suppressor. These results also confirm that while *ARF* acts as a regeneration suppression in the context of zebrafish fin regeneration, its hallmark function as a tumor suppressor is not lost.

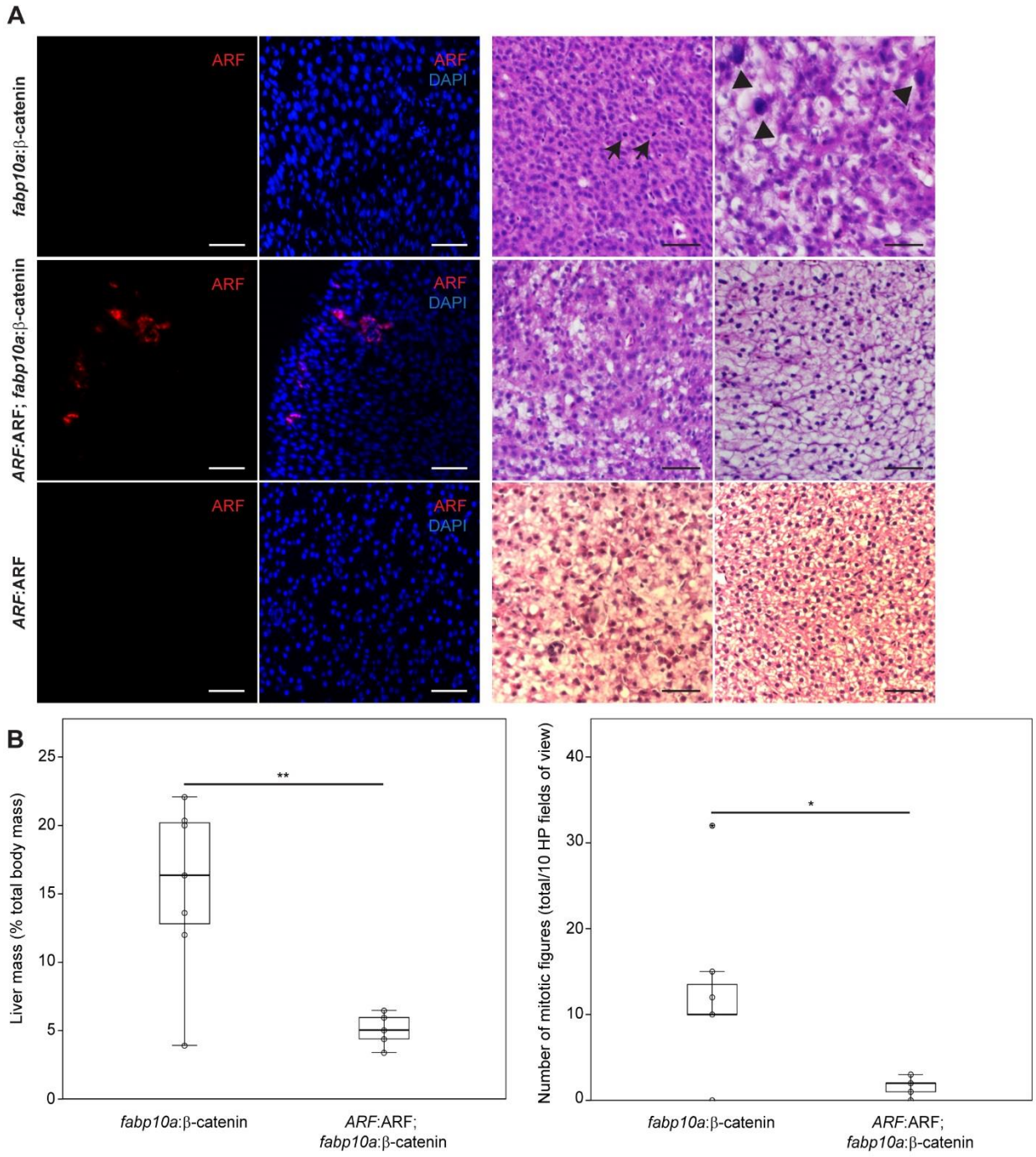

Figure 7. *ARF* acts as a tumor suppressor in a zebrafish model of hepatocellular carcinoma. (A) Representative images of ARF expression in *fabp10a*:β-catenin, *ARF*:ARF; *fabp10a*:β-catenin and *ARF*:ARF livers (left). Scale bars: 50 μm. ARF is only expressed in the presence of the *fabp10a*:pt-β-cat transgene. Representative images of H&E stained *fabp10a*:β-catenin, *ARF*:ARF; *fabp10a*:β-catenin and *ARF*:ARF livers (right). Scale bars: 20 μm. *fabp10a*:β-catenin livers have numerous pathological abnormalities including high numbers of mitotic cells (arrows) and cells with enlarged nuclei (arrow heads). Livers expressing ARF do not have these abnormalities. (B) Quantification of liver mass as a percentage of total body mass (left). Livers expressing ARF are significantly smaller than livers lacking ARF expression (N=7, $p<0.01$). Quantification of the total number of mitotic figures present in 10 high powered fields of view of H&E stained slides (right). Livers expressing ARF have significantly fewer mitotic figures than livers lacking ARF expression (N=7, $p<0.05$). The circled asterisk represents an outliner.

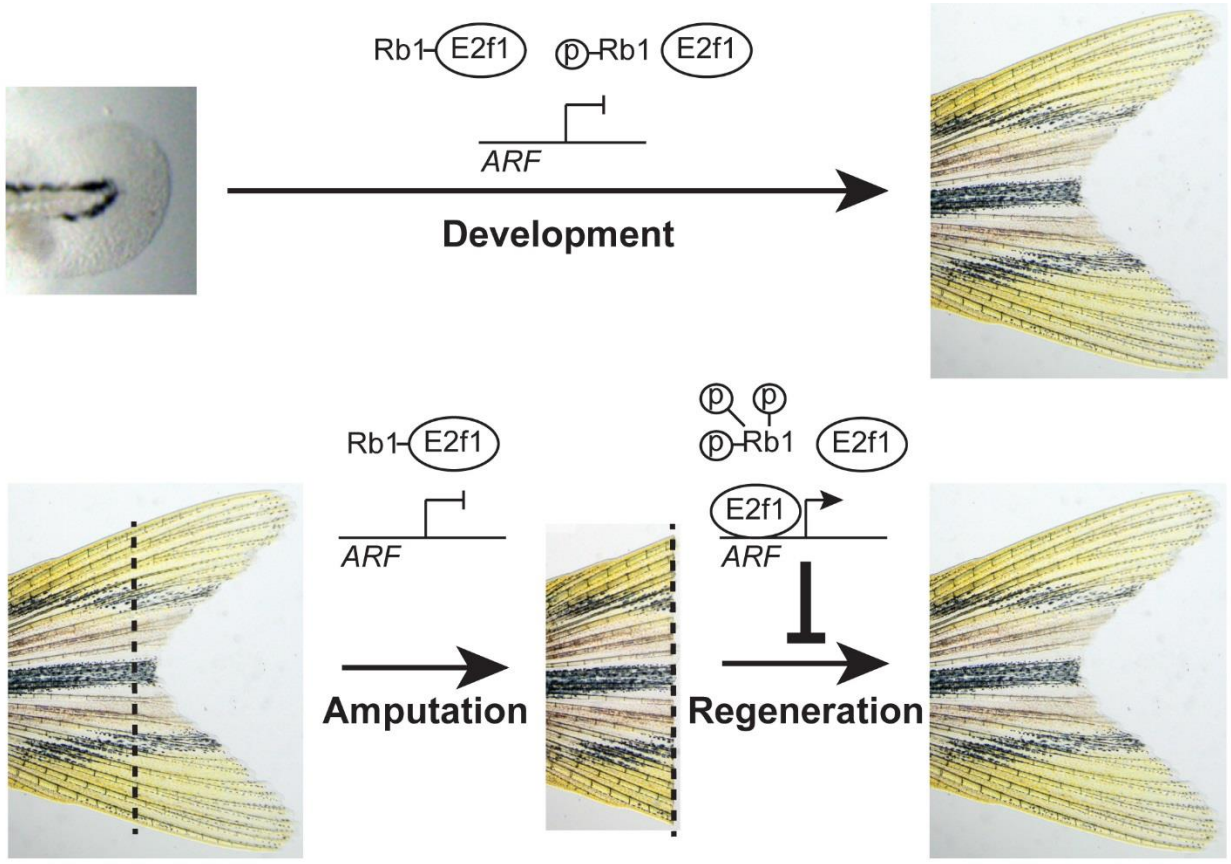

Figure 8. Model of *ARF* function in the context of Rb pathway activity during zebrafish development and fin regeneration. *ARF* is not active during development during which a moderate level of mitogenic signaling causes modest phosphorylation of Rb1 (top); however, during regeneration, high mitogenic signaling induces Rb1 hyperphosphorylation and abundant free E2f1, which activates *ARF* and leads to inhibition of regeneration (bottom). The dashed lines represent the amputation plane.

Discussion

In this study, I experimentally tested the hypothesis that tumor suppressor evolution may impact regenerative capacity. I found that the core mammalian tumor suppressor *ARF* senses regeneration signals and specifically responds to negatively alter the proliferative balance in the zebrafish blastema, greatly perturbing regeneration. My findings provide the first *in vivo* experimental evidence that evolution of tumor suppressors can negatively impact solid tissue regeneration potential.

Although the core tumor suppressors as a whole support regenerative processes, the properties of *ARF* identified in this study are at odds with epimorphic regeneration. This new example of antagonistic pleiotropy adds to previously recognized trade-off characteristics of tumor suppressor genes affecting mammalian stem cell function, reviewed in (Pardal et al., 2005, Greaves, 2007, Pomerantz and Blau, 2013, Rodier et al., 2007) and shows that *ARF* antagonistic properties also manifest in the context of the blastema. The evidence that ARF is a critical tumor suppressor in mammals (Sherr, 2006, Sharpless, 2005) but opposes regeneration functions (Sharpless and DePinho, 2007), this study) suggests that the selective pressure that has driven the evolution of ARF has primarily enhanced tumor suppression either at the expense of or in the absence of regeneration pressures. Although my experiments and those of others (Gemberling et al., 2013, Poss et al., 2003) show that the regenerative capacity of zebrafish is vulnerable to single gene alterations, whether altering function of a single gene in mammals would induce the emergence of robust epimorphic regenerative capacity is a much more complex issue. Indeed, the multifactorial genetic differences of highly and less regenerative vertebrates make it unlikely that manipulation of a single gene could enable regeneration. It is notable, however, that *Cdkn1a* (*p21*) knockout mice do possess a somewhat enhanced ability to regenerate solid structures

(Heber-Katz et al., 2013, Clark et al., 1998) such as pinnae, which lack the complex tissue structure of a digit, but nonetheless, demonstrate that alteration of cellular growth control mechanisms can impact regeneration. Moreover, the importance of active repression of ARF to maintain stem cell function (Molofsky et al., 2005), and of ARF reduction to facilitate dedifferentiation (Pajcini et al., 2010) have been documented.

Among the core tumor suppressor genes that are frequently inactivated in mammalian tumors, *ARF* is unique in that it does not have orthologues represented in most vertebrates including highly regenerative species. By contrast, *Tp53*, *Pten*, and *Ink4a* have distant orthologues, being present in invertebrates and vertebrates alike. The transgenesis approach I used to study ARF in fin regeneration made it possible to study ARF with its human regulatory components but without increasing *CDKN2A* CKI gene dosage which could have been a complicating factor in a transgenic harboring the entire *CDKN2A (INK4A/ARF)* locus. This study extends our group's previous observations (Pajcini et al., 2010) that ARF prevents dedifferentiation in muscle cells in culture and provides new evidence that ARF functions *in vivo* to oppose tissue regeneration. Future experiments will determine whether ARF prevents dedifferentiation *in vivo*, such as the dedifferentiation of osteoblasts in regenerating fins, or whether it acts on proliferating blastema cells after they have dedifferentiated. Combined, my findings suggest that zebrafish cells are more promiscuous in terms of tolerance to high levels of mitogenic activity, thus permitting the cellular processes required for epimorphic regeneration. It follows that regenerating cells in organisms that have an *ARF* gene would need to prevent ARF activation or would be inherently more restricted in these activities.

I found that ARF recapitulates its core mammalian mechanistic functions in zebrafish cells and tissues. As in mammals, when ARF is overexpressed in zebrafish cells, it associates

with Mdm2, stabilizes Tp53, and induces cell cycle arrest or apoptosis. This functional conservation over an evolutionary distance demonstrates that cross-species genetic variations can be experimentally examined in the study of regeneration. When ARF expression is driven by its endogenous human promoter in zebrafish cells, activation of the p53 axis occurs specifically in the blastema-regeneration scenario. In the developing or adult uninjured state, E2f1 is sequestered and inhibited by Rb1, and *ARF* is inactive. However, during blastema formation and regeneration, Rb1 hyperphosphorylation is associated with sufficient free E2f1 to activate *ARF*, which inhibits fin regeneration via a Tp53-dependent mechanism (Figure 8). My findings and model are in agreement with the recent proposal that in salamanders the absence of ARF permits downregulation of Tp53 during blastema formation (Yun et al., 2013). The responsiveness of *ARF* to the Rb pathway proliferative signaling characteristic of zebrafish fin regeneration implies that similar mitogenic signaling occurring in a mammalian context would be detected as aberrant, activate ARF-MDM2-TP53 tumor suppressor mechanisms, and oppose regeneration. My findings are compatible with previous mouse studies showing that ARF is a potent tumor suppressor that is dispensable for normal development (Serrano et al., 1996, Kamijo et al., 1997). Although the majority of tumor suppressors probably function in regeneration as they do in normal development, the findings of the present study indicate that *ARF* represents an unusual departure from that paradigm in that the properties that cause it to respond specifically to tumorigenesis also cause it to distinguish regeneration contexts from developmental ones.

I also found that ARF recapitulates its core mammalian mechanistic functions in the context of tumorigenesis. Using a zebrafish model of hepatocellular carcinoma (HCC) that specifically expresses constitutively active β-catenin in the liver (Evason et al., 2015), I discovered that *ARF* not only detected oncogenic signaling, but also responded to it to prevent

histological anomalies and reduce tumor burden. While ARF did not prevent all signs of disease, it was effective in an objectively severe model of HCC (Evason et al., 2015). This line of experimentation confirms that while ARF may serve as a regeneration suppressor in the context of zebrafish fin regeneration, its function as a tumor suppressor is conserved.

I show here how examination of zebrafish that are humanized with respect to candidate regeneration modifiers is informative for understanding disparate regenerative capacities. Such an approach should prove useful for examining other candidate genes and pathways of interest. My findings with respect to ARF strongly suggest that it is a barrier to mammalian epimorphic regeneration because it interprets the regeneration context as similar to tumorigenesis. It follows conceptually that approaches to induce epimorphic regeneration clinically would need to disrupt ARF-MDM2-TP53 axis activation.

Chapter 2. *Arf* null mice do not have superior regenerative abilities

Introduction

While mammals cannot regenerate their limbs like teleost fish and urodele amphibians, there are some examples of mammalian regenerative responses to injury. Mammalian digit tips are capable of some degree of regeneration upon injury or amputation as demonstrated by case reports in children (Rosenthal et al., 1979, Vidal and Dickson, 1993) and studies in neonatal and adult mice (Borgens, 1982, Muller et al., 1999). It has been postulated that this regenerative response is an example of epimorphic regeneration in that a blastema forms and subsequently gives rise to the regenerate (Muneoka et al., 2008, Fernando et al., 2011, Rinkevich et al., 2011). The regenerative response is characterized by bony regrowth rather than the simple soft tissue repair that occurs during wound healing (Muller et al., 1999). While epimorphic regenerative responses are thought to recapitulate developmental processes, bony regrowth of the distal phalanx in mouse digit tip regeneration occurs via direct intramembranous ossification rather than endochondral ossification that occurs during development (Muller et al., 1999, Neufeld and Zhao, 1993, Neufeld and Zhao, 1995). The only vital solid organ known to regenerate in mammals is the liver, which can regenerate its full mass after removal of up to 70% of the organ (Taub, 2004). While liver regeneration is extremely fascinating, the mechanism underlying this regenerative response is one of tissue regeneration instead of epimorphic regeneration.

Regeneration of mouse digit tips is similar to reported human digit tip regeneration, which makes the mouse a good model system to use for digit regeneration studies (Han et al., 2008). The mouse model of digit tip has also become a popular mammalian model of regeneration in recent years (Agrawal et al., 2010, Rinkevich et al., 2011, Fernando et al., 2011). While regeneration of the digit is extremely limited, adult mice can variably regenerate distal-

most amputations near the nail bed over the course of about 70 days via a process that results in regeneration of skin, nerve, bone and nail. Amputations made proximal to the nail bed or proximal to the interphalangeal joint do not regenerate in adult mice. The mouse homolog of ARF, $p19^{Arf}$ (Arf), is also a negative cell cycle regulator that connects the Rb and p53 pathways, and it may be involved in the observed lack of regeneration of digits injured proximal to the nail bed in mice because it can disrupt regenerative processes.

To determine the effects of *Arf* on mouse digit tip regeneration, I used a mouse model that is genetically deficient for *Arf* (Zindy et al., 2003) or the entire *Cdnk2a* locus (Serrano et al., 1996). Since *Arf* is a mammalian gene that can disrupt regenerative processes as observed in my zebrafish models, I hypothesized that the genetic elimination of *Arf* or *Cdkn2a* would enable regeneration in contexts where it would not normally occur such as proximal digit amputations.

Methods and Materials

Mouse Model

Juvenile (2 weeks old), young adult (2-3 months old), and adult (6-7 months old) *Arf*+/+ (WT) and *Arf*-/- (KO) mice (Zindy et al., 2003) were used for digit tip regeneration studies. Digit tip regeneration experiments were also performed on adult (2-7 months old) *Cdkn2a*+/+ (WT) and *Cdkn2a*-/- (KO) mice (Serrano et al., 1996). All experiments were approved by the IACUC of UCSF.

Digit Tip Regeneration

Digit amputations were performed under isoflurane anesthesia using a scalpel at pre-determined points either distal to the distal interphalangeal joint or proximal to the interphalangeal joint. Both forelimbs and hindlimbs were used, and a maximum of three digits were amputated per limb. Non-amputated digits were used as internal controls. Three amputation planes were analyzed (Figure #A). When the amputations were performed, pressure was applied for 40 seconds to control bleeding and then the animal was woken from anesthesia. Animals were monitored continuously for 6 hours after surgery. During the initial recovery period, the animals were kept in a warm environment (heat lamp). Animals were monitored twice daily for first 3 days post-surgery and then daily until euthanasia. Juvenile mouse digit tips were examined and imaged daily post-surgery for 21 consecutive days up to a total of 30 days.

Histological Analysis

Hematoxylin and eosin (H&E) staining of sagittal paraffin sections was performed as follows. Xylene 5 minutes 2X, 100% EtOH 5 minutes 2X, 95% EtOH 5 minutes, 80% EtOH 5 minutes,

rinsed with tap H_2O 3-4X, 3x Gills Hematoxylin 4 minutes, rinsed with tap H_2O 3-4X, Scotts H_2O 3 minutes, rinsed with tap H_2O 3-4X, Eosin 2 minutes, rinsed with tap H_2O 3-4X, 80% EtOH 1 minute, 95% EtOH 2 minutes 2X, 100% EtOH 3 minutes 2X, Xylene 2 minutes 2X, mounted with Permount.

Masson's trichrome staining of sagittal paraffin section was performed as follows. Hydrated with tap H_2O, Bouin's Fixative overnight, rinsed with tap H_2O, Weigert's Iron Hematoxylin 5 minutes, rinsed with H_2O, Bieberich Scarlet 15 minutes, rinsed with ddH_2O 3X, Phosphot ungstic/Phosphomolybdic Acid Solution 10-15 minutes, Aniline Blue 5-10 minutes, rinsed with ddH_2O 3X, 1% acetic acid 3-5 minutes, 80% EtOH 2 minutes, 95% EtOH 2 minutes 2X, 100% EtOH 3 minutes 2X, Xylene 3 minutes 2X, mounted with Permount.

Gross Morphological Analysis

Regeneration of digits was progressively graded from 0 to 3 compared to non-amputated internal controls. A score of 0 signified that no regeneration had occurred. A score of 1 signified that only slight regeneration had occurred. A score of 2 signified that incomplete regeneration had occurred. Finally, a score of 3 signified that regeneration had completed in full.

Micro-Computed Tomography (CT)

Bone imaging was performed on isolated mouse digits with micro-CT scans at various time points following standard operating procedures outlined by the UCSF Bioengineering & Biomaterials Micro-CT and Imaging Facility.

Results

In adult mice, amputations were consistently performed at three amputation planes. Of the planes considered, two were distal to the distal interphalangeal joint, one distal (Figure 9A, plane 1) and the other proximal (Figure 9A, plane 2) to the nail bed. The third amputation plane was proximal to the distal interphalangeal joint (Figure 9A, plane 3). Regeneration was analyzed at 5, 10, 20, 30, and 60 days post amputation (dpa) by histological and gross morphological analysis. Histological analysis consisted of H&E or Masson's trichrome stained sagittal sections of paraffin embed digits (Figure 9B, right). At 30 dpa, WT and KO mice had equally fully regenerated amputations distal to the nail bed, distal to the distal interphalangeal joint with average regeneration scores of 3.0 ± 0.0 and 2.7 ± 0.7, respectively ($N=21$ digits per genotype, $p>0.05$) (Table 1). KO mice did not seem to regenerate distal amputations more quickly than WT mice. However, neither genotype was able to fully regenerate amputations proximal to the nail bed, distal to the distal interphalangeal joint or proximal to the distal interphalangeal joint by 60 dpa. No statistically significant difference was observed at any amputation plane. Histological analysis of amputated and non-amputated digits of WT and KO mice at multiple time points along the three amputation planes provided little insight as no gross difference in digit tip regeneration between WT and KO mice could be observed. When digits were analyzed with micro-CT scans, minimal bony deposition was observed at 20 dpa in both WT and KO digits at the distal and proximal amputation planes distal to the distal interphalangeal joint (Figure 9B, left). However, callous formation seemed to be more pronounced in KO digits amputated proximal to the nail bed, distal to the distal interphalangeal join than WT digits amputated at the same plane. A total of 2 WT and 2 KO digits, one amputated distal to the nail bed and one amputated proximal to the nail bed per

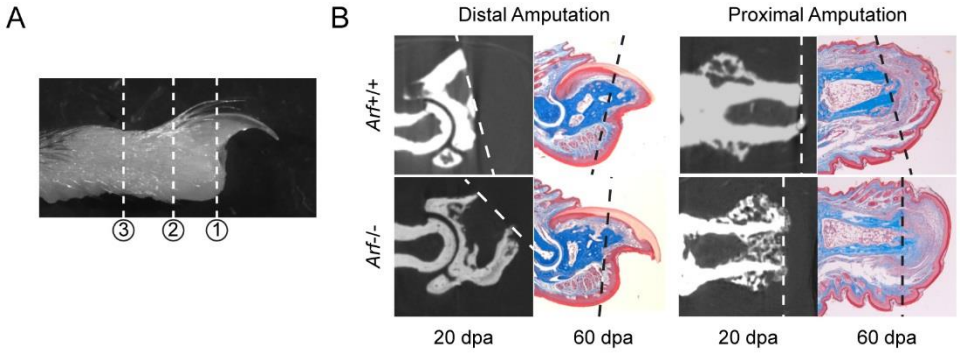

Figure 9. Regardless of *Arf* genetic dosage, distal, but not proximal, digit amputations regenerate in adult mice. (A) Schematic of digit amputation planes used in adult and juvenile digit regeneration experiments. Amputation plane 1 represents a plane distal to the nail bed, distal to the distal interphalangeal joint. Amputation plane 2 represents a plane proximal to the nail bed, distal to the distal interphalangeal joint. Amputation plane 3 represents a plane proximal to the distal interphalangeal joint. (B) Regeneration of *Arf*+/+ (WT) and *Arf*-/- (KO) digits amputated at amputation planes 1 (distal) and 2 (proximal). Sagittal micro computed tomography (CT) scans were performed on digit at 20 dpa (left). Sagittal Masson's trichrome stained sections of digits at 60 dpa (right). Dashed lines represent amputation planes.

genotype, were analyzed with micro-CT scans, thus the callous observation is not supported by a sufficient number of replicates to determine if it is a true observation or one observed by chance.

Table 1. Quantification of adult digit tip regeneration at 30 dpa.

Adult digit tip regeneration (30 dpa)	Amputation Plane	None	Slight	Incomplete	Complete
Arf+/+ (WT)	1	0	0	0	21
	2	0	3	0	0
	3	1	0	0	0
Arf-/- (KO)	1	0	2	1	18
	2	0	3	0	0
	3	0	1	0	0

Similar experiments were performed on juvenile mice beginning at 2 weeks of age. Gross morphological analysis of digit regeneration yielded similar results to those of adult mice; by 30 dpa, amputations distal to the nail bed, distal to the distal interphalangeal joint regenerated, but amputations proximal to the nail bed, distal to the distal interphalangeal joint and amputations proximal to the distal interphalangeal joint did not regenerate regardless of genotype (Table 2).

Table 2. Quantification of juvenile digit tip regeneration at 30 dpa.

Juvenile digit tip regeneration (30 dpa)	Amputation Plane	None	Slight	Incomplete	Complete
Arf+/+ (WT)	1	0	0	0	7
	2	0	7	0	0
	3	3	3	1	0
Arf-/- (KO)	1	0	0	0	3
	2	0	3	0	0
	3	1	2	0	0

Digit tip regeneration experiments were also performed on mice harboring a mutated *Cdkn2a* locus (Serrano et al., 1996), the locus from which p16Ink4a and Arf are expressed. Since no overt phenotype was observed with *Arf*-/- mice, it was hypothesized that disruption of the

entire locus may lead to a more pronounced phenotype. However, digit tip regeneration in *Cdkn2a*-/- mice progressed similarly to that in *Arf*-/- mice; complete regeneration was only observed at the amputation plane distal to the nail bed, distal to the distal interphalangeal joint in both juvenile and adult mice (Table 3).

Table 3. Quantification of digit tip regeneration in juvenile and adult *Cdkn2a* mice at 30 dpa.

Digit tip regeneration (30 dpa)	Amputation Plane	None	Slight	Incomplete	Complete
Cdkn2a+/+ (WT)	1	0	0	2	10
	2	0	4	0	0
	3	0	3	1	0
Cdkn2a-/- (KO)	1	0	0	0	13
	2	0	5	0	0
	3	4	1	0	0

Discussion

The critical limit for successful regeneration after digit tip amputation seems to lie distal to the nail bed, distal to the distal interphalangeal joint. The location of this critical limit is most likely due to stem cells in the nail bed matrix (Takeo et al., 2013, Rinkevich et al., 2011, Zhao and Neufeld, 1995). These epithelial stem cells require Wnt activation, which also assists in the attraction of nerves to promote mesenchymal blastema formation and growth leading to the regeneration of the digit tip (Takeo et al., 2013). If the activation of the nail bed stem cell pool is the predominant driving force behind digit tip regeneration, then my observations of regenerative failure proximal to this pool are in agreement with and lend credence to the literature. Most epithelial stem cells expresses Bmi1, a member of the Polycomb Repressive Complex (Pietersen et al., 2008, Tanaka et al., 2013, Tian et al., 2011), so it would not be very surprising if nail bed stem cells express Bmi1 as well. Bmi1 is a known negative regulator of the *Cdkn2a* locus (Molofsky et al., 2005), so it is possible that the lack of *Arf* or *Cdkn2a* in my experiments would not promote regeneration in a context in which it is normally transcriptionally repressed i.e. the nail bed.

Amputations made proximal to the nail bed seem to default to a wounding healing response rather than a regenerative one. It is possible that Wnt signaling and subsequent nerve attraction influence the fate of cells responding to the injury as well as the surrounding mesenchyme. It has recently been identified that macrophages are essential for limb regeneration in salamanders (Godwin et al., 2013) and fin regeneration in zebrafish (Petrie et al., 2014). Ablation of macrophages caused dysregulation of blastema markers, stunted activation of MMP9 and MMP3, and a lack of matrix remodeling (Godwin et al., 2013), which is necessary for successful limb regeneration (Vinarsky et al., 2005). Macrophage matrix metalloprotease genes

are implicated with successful limb regeneration, and their expression is sensitive to denervation (Yang et al., 1999). If nerves are recruited by Wnt signaling or the paracrine factor(s) secreted from Wnt-activated cells in the nail bed (Takeo et al., 2013), then that could explain why a presumed blastema forms there and not at locations proximal to the nail bed. Nerves are essential for regeneration and their recruitment seems to be an initiator of blastema formation (Mullen et al., 1996); the exact mechanism responsible for nerve-dependent promotion of blastema formation remains an open and actively investigated issue in regeneration biology.

With regards to blastema formation and the mesenchyme that contributes to it, there has been a fair amount of debate whether or not the cell mass that gives rise to the mammalian digit tip regenerate is analogous to blastemas observed during urodele amphibian and teleost fish regeneration and can be called a true blastema. Blastema formation in urodele amphibians and teleost fish involves the process of dedifferentiation (Han et al., 2005), which is the term ascribed to mature, post-mitotic cells at the site of injury reverting to a more proliferative, but still fate-restricted, state. Since digit tip regeneration proceeds from stem or progenitor cells in the nail bed instead of dedifferentiation, many groups consider mammal regeneration to be devoid of a true blastema (Muneoka et al., 2008, Agrawal et al., 2010, Brockes and Kumar, 2005, Rinkevich et al., 2011, Reginelli et al., 1995). Other groups disagree and consider the mass of proliferative cells at the digit tip a blastema regardless of cellular origin (Fernando et al., 2011, Han et al., 2008).

It is likely that proximal amputations default to a wound healing response because the lack of signaling essential for nerve recruitment and matrix remodeling renders the injury site non-permissive for a blastema-like structure to form regardless of *Arf* or *Cdkn2a* dosage. Lack of *Arf* or *Cdkn2a* may expedite proliferative events, but regeneration requires more than

proliferation to be successful. The first step to successful regeneration is the assembly of a permissive niche. Since this presumably does not occur at proximal amputation sites, cells that would contribute to the regenerate are not activated nor aggregated. The lack of *Arf* or *Cdkn2a* does not promote regeneration in contexts where it does not normally occur because the proliferative advantage of *Arf* or *Cdkn2a* loss is never realized; a blastema-like structure is never formed at proximal amputation planes.

Additionally, lack of key regulators of the differentiated state such as *Arf* or *Cdkn2a* could conceivably be detrimental to regeneration. Regeneration requires a permissive or inductive niche, proliferative ability, and tight developmental regulation in order to reproduce near identical copies of lost structures. This tight regulation is essential for cellular differentiation at the end of successful regeneration, and it would most likely be disrupted in the context of *Arf* or *Cdkn2a* loss.

While out of the scope of this work, an interesting and relatively unexplored area of regeneration regards the mechanisms by which mammals can regenerate the liver in the presence of *Arf*. In keeping with my hypothesis that *Arf* plays a large role in regenerative success, I hypothesize that *Arf* is somehow being inhibited during liver regeneration or that the blastema signaling that activates *Arf* is somehow different from the liver regeneration *milieu*. Several groups have reported that hepatocyte proliferation drives liver regeneration (Michalopoulos, 2007, Mitchell and Willenbring, 2008) and that microRNAs control hepatocyte proliferation (Song et al., 2010). It has also been reported that *Arf* is targeted and inhibited by a number of microRNAs (Mudhasani et al., 2008) including miR-24 (To et al., 2012) and miR-125b (Amir et al., 2013). However, microRNAs can also support the differentiation-promoting activities of *Arf* depending on cellular contexts including miR-34a (Iqbal et al., 2014) and even miR-125b (Liang

et al., 2010). Long non-coding RNAs could also play a role in *Arf* inhibition, particularly the long non-coding RNA ANRIL, which is a product of the INK4 locus (Pasmant et al., 2011, Wan et al., 2013). ANRIL has been shown to directly bind the *CDKN2B* transcript and is capable of recruiting the Polycomb Repressor Complex (PRC) to inhibit expression from the INK4 locus (Kotake et al., 2011, Yap et al., 2010).

With all of this in mind, it seems likely that *Arf* and other Ink4 products could be inhibited during liver regeneration. Future experiments, could make use of the *Arf*-GFP knock-in mouse model (Zindy et al., 2003) to investigate if *Arf* is activated during liver regeneration. ChIP experiments could also be performed to investigate E2f binding of the *Arf* promoter during liver regeneration. If *Arf*-GFP is observed, then that would suggest that Arf is being regulated at a post-transcriptional or post-translational level, which may necessitate investigating potential inhibitors of Arf such as microRNAs, long non-coding RNAs, and PRC components including Bmi1.

In the next chapter, I examine another key regulator of the differentiated state and what happens when it is disrupted.

Chapter 3. The role of the Rb pathway during zebrafish fin regeneration

Introduction

Urodele amphibians and teleost fish are unique among vertebrates in that they possess the innate ability to regenerate lost structures such as limbs and fins. This regeneration, termed epimorphic regeneration (Morgan, 1901), occurs in the axolotl and zebrafish through several defined steps. First, epithelial cells migrate to close the wound and form the wound epithelium. Mesenchymal cells subjacent to the wound epithelium then dedifferentiate to form the blastema. The wound epithelium subsequently matures into an apical epithelium cap, and through proposed epithelial-mesenchymal interactions, the blastema elongates and is patterned into a functional copy of the lost tissue (Tsonis, 1996, Brockes and Kumar, 2002, Nacu and Tanaka, 2011, Poss et al., 2003). The cellular source of blastema cells is being actively investigated; both undifferentiated cells arising by dedifferentiation and stem cell populations likely contribute to the blastema (Stocum and Cameron, 2011, Hyun et al., 2012).

The cellular process of dedifferentiation is still controversial in the field of regeneration biology even though the term was originally introduced in 1902 by Driesch (Tsonis, 1996). The controversy stems from limitations of early studies that provided descriptive evidence of the existence of the process along with clear evidence for stem cell populations driving many regenerative processes. However, multiple investigators have recently documented that cellular dedifferentiation is an important natural process in regenerating tissues in zebrafish (Kikuchi et al., 2010, Jopling et al., 2010, Knopf et al., 2011, Singh et al., 2012, Stewart and Stankunas, 2012, Sousa et al., 2011). I define dedifferentiation as the process by which a cell loses its differentiated state to adopt a more proliferative, progenitor-like one. Cellular dedifferentiation is exemplified by osteoblasts in the zebrafish caudal fin; it has been observed that mature

osteoblasts lose their differentiated characteristics and adopt qualities of less differentiated cells during the early stages of regeneration (Knopf et al., 2011). Osteoblast differentiation is well described, and promoters for genes such as *runx2*, *sp7* (*osterix*), and *bglap* (*osteocalcin*) have been used to specifically identify preosteoblasts and intermediate and mature osteoblasts, respectively (Knopf et al., 2011). *Runx2* promotes the differentiation of mesenchymal stem cells into preosteoblasts, and reporters driven by these promoters have aided in assessing the differentiation state of osteoblasts during epimorphic regeneration (Komori, 2006).

Cell cycle regulators are intimately tied to the terminally differentiated state of mesodermal cell types (Jacks et al., 1992). The retinoblastoma gene *Rb1* is critical for the control of cell cycle entry, and in cancer, the Rb pathway is generally compromised (Meuwissen et al., 2003). During the normal cell cycle, the inactivation of Rb1 through phosphorylation by cyclin-dependent kinases leads to the release of E2F transcription factors, which promote entry into S-phase. Interestingly, if Rb1 is inactivated in urodele muscle cells, the terminally differentiated state is lost (Tanaka et al., 1997). However, in mammals, which possess the *Cdnk2a* locus, the terminally differentiated state is maintained as a result of upregulation of Arf (Pajcini et al., 2010). Arf acts as a fail-safe for aberrant Rb pathway inhibition in mammals, so it can be predicted that the cells of urodele amphibians and teleost fish, which lack an orthologue of Arf, are more plastic than their mammalian counterparts. Differences in cell plasticity with regard to differentiation states could play a large role in the differences observed in regenerative ability of vertebrate species. In this chapter I will discuss experiments designed to investigate the role of Rb1 in control of the terminally differentiated state and the induction of dedifferentiation through modulation of the Rb pathway.

Materials and Methods

Morpholino Oligomer (MO) Design and Injections

The following Morpholino oligomers (Gene Tools, LLC, Philomath, OR) were used to knockdown zebrafish *rb1*. Both Morpholino oligomers were designed to interact with the 5' untranslated region (UTR) of zebrafish *rb1* at different and non-overlapping areas to prevent ribosome processing of the bound mRNA, and both Morpholino oligomers were manufactured with a 3'fluorescein tag to aid in visual assessment as well as electroporation of the Morpholino oligomer into zebrafish tissue.

Gene	RefSeq ID	Morpholino Oligomer Name	Morpholino Oligomer Sequence
rb1	NM_001077780.1	Rb1 ATG MO1	5'-CGT TCA CTC TCA GCA CAG CGA GCG A-3'
rb1	NM_001077780.1	Rb1 ATG MO2	5'- TCA CGA GTT GTG TTG TGA TGT TTC T-3'

Morpholino oligomers were injected into 2 dpa blastemas and electroporated as previously described (Hyde et al., 2012). Briefly, fluorescent Morpholino oligomers were reconstituted for 5 minutes at 65°C, loaded into a microinjection needle, and approximately 75 nL was delivered into each fin ray blastema on the dorsal lobe of the caudal fin. The two lobes were then individually electroporated using a square wave producing electroporator with each of 10 pulses being 15V in amplitude and 50 milliseconds in length with 1 second in between pulses.

For embryo injections, 2 nL of MO was injected into either the cytoplasm or yolk sac at the single cell stage. For coinjections, 2 nL of MO and mRNA was injected into either the cytoplasm or yolk sac at the single cell stage.

A 3'fluorescein tagged standard control MO (5'-CCT CTT ACC TCA GTT ACA ATT TAT A-3') was used to control for non-specific Morpholino oligomer effects, and the non-injected ventral lobe of the caudal fin was used to control for non-specific electroporation effects. To

control for non-specific effects of Rb1 ATG MO1 and Rb1 ATG MO2, RNA of zebrafish *rb1* lacking the 5'UTR was coinjected. This construct was created by cloning zebrafish rb1 using the following primers to remove the 5'UTR: 5'- TTA CTA CAA TTG ATG CCG CCG AAG AAG CGC AG-3' and 5'-CCT CCT CGA GTT CAA ACA TGT CAG TTG TTA-3'. These primers added an MfeI site and an XhoI site (underlined) to the 5' and 3' ends of zebrafish *rb1*, respectively. The PCR product was then cut with MfeI and XhoI and subcloned into a multiple cloning site. *In vitro* transcription of RNA was performed using the mMESSAGE mMACHINE SP6 and T7 transcription kits (Life Technologies) according to the manufacturer's instructions.

Transgene Design and Transgenic Zebrafish

Tol2-mediated transgenesis was used to generate transgenic animals (Kwan et al., 2007). Transgenic animals were detected based on their GFP-positive hearts, due to the transgenes containing a *cmlc2*:GFP cassette.

An Rb1 overexpression transgene, Tg(*hsp70l*:Rb1), was created by subcloning the cDNA of zebrafish Rb1 downstream of the promoter sequence of zebrafish *hsp70l* (Halloran et al., 2000). The following primers were used to clone the cDNA zebrafish Rb1 and add attB1 and attB2 sites (underlined) to the 5' and 3' ends of the sequence, respectively, in order to subclone the fragment into a Gateway cloning (Life Technologies) entry vector: 5'-GGG GAC AAG TTT GTA CAA AAA AGC AGG CTC GGA GAG TTG CGG ACG CAA AC-3' and 5'-GGG GAC CAC TTT GTA CAA GAA AGC TGG GTT CA AAC ATG TCA GTT GTT AA-3'.

A mature bone cell specific CreER expression transgene, Tg(*bglap*:CreER^{T2}), was created by subcloning the CreER^{T2} cassette downstream of the promoter sequence of zebrafish *bglap* (Singh et al., 2012). The following primers were used to clone the CreER^{T2} cassette. 5'-CGA ATT CAT

GTC CAA TTT ACT GAC C-3' and 5'-TGA GCT CTC AAG CTG TGG CAG GGA A-3'. The following primers were used to clone the promoter sequences of zebrafish *bglap*. 5'-CGA CTC ACT ATA GGG CGA ATT G-3' and 5'-GGC TAA CAG GTT CAA AGC AAA G-3'. The promoter sequences were then subcloned into a multiple cloning site modified to include an MfeI restriction site.

The creation of an osteoblast differentiation reporter zebrafish line was attempted by crossing Tg(*runx2*:EGFP) (Knopf et al., 2011) fish with Tg(*bactin2*:loxP-STOP-loxP-DsRed-express)^{sd5} (Bertrand et al., 2010) fish and then finally crossing the progeny of that cross with Tg(*bglap*:CreER^{T2}) fish. In this way, mature osteoblasts would be permanently DsRed-positive and immature osteoblasts would be transiently EGFP-positive. Mature osteoblasts would be marked before injury with 4-hydroxytamoxifen (Sigma) to stimulate CreER-mediated recombination in mature osteoblasts. Dedifferentiated cells would be identified as those that were both DsRed-positive and EGFP-positive.

Tg(runx2:EGFP) fish were genotyped by examining them under a fluorescent stereoscope between at 48 hpf. Tg(*bactin2*:loxP-STOP-loxP-DsRed-express)^{sd5} were genotyped using the following primers: 5'-TGA ATG TCG AAA TCT GTT CC-3' and 5'-ACC AAA TTA AGG GCC AGC TC-3'. The positive PCR product was approximately 600 bp in length.

Rb1 Gene Trap Design and Mutation Analysis

To create a genetic model of *rb1* loss, I attempted to place a silent gene trap into the first intron on zebrafish *rb1*. The strategy was to use attP and attB recombination chemistry to irreversibly incorporate a gene trap in the form of a strong splice acceptor followed by a fluorescent marker and a STOP cassette. To make the gene trap silent, it was inverted and placed between two

mutated loxP sites facing each other. This orientation of the loxP sites would cause the intermediate DNA to invert, and the use of mutated loxP sites would place a strong preference on the DNA inverting only once, thus disrupting zebrafish *rb1* and marking the recombined cell with a fluorescent reporter. The first step was to incorporate an attP site into intron 1 of zebrafish *rb1*. This first step was necessary because only short sequences could be added. The attP site served as a landing site for the rest of the gene trap, which was too large to incorporate in a single step. The gene trap vector was designed to have an attB site so that it could recombine with the attP site in the intron. First, the sequence between exons 1 and 2 of zebrafish *rb1* was cloned using the following primers: 5'-CAC CGA CTA CCA ACC ACT AAC-3' and 5'-CTC CTC GCT GAG AAA CAC AA-3'. This allowed us to accurately design single/short guide RNAs (sgRNAs) to use the CRISPR/Cas9 system (Hwang et al., 2013) to target intron 1 of *rb1*. Four targets were tested, sgRNA1 (5'- GGC AAA GAA TGT TAA AAT AC-3'), sgRNA2 (5'-GGA GAA TTC CGG CAA AAA TG-3'), sgRNA3 (5'-GGG ACA GAA GAG TAA AAT AT-3'), and sgRNA4 (5'-GGG AGA ATT CCG GCA AAA AT-3'). Each sgRNA target was cloned immediately upstream of a T7 promoter and transcribed *in vitro* using a MAXIscript T7 kit (Life Technologies) according to manufacturer's instructions. Cas9 mRNA was transcribed *in vitro* using a mMESSAGE mMACHINE T7 transcription kit (Life Technologies) according to the manufacturer's instructions. Both Cas9 mRNA and sgRNA were injected into single cell embryos. The most efficient was sgRNA3 as determined by T7 Endonuclease I assay performed as described below. Next, single-stranded DNA oligos were tested for recombination efficiency. Homology arms of 5, 10, or 20 base pairs were tested, and oligos with 10 base pair long homology arms seemed to work best. An attP site was introduced into intron 1 of zebrafish *rb1* by coinjecting Cas9 mRNA, sgRNA3, and an oligo of attP (underlined) flanked by homology

arms of 10 base pairs (5'-AAG AGT AAA ACC CCA ACT GAG AGA ACT CAA AGG TTA CCC CAG TTG GGG TAT GGG AGA A-3'). With attP in the first intron of zebrafish *rb1*, I set out to create the attB gene trap vector. Using gBlocks Gene Fragments (Integrated DNA Technologies, Coralville, IA) and pBAD-mTagBFP2 (Addgene, Cambridge, MA) as a backbone, I constructed the attB gene trap vector, which contained an FRT site (+), attB (+), lox66 (+), a STOP cassette (-), mTagBFP2 (-), a splice acceptor (-), lox71 (-), and finally another FRT site (+). (+) designates that the DNA reads 5' to 3' on the positive strand and (-) designates that the DNA reads 5' to 3' on the negative strand. FRT sites were included to remove extraneous plasmid DNA after the attP and attB sites recombined.

However, before incorporating the gene trap, I needed to assess the mutation state of the attP-containing zebrafish because the CRISPR/Cas9 system has been known to cause off-target (OT) mutations (Yang et al., 2013). When the sgRNA3 sequence was BLAST (NCBI) searched against the zebrafish genome with a tolerance of up to 3 or 4 base pair mismatches, 10 regions of varying similarity to sgRNA3 were detected. These regions were then tested for mutations with T7 Endonuclease I assays as described below. Zebrafish with attP but without mutations at the 10 regions were used for the second step of creating the Rb1 gene trap line, incorporating the attB gene trap. First, FLPe mRNA was transcribed *in vitro* from pCSFLPe (Addgene) using a mMESSAGE mMACHINE SP6 transcription kit (Life Technologies) according to the manufacturer's instructions. Then, 2 nL of 25 ng/μL attB gene trap vector, 35 ng/μL FLPe mRNA, 1X BP Clonase (Life Technologies), and 1X Phenol Red was injected into individual single cell embryos of a *rb1* attP outcross. BP Clonase (Life Technologies) contains an integrase that catalyzes the recombination of attP and attB. Fish were raised and genotyped using the

following primers for mTagBFP2: 5’-CGT GGA CAA CCA TCA CTT CA-3’ and 5’-CCA GGC ATC TTG AGG TTC TTA G-3’.

T7 Endonuclease I Assay

This assay was performed to determine the presence of mutations after DNA was cut *in vivo* using the CRISPR/Cas 9 system (Hwang et al., 2013). T7 endonuclease I cuts DNA when mismatched base pairs are detected. To assay for mismatches, DNA strands are dissociated and then rehybridized. Genomic DNA was generated by incubating individual 24 hpf embryos in 0.1 mg/mL proteinase K in 50 μL DirectPCR Lysis Reagent (Viagen Biotech, Los Angeles, CA) overnight 60°C. Lysates were then incubated for 10 minutes 95°C to inactivate the proteinase K. Genomic regions of interest (see table below) were then amplified using 2 μL of lysate and Phusion high-fidelity PCR kit (New England Biolabs, Ipswich, MA) with high-fidelity buffer according to the manufacturer’s instructions. PCR products were purified using a QIAquick PCR purification kit (Qiagen). Then 200 ng of purified PCR product, 2 μL NEBuffer 2, and water were combined to the total volume of 19 μL. Hybridization was then performed as follows: 5 minutes 95°C, 95°C to 85°C at -2°C/s, 85°C to 25°C at -0.1°C/s, hold at 4°C. 1 μL of T7 endonuclease I is then added to the mixture and incubated for 15 minutes 37°C. 2 μL 0.25M EDTA is added to stop the reaction, which is then run on an agarose gel containing a DNA dye for analysis. The presence of DNA products less than the expected length are considered evidence of a mutation in that region. Uninjected embryos were used as controls for polymorphisms in each amplified region of interest.

T7 Endonuclease I Assay Primers

Target	Product	Forward Primer	Reverse Primer
sgRNA1	687 bp	5’-GTG CAT CAA TCA TTG GCC TTC-3’	5’-TGT ATT GCT TGC GTT TGT TCA T-3’
sgRNA2	687 bp	5’-GTG CAT CAA TCA TTG GCC TTC-3’	5’-TGT ATT GCT TGC GTT TGT TCA T-3’
sgRNA3	415 bp	5’-CTC TCA TTT ATG GAT ATG CCA GAT GTA-3’	5’-GTG CCG CAT TCC CTG ATT-3’
sgRNA4	415 bp	5’-CTC TCA TTT ATG GAT ATG CCA GAT GTA-3’	5’-GTG CCG CAT TCC CTG ATT-3’
OT1	185 bp	5’-GCT CGG CTG TTC AAA GAA AA-3’	5’-AAG CAT CAT AAA GGG CAT GG-3’
OT2	931 bp	5’-TGT TGT AAT GGC CTA ACC TAC C-3’	5’-ACA AAG GGA GAG CAC AGA AC-3’
OT3	506 bp	5’-AGT GAA AGG CGA CAA TCA GC-3’	5’-GCC ATT TCA TGC CAC TCT TT-3’
OT4	221 bp	5’-TCC TGT CTC GTC GTT TTT CC-3’	5’-GAT GGT TGA CGC ACA GCT AA-3’
OT5	467 bp	5’-TTC TCC CGG CTA AAC ACA TAT C-3’	5’-TCT GTT CAC TTC ACT CCC ATT T-3’
OT6	310 bp	5’-CGA CGG CAC CTG TAA TCA A-3’	5’-TCC CTT CCT GCT CTT CAG ATA-3’
OT7	340 bp	5’-CCC CCA CTT TAG CTC CTC TT-3’	5’-GTT CCC TCG CAA AAC CAT T-3’
OT8	323 bp	5’-CCT GGT GGT TTG ACG ATA CA-3’	5’-AAG GGA CTA AGC TGA CAA GAA A-3’
OT9	341 bp	5’-CCA AAG TGG CTC CGT TAC ATA-3’	5’-GTC CAT CCT CAT AGT GAA CAT ACC-3’
OT10	247 bp	5’-CCA CAG AAC AGA CTC GCA TTT A-3’	5’-CAG AGA CAG GAG CGA CAT AGA-3’

Fin Regeneration

Caudal fin amputations were performed with a razor blade on fish anesthetized with 0.016% tricaine in aquarium water; consistently only the distal halves of fins were amputated. Heat shocks were delivered by housing fish in a water bath set to 37°C with bidiurnal water exchanges. The water bath achieved 37°C within 15 minutes, maintained that temperature for 1 hour, and then passively cooled to fish room temperature (26-28°C). An automatic digital timer (Intermatic) was used to turn on and off the water bath. For heat shock experiments, an initial

heat shock was delivered and then fins were amputated 3 hours later. Heat shocks were subsequently delivered every 6 hours for the duration of the experiment. For Morpholino oligomer injected fins, regenerates were visually assessed under a fluorescent stereoscope at 0 days post transfection (dpt) (2 dpa), 1 dpt (3 dpa), and 2 dpt (4 dpa). Quantification of fin regenerate length and area was performed in ImageJ.

Drug Treatments

Adult zebrafish were treated with 5 μM 4-hydroxytamoxifen (4OHT, Sigma) in EtOH (1 mM stock). Water was exchanged daily.

For EdU pulse-chase experiments, 5 μL of 5 mg/mL of EdU (Life Technologies, Carlsbad, CA) in saline was injected intraperitoneally into anesthetized fish 30 minutes before tissue harvest.

Histological Analysis

EdU incorporation was detected using the Click-iT EdU imaging kit per the manufacturer's instructions (Life Technologies). Briefly, fin tissue was fixed flat in 4% PFA 1 hour, and then incubated in 80% MeOH, 20% DMSO overnight 4°C. Tissue was rehydrated in 75%, 50%, and finally 25% MeOH in PBS 5 minutes each, permeabilized in acetone 20 minutes -20°C, PBS 5 minutes 2X, 0.5% PBTx 30 minutes, PBS 5 minutes 2X. The Click-iT cocktail was prepared fresh and 50 μL was applied per fin, incubated 30 minutes dark, PBS 5 minutes, 3X, mounted with Vectashield mounting medium with DAPI (Vector Laboratories).

TUNEL detection was performed using the In Situ Cell Death Detection Kit (Roche, Basel, Switzerland) per the manufacturer's instructions. Briefly, fin tissue was fixed flat in 4% PFA 1 hour, and then incubated in 80% MeOH, 20% DMSO overnight 4°C. Tissue was rehydrated in

75%, 50%, and finally 25% MeOH in PBS 5 minutes each, permeabilized in acetone 20 minutes -20°C, PBS 5 minutes 2X, 0.5% PBTx 30 minutes, PBS 5 minutes 2X. The labeling/enzyme mix was prepared fresh and 50 μL was applied per fin, incubated 30 minutes dark and humid, PBS 5 minutes, 3X, mounted with Vectashield mounting medium with DAPI (Vector Laboratories).

Alizarin red staining was performed as follows. Fin tissue was fixed flat in 4% PFA 1 hour, and then incubated in 80% MeOH, 20% DMSO overnight 4°C. Tissue was rehydrated in 75%, 50%, and finally 25% MeOH in PBS 5 minutes each, bleached with 0.8% KOH, 0.6% H_2O_2 30 minutes, ddH2O 5 minutes 2X, stained in a saturated Alizarin red solution in 1% KOH 20 minutes, ddH2O 5 minutes 4X, mounted through a gradual glycerol/PBS series from 25% to 50% to 80% glycerol. Finally, fins were imaged in 80% glycerol.

Images were quantified in ImageJ. The percent of EdU- or TUNEL-positive cells was quantified by first counting the number of positive cells in the regenerate and then dividing that count by the number of nuclei in the field counted. The percentage of bone present in the regenerate was calculated by measuring the length of the longest alizarin red stained bony fin ray in the regenerate and dividing that number by the length of the regenerate.

Reverse Transcriptase Polymerase Chain Reaction (RT-PCR)

RT-PCR was performed using the SuperScript III One-Step RT-PCR System with Platinum Taq (Life Technologies) according to the manufacturer's instructions with the following primers.

Target	Product	Forward Primer	Reverse Primer
Cre	607 bp	5'-GCA AAA CAG GCT CTA GCG TTC G-3'	5'-CTG TTT CAC TAT CCA GGT TAC GG-3'
β-actin	102 bp	5'- CGA GCA GGA GAT GGG AAC C -3'	5'- CAA CGG AAA CGC TCA TTG C -3'

Results

Knockdown of zebrafish *rb1* inhibits fin regeneration

To determine the role of Rb1 in the maintenance of the differentiated state, I designed two Morpholino oligomers (MOs) to target the 5' untranslated region (UTR) of zebrafish *rb1*, Rb1 ATG MO1 (MO1) and Rb1 ATG MO2 (MO2, *rb1* MO). The MOs were tagged with fluorescein tags to aid cellular incorporation of the MO as well as visualization. Since MOs are inherently uncharged, the fluorescein tag adds a charge to the molecule and allows for its electroporation into the cells of the fin.

To confirm *rb1* knockdown, both MOs were tested at multiple concentrations in zebrafish embryos. 0.6 mM did not seem effective with either MO, and 2.4 mM caused non-specific effects. 1.2 mM MO2 produced a pronounced effect on Rb1 expression levels in 48 hpf embryos (Figure 10A), and all further experiments use this combination of concentration and MO (*rb1* MO). Specificity of knockdown was assessed by coinjecting embryos with *rb1* MO as well as an mRNA of zebrafish *rb1* lacking the targeted 5' UTR (*rb1* -5' UTR). After 48 hours, embryos were photographed and a noticeable difference in survival and appearance was observed between embryos injected with only *rb1* MO and those coinjected with *rb1* MO and *rb1* -5' UTR mRNA (Figure 10B). These analyses show that *rb1* MO can specifically knockdown zebrafish *rb1*.

During zebrafish fin regeneration, mature cells dedifferentiate to give rise to the blastema. As regeneration progresses and enters the outgrowth phase, these cells redifferentiate and form the regenerate. To determine the role *rb1* in the redifferentiation observed during outgrowth, I injected and electroporated *rb1* MO into 2 dpa blastemas (0 dpt) and then assessed fin regeneration at 4 dpa (2 dpt). It was observed that the *rb1* MO but not the standard control

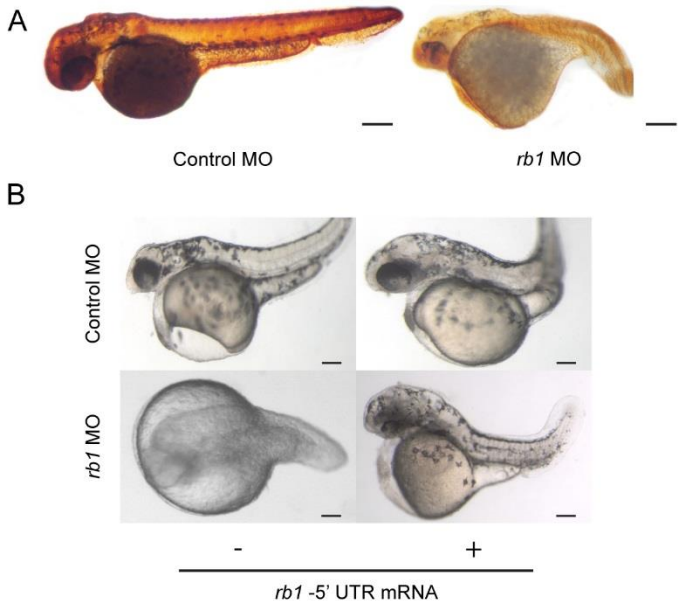

Figure 10. *rb1* MO specifically targets *rb1* mRNA transcripts for knockdown. (A) Immunostaining for Rb1 in 48 hpf embryos injected with 1.2 mM standard control MO or 1.2 mM *rb1* MO at the single cell stage. Scale bars: 100 μm. (B) Representative images of 48 hpf embryos injected with 1.2 mM standard control MO or 1.2 mM *rb1* MO and coinjected with or without 400 pg of rb1 -5'UTR mRNA at the single cell stage. Scale bars: 100 μm.

MO (Gene Tools, LLC) significantly inhibited fin regeneration by 45% (Figure 11A) (N=5, $p<0.001$). To determine why fin regeneration was inhibited with *rb1* knockdown, cell cycle and apoptosis analyses were performed by staining injected fins for EdU incorporation and TUNEL reactivity, respectively. I found that *rb1* MO injected fin blastemas were 107% more proliferative than control MO injected fins (N=3, $p<0.01$) (Figure 11B). However, no significant difference was found with regard to the incidence of apoptosis (N=3, $p>0.05$) (Figure 11C). Alizarin red staining was performed to observe the development of the bony fin rays. Alizarin red is used to identify calcium such as that present in mature bone. When the percentage of bone present in the regenerate (stained bone length per regenerate length) was assessed, it was found that *rb1* MO injected fins were significantly underdeveloped compared to control MO injected fins (N=6, $p<0.05$) (Figure 11D). These findings suggest an essential differentiation promoting role for Rb1 during the redifferentiation phase of regenerative outgrowth.

Rb1 gain of function model is insufficient to prevent dedifferentiation

While loss of function of Rb1 prevented differentiation, I sought to investigate the role of *rb1* in dedifferentiation by using a gain of function model to reinforce Rb1 expression and prevent the dedifferentiation that occurs with fin regeneration. I created the transgenic line Tg(*hsp70l*:Rb1) (*hs*:Rb1) to accomplish this. The *hs*:Rb1 line incorporated the coding sequence of zebrafish *rb1* under the control of the zebrafish heat shock inducible promoter, *hsp70l*, to overexpress Rb1.

Using the same heat shock regimen as the *hs*:ARF experiments in Chapter 1, WT and *hs*:Rb1 fish fins were amputated and heat shocked. When regeneration was assessed at 6 dpa, no

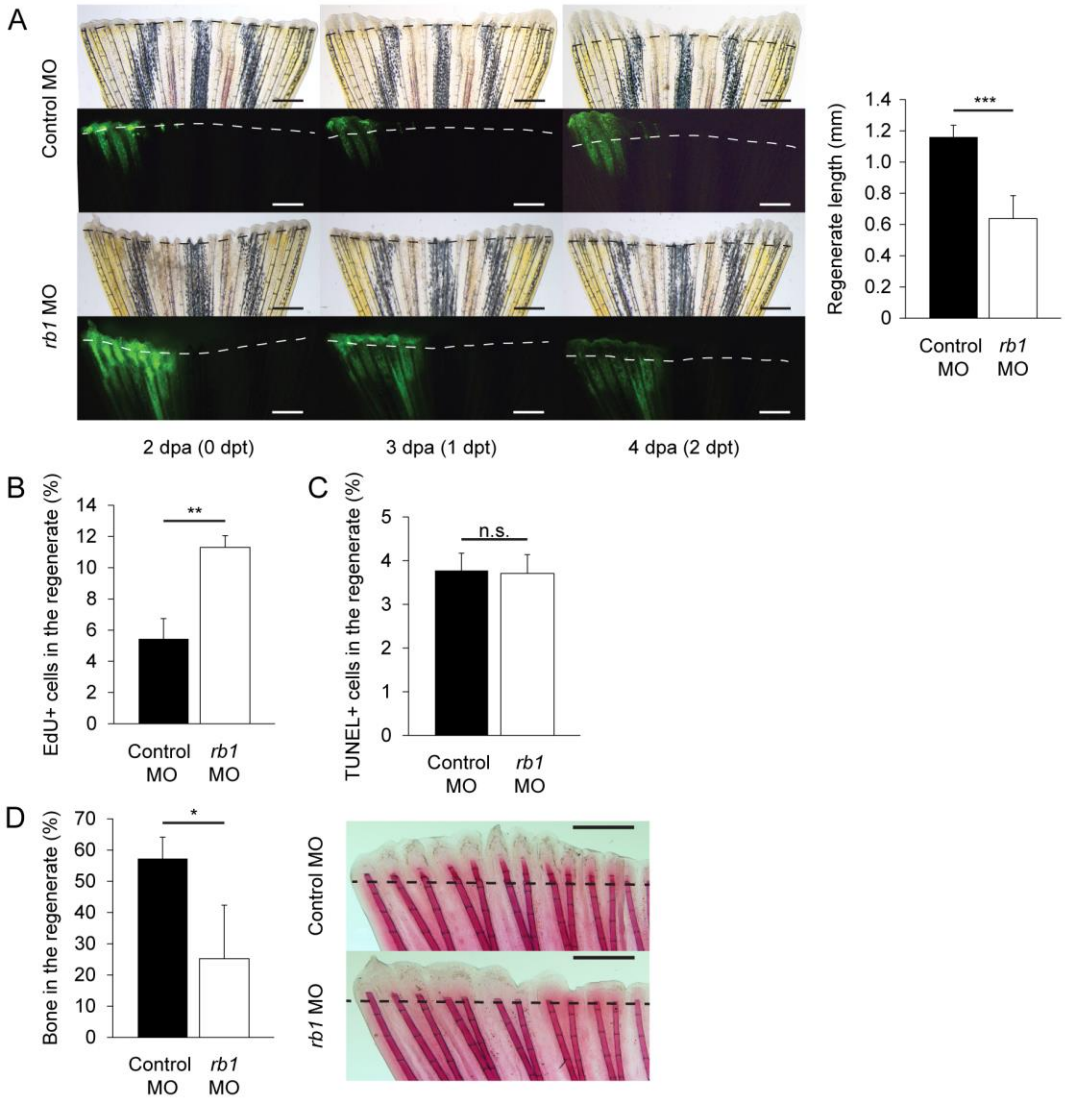

Figure 11. Knockdown of *rb1* inhibits fin regeneration by promoting proliferation and preventing differentiation of osteoblasts. (A) Representative images of fin regeneration at 0, 1, and 2 days post transfection (dpt) in zebrafish fins injected and transfected with 1.2 mM standard control MO or 1.2 mM *rb1* MO (left). Fluorescent images demonstrate the dorsal localization of the injected and transfected fluorescence-tagged MOs. Scale bars: 1 mm. Quantification of regenerate length at 2 dpt (4 dpa) in zebrafish fins injected and transfected with 1.2 mM standard control MO or 1.2 mM *rb1* MO (right; N=5, $p<0.001$). (B) Quantification of EdU staining at 2 dpt (4 dpa) in zebrafish fins injected and transfected with 1.2 mM standard control MO or 1.2 mM *rb1* MO (N=3, $p<0.01$). (C) Quantification of TUNEL staining at 2 dpt (4 dpa) in zebrafish fins injected and transfected with 1.2 mM standard control MO or 1.2 mM *rb1* MO (N=3, $p>0.05$). (D) Quantification of the percentage of mature bone in the regenerate at 2 dpt (4 dpa) in zebrafish fins injected and transfected with 1.2 mM standard control MO or 1.2 mM *rb1* (left; N=6, $p<0.05$). The percentage was calculated by measuring the length of Alizard red stained bone in the regenerate and dividing the longest length by the total regenerate length. Representative images of Alizard red staining at 2 dpt (4 dpa) in zebrafish fins injected and transfected with 1.2 mM standard control MO or 1.2 mM *rb1* MO (right). Scale bars: 1 mm. Dashed lines represent amputation planes. Results are shown as mean ± SD.

significant difference in regenerate length or area was observed (Figure 12A) (N=30, $p>0.05$). Other heat shock regimens were also attempted with similar results.

To confirm Rb1 overexpression with heat shock, I performed a series of Western blots for Rb1 and phosphorylated-Rb1 (p-Rb1) on heat shocked WT and *hs*:Rb1 fish. Protein was isolated at 0 dpa and 4 dpa. The Western blots showed that Rb1 was overexpressed with heat shock in *hs*:Rb1 but not WT fish; however, the Western blot also showed that while Rb1 was overexpressed with heat shock, p-Rb1 levels also rose with Rb1 expression (Figure 12B). This simultaneous increase in Rb1 and p-Rb1 levels suggests that even though Rb1 is being overexpressed, it is not enough to saturate the cyclin dependent kinases active during regeneration. These results explain why WT and *hs*:Rb1 fins regenerate equally well; Rb1 is overexpressed, but it is phosphorylated, thus not preventing Rb1 inhibition and presumably dedifferentiation as a result. Had dedifferentiation been prevented, inhibition of regeneration would have been expected.

Attempted creation of a transgenic zebrafish osteoblast differentiation report line

I began creating a transgenic zebrafish osteoblast differentiation reporter line by first identifying and collecting necessary, pre-existing transgenic zebrafish lines. The transgenic lines Tg(*runx2*:GFP) (Knopf et al., 2011) and Tg(*bactin2*:loxP-STOP-loxP-DsRed-express)^{sd5} (Bertrand et al., 2010) were identified from publications, and both Shannon Fisher's and David Traver's groups very generously provided fish. Tg(*runx2*:GFP) transiently marks immature osteoblasts with GFP, and Tg(*bactin2*:loxP-STOP-loxP-DsRed-express)^{sd5} permanently marks Cre expressing cells with DsRed.

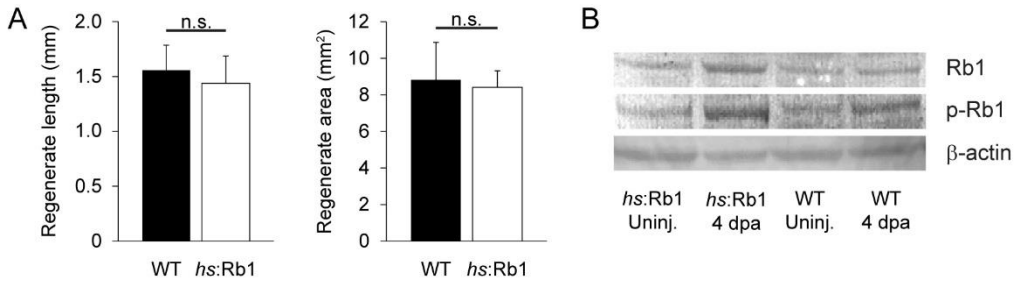

Figure 12. Overexpression of Rb1 does not prevent dedifferentiation during zebrafish fin regeneration. (A) Quantification of regenerate length and area at 6 dpa in WT and *hs*:Rb1 fins exposed to heat shock (N=30, p>0.05). (B) Representative Western blot of 3 replicates of Rb pathway components, Rb1 and hyperphosphorylated Rb1 (p-Rb1), before injury (Uninj.) and at 4 dpa in WT and *hs*:Rb1 zebrafish fins. b-actin is used as a loading control. Results are shown as mean ± SD.

To be certain that I received the correct fish, I tested both lines. Genotyping Tg(*runx2*:GFP) fish is easy because they express GFP brightly in all forming skeletal structures. It was particularly easy to observe at 48 hpf. In order to test Tg(*bactin2*:loxP-STOP-loxP-DsRed-express)^{sd5} fish, I injected embryos at the single cell stage with 100 ng/μL Cre mRNA. The addition of Cre excised the STOP cassette and allowed for the expression of DsRed throughout the embryos (Figure 13).

The next step was to create a transgenic zebrafish line expressing CreER^{T2} under the control of the zebrafish osteocalcin (*bglap*) promoter, Tg(*bglap*:CreER^{T2}), in an effort to permanently mark mature osteoblasts with DsRed. The *bglap* promoter was subcloned from a vector generously provided by the Kenneth Poss's group (Singh et al., 2012), and the CreER^{T2} cassette was subcloned downstream of the promoter. Transgenic zebrafish were generated, and then Cre expression was confirmed by reverse transcriptase polymerase chain reaction (RT-PCR). Next, confirmed Tg(*bglap*:CreER^{T2}) fish were mated to Tg(*bactin2*:loxP-STOP-loxP-DsRed-express)^{sd5} fish to produce the mature osteoblast marking component of the osteoblast differentiation reporter line. However, when treated with 4-hydroxytamoxifen (4OHT) for 24 hours in the dark, no DsRed expression could be detected at 1 or 2 days post treatment. Since this treatment regimen has been published to be successful (Singh et al., 2012) and the Tg(*bactin2*:loxP-STOP-loxP-DsRed-express)^{sd5} is functional, these results led us to believe that the problem lies with the Tg(*bglap*:CreER^{T2}) line. While Cre is expressed in this transgenic zebrafish line, it may not be expressed at sufficient levels to induce recombination.

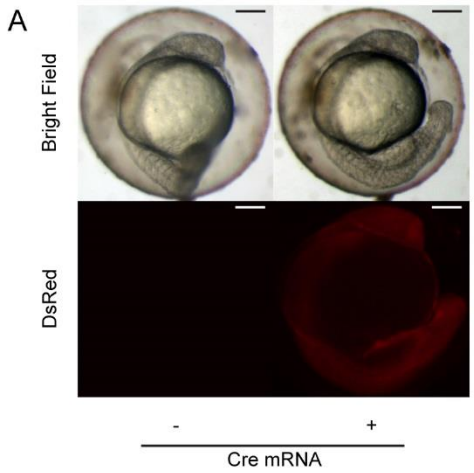

Figure 13. Imported transgenic zebrafish lines function appropriately. Representative images of 24 hpf Tg(*bactin2*:loxP-STOP-loxP-DsRed-express)^{sd5} transgenic zebrafish injected with or without 100 ng/mL Cre mRNA at the single cell stage. Embryos develop normally (top), but only Cre-injected embryos are fluorescent (bottom). Scale bars: 200 μm.

Attempted creation of a conditional, inducible *rb1* loss of function model

While zebrafish *rb1* knockdown experiments suggested a role for Rb1 in the redifferentiation phase of zebrafish fin regeneration, it was necessary to create a genetic loss of function model to examine the role of *rb1* in dedifferentiation. Since Rb1 in an important cell cycle regulator in many tissue types especially early in development, I decided to create a conditional, inducible loss of function zebrafish model. I set out to do this through a series of steps. First, I planned to mutate the first intron of zebrafish *rb1* with the recently documented CRISPR/Cas9 (Hwang et al., 2013), which has since very quickly been widely adopted and modified to fulfill a wide variety of tasks, to insert an attP site. Next, I planned to use the incorporated attP site as a landing site to insert a gene trap including an attB site through attP/B site recombination. I designed the gene trap such that it was silent until recombination with Cre. With Cre expression, the gene trap cassette would invert and prevent splicing of exons 1 and 2 of *rb1* thus creating a nonsense allele while also marking the recombined cells with a fluorescent tag. Mating this model with a conditional Cre line such as Tg(*bglap*:CreER^{T2}), would ensure that *rb1* would only be lost in mature osteoblasts in an inducible manner. I predicted that this model would be very useful for experiments with uninjured tissue. I planned to induce recombination in mature osteoblasts to determine if loss of *rb1* would promote dedifferentiation.

First, I needed to mutate the first intron of zebrafish *rb1* to insert an attP site. I started by sequencing the first exon, first intron, and second exon of rb1 to generate precise target sites for the CRISPR/Cas9 system. Four target sites were identified and tested. One, sgRNA3, produced mutations in the first intron with an efficiency of 50% (Figure 14A), which far surpassed the other target sites. This target sites was chosen, and experiments to insert an attP site were performed. I tested three lengths of homology arms flanking the attP, and it was determined that

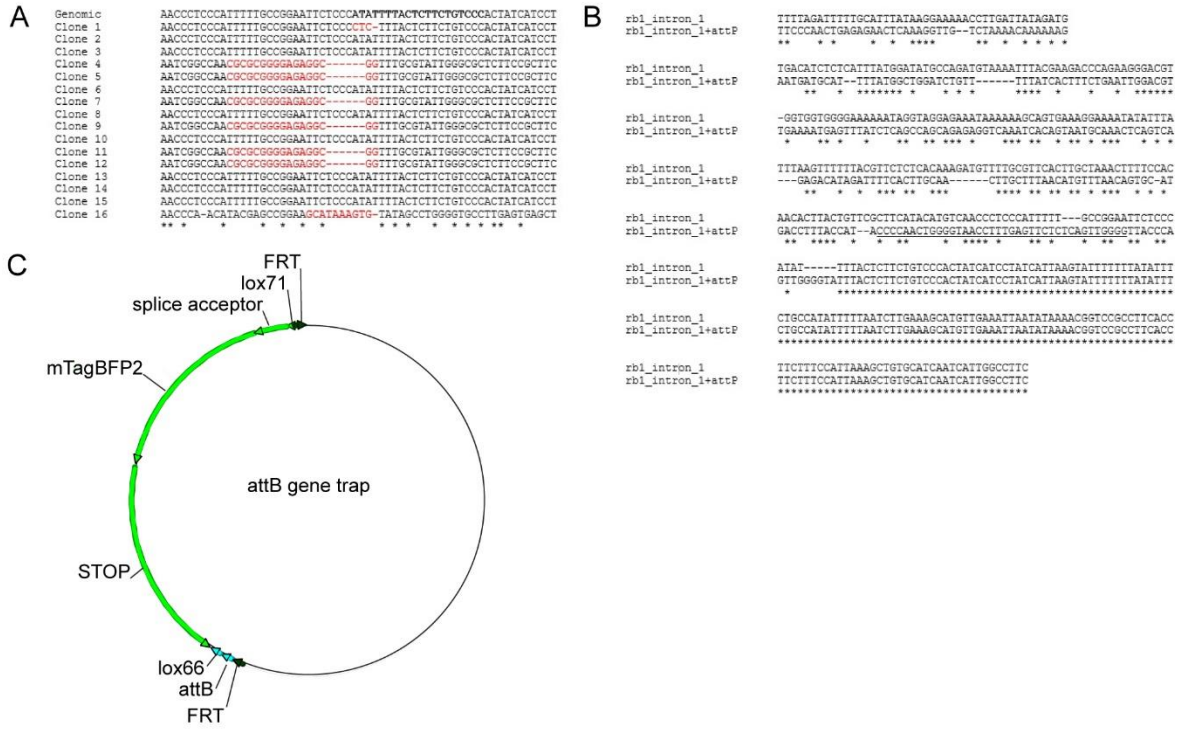

Figure 14. Use of the CRISPR/Cas9 system to create an inducible, conditional nonsense allele of *rb1*. (A) Sequencing results of a mutation analysis of sgRNA3-induced mutations in the first intron of *rb1*. Mutated sequences are highlighted in red. (B) Comparison of sequencing results of the first intron of *rb1* in zebrafish with or without CRISPR/Cas9-mediated mutations to introduce an attP recombination site (underlined). (C) Schematic of the attB gene trap vector used to recombine with the introduced attP recombination site in the first intron of *rb1*.

10 bp homology arms were most efficient. The region was sequenced again to confirm the incorporation of the attP site (Figure 14B) before continuing to the next step, generation and incorporation of the attB gene trap.

The attB gene trap was generated by subcloning gBlocks Gene Fragments (Integrated DNA Technologies) into the backbone, pBAD-mTagBFP2 (Addgene). The final construct included a flanking pair of head-to-tail FRT sites, the attB site, and a pair of head-on lox66 and lox71 sites flanking the gene trap cassette, which included a splice acceptor, the coding sequence for mTagBFP2, a STOP cassette (Figure 14C). In theory, the splice acceptor would intercept the splice donor of *rb1* exon 1 and link it to the mTagBFP2 before terminating the transcript. Flanking FRT sites were included to remove extraneous plasmid DNA after the attP/B recombination.

Before inserting the attB gene trap, I assessed the attP mutants for off target (OT) mutations (Yang et al., 2013). Ten regions of varying similarity to sgRNA3 were detected by BLAST (NCBI), and each region was tested for potential mutations with T7 Endonuclease I assays. Of the 10 regions, 7 did not contain any mutations in the four fish assayed (Table 4).

Table 4. Off-target mutation analysis.

Site Name	Sequence	Mutation Frequency	Coordinate
sgRNA3	5'-GGG ACA GAA GAG TAA AAT ATG GG-3'	/	chr21: 22979146-22979168
OT1	5’-GGG AtA GAA cAG TAA AAT ATG GG-3’	0/4	chr19: 42357455-42357477
OT2	5’-GGG ACA GAA ctG TAA AAT ATG GG-3’	0/4	chr21: 33616661-33616683
OT3	5’-GGG ACA GAA tgG TAA AAT ATG GG-3’	0/4	chr4: 71915102-71915124

OT4	5’-GGG AtA GAA tAG TAA AAT ATG GG-3’	0/4	chr1: 10934719-10934741
OT5	5’-GGG AtA GAA GgG TAA AAT ATG GG-3’	2/4	chr20: 10576166-10576188
OT6	5’-GGG AaA GAA cAG TAA AAT ATG GG-3’	1/4	chr23: 5818358-5818380
OT7	5’-tGG ACA GAA tgG TAA AAT ATG GG-3’	0/4	chr17: 35380526-35380548
OT8	5’-Gtc ACA GAA cAG TAA AAT ATG GG-3’	0/4	chr9: 16798649-16798671
OT9	5’-caG ACA GAA tgG TAA AAT ATG GG-3’	2/4	chr23: 9844450-9844472
OT10	5’-GaG ACA GAA ctG TAA AAT ATG GG-3’	0/4	chr17: 762325-762347

Once attP mutants lacking OT mutations were identified, they were mated, and embryos were injected at the single cell stage with a cocktail containing the attB gene trap vector, FLPe mRNA to excise extraneous plasmid DNA, 1X BP Clonase (Life Technologies) to induce attP/B site recombination, and 1X Phenol Red to visualize the injection. Fish were raised and then genotyped using primers for mTagBFP2. Fish positive for mTagBFP2 were identified and separated for breeding purposes.

To test the function of the gene trap, I mated mTagBFP2-positive fish and injected Cre mRNA into the resulting embryos at the single cell stage. Even though multiple concentrations of Cre mRNA were tested, blue fluorescence was never detected despite positive mTagBFP2 genotyping of the injected embryos. Since I know that the Cre mRNA is functional (Tg(*bactin2*:loxP-STOP-loxP-DsRed-express)^{sd5} testing), the problem most likely lies with a component of the attB gene trap vector. I was successful in my attempt to use the CRISPR/Cas9

system to incorporate an inducible gene trap into the first intron of zebrafish *rb1*, but there seem to be unresolved issues with either the design or components of the gene trap itself.

Discussion

While attempts to create a transgenic zebrafish osteoblast differentiation reporter line and a conditional, inducible genetic loss of function model were unsuccessful, the experiments included in this chapter did succeed in elucidating roles for Rb1 during zebrafish fin regeneration.

Knockdown of *rb1* with a Morpholino oligomer (MO) injected and electroporated into fin blastemas was surprisingly effective. I had anticipated that the other Rb family members, *rbl1* and *rbl2*, would compensate for the loss of *rb1*. The effect size of the *rb1* knockdown suggests that *rbl1* and *rbl2* are not major players and are incapable of compensating for an acute loss of *rb1*. One limitation of the MO knockdown experiments was that only already formed blastemas could be injected. I attempted to inject uninjured fin tissue to determine if *rb1* loss could promote the initial phases of regeneration, particularly dedifferentiation, but it proved to be too technically difficult. Another limitation is that MOs are only effective for 48 hours post injection and electroporation (Thummel et al., 2006). The efficiency of MO incorporation is another thing to consider because the technical process of injecting the blastemas and then electroporating the fin tissue can lead to variability in observed phenotypes.

Even with these limitations, the experiments strongly suggested a role for Rb1 during the redifferentiation and outgrowth phase of zebrafish fin regeneration. With *rb1* knockdown, proliferation increased, bone development was reduced, and the incidence of apoptosis remained constant. These results signify that without Rb1, osteoblasts are not able to redifferentiate, which could lead to the observed inhibition of regeneration because there is no new tissue on which to grow. Regeneration is highly controlled not only so that cells can proliferate and contribute to the blastema without causing cancer, but also so that cells can appropriately differentiate to form the

stable, mature regenerate. As zebrafish regeneration proceeds, the tailing edge of the proximal blastema begins to differentiate, thus providing the blastema with tissue on which to grow (Poss et al., 2003). This appropriately timed differentiation promotes outgrowth of the regenerate, and disruption of this process will predictably lead to regenerative failure.

The creation of and experiments with the *hs*:Rb1 transgenic zebrafish line did not produce the desired effect on differentiation reinforcement, but they did teach us about the cellular plasticity of zebrafish cells dedifferentiating to contribute to the blastema. Even though Rb1 was overexpressed with heat shock in this line, it was not enough to prevent dedifferentiation. This result, while negative, is telling. It suggests that zebrafish cells are incredibly plastic. The amount of signaling leading to Rb1 inhibition is so great that it can overcome an excess of Rb1. While there must be a saturation point for the cyclin-dependent kinases that inhibit Rb1, the limits seems to be very high. For future experiments, I recommend using the product of a cross of an osteoblast conditional, inducible Cre line and a loxP-STOP-loxP-Rb1 transgenic line. This model will allow for permanent, stable overexpression of Rb1, and it may be more effective for differentiation reinforcement than the *hs*:Rb1 transgenic zebrafish line because of the expression fluctuation associated with heat shock driven overexpression.

The Tg(*bglap*:CreER^{T2}) transgenic zebrafish line that I created was not an effective conditional, inducible Cre line. However, I do not believe that the problem lies with the transgene construct. The promoter sequences were subcloned from an existing transgene (Singh et al., 2012), and the CreER^{T2} cassette was subcloned from another functional plasmid. I think that *bglap* is the best promoter to use since it is active in only mature osteoblasts. However, other osteoblast-specific Cre lines do exist and have been published. One example is the

Tg(*osterix*:mTagBFP-2A-CreER)^{pd45} transgenic line (Singh et al., 2012), which uses the intermediate osteoblast promoter *osterix* (*sp7*) to drive CreER expression. For future experiments, I recommend performing Tg(*bglap*:CreER^{T2}) injections again and carefully selecting for a transgenic line that strongly expresses CreER.

I was successful in using the CRISPR/Cas9 system to mutate the first intron of zebrafish *rb1* to insert a silent gene trap with the intension of creating a nonsense allele with Cre-mediated recombination. However, the gene trap was too silent; when gene trap containing embryos were injected with Cre mRNA, no recombination was detected in the form of blue fluorescence from the included mTagBFP2 tag. I believe that the failure of the gene trap can be attributed to the included splice acceptor. I do not think that the gene trap splice acceptor was strong enough to outcompete the splice acceptor of the second exon of *rb1*.

I used a two-step mutation/insertion strategy to insert the gene trap into the first intron of *rb1* because, at the time, only short sequences had been reported to have been successfully inserted into particular genetic loci with a reasonable degree of efficiency. However, that is no longer the case. Several groups have used homologous recombination-like techniques to insert whole reporter genes or promoter regions to create knock-in transgenic zebrafish (Auer et al., 2014, Kimura et al., 2014). For future experiments, I would use a very strong splice acceptor and the CRISPR/Cas9 system in a single step to create a similar inducible loss of function model.

The aforementioned experiments identified roles for Rb1 during zebrafish fin regeneration. It is essential during the redifferentiation and outgrowth phase of regeneration, and it may have a deeply involved role in dedifferentiation as well. While there were shortcomings with model creation, these can be overcome with careful selection of transgenic lines and the use of the latest techniques involving the CRISPR/Cas9 system for genetic engineering. I believe that

this project, when completed, will provide valuable insights into the mechanisms governing dedifferentiation and epimorphic regeneration as a whole.

Chapter 4. The evolution of *ARF*: an oxidative stress hypothesis

Introduction

Arf is an unusual tumor suppressor in that it is poorly conserved in non-mammalian lineages. The *Cdkn2a/b* locus of teleost fish, including zebrafish (*Danio rerio*) and fugu (*Takifugu rubripes*) (Gilley and Fried, 2001), exists as a single protein producing unit that only encodes for a CKI. During evolution, *Cdkn2a* and *Cdkn2b* developed into two separate but related genes encoding for biochemically related CKIs. Arf is not a CKI and, on an amino acid level, is not closely related to either Cdkn2a or Cdkn2b. Arf is thought to be the product of a genetic duplication caused by either an insertion or transposition into the *Cdkn2a/b* locus (Gil and Peters, 2006). Of the highly regenerative species for which genomes have been completely sequenced, none possess an orthologue of *Arf* (Flicek et al., 2014, Karolchik et al., 2014). The earliest documented orthologue of *Arf* exists in the chicken genome (Kim et al., 2003). The question of why this tumor suppressor evolved and has been reported to be present only in avian and mammalian genomes has unfortunately gone largely unnoticed.

In addition to being an important regulator of the cell cycle, Tp53 is also an important regulator of metabolic processes such as the balance between oxidative phosphorylation and glycolysis (Berkers et al., 2013, Maddocks and Vousden, 2011). Arf, which serves as a bridge between the Rb and p53 pathways, has Tp53-dependent functions such as those explored in pervious chapters, but it also serves numerous Tp53-independent roles including controlling ribosome biogenesis and responding to oxidative stress (Sherr, 2006, Weber et al., 2000, Damalas et al., 2011, Menendez et al., 2003). In mammalian cells, Arf and Tp53 form an axis of regulation that controls both proliferative and metabolic states. In lower vertebrates including zebrafish, the p53 pathway is less complex partly because there is no Arf orthologue.

Reactive oxygen species (ROS) have been reported to not only be present during zebrafish fin regeneration (Gauron et al., 2013) and *Xenopus* tadpole tail regeneration (Love et al., 2013), but also necessary for successful regeneration. If not tightly controlled and properly balanced by antioxidants, ROS can cause oxidative stress and even DNA damage and tumorigenesis (Maddocks and Vousden, 2011). Since ARF can respond to oxidative stress by causing cell death (Damalas et al., 2011), ROS production during zebrafish fin regeneration may contribute to the ARF-Tp53 axis activation observed in Chapter 1.

The risk of DNA damage and tumorigenesis as a consequence of unchecked mitochondrial ROS production and oxidative stress is a potential pressure that drove the evolution of *Arf*. It is known that the mitochondria of endothermic species are more active than those of ectothermic species (Hulbert and Else, 1989); therefore, without properly evolved controls, endothermic species would be at a higher risk of developing tumors spontaneously due to oxidative stress-induced DNA damage. I hypothesize that cellular metabolic changes associated with the transition of vertebrates from ectothermic to endothermic regulation over the course of evolutionary history play a large role in the evolution of the *Cdkn2a* locus, and the following experiments are designed to investigate this hypothesis.

Material and Methods

Metabolic Profiling of Zebrafish

Metabolic profiles of embryonic zebrafish (72 hpf) and adult zebrafish fin tissue at multiple time points (0, 1, 2, 3, and 4 dpa) during fin regeneration were created using an XF^{e}24 Extracellular Flux Analyzer (Seahorse Bioscience, North Billerica, MA). Oxygen consumption rates (OCR), a measure of oxidative phosphorylation, and extracellular acidification rates (ECAR), a measure of glycolysis, of zebrafish tissue were recorded in 700 μL of XF assay medium (Seahorse Bioscience) at 29°C ± 1°C. XF24 Islet Capture Microplates (Seahorse Bioscience) and XF^{e}24 FluxPaks (Seahorse Bioscience) equilibrated with XF Calibrant (Seahorse Bioscience) overnight at 29°C ± 1°C were used for all experiments. A standard program of 6 measurement cycles was used to determine the basal OCR and ECAR values of each well of a 24-well plate. At least 4 wells were used as biological replicates per condition, and 4 evenly spaced wells of each plate were used as blanks to control for temperature fluctuations. 72 hpf zebrafish were individually placed into wells and then secured with Islet Capture Screens (Seahorse Bioscience). For fin regeneration experiments, only regenerates were used, and all time points required the placement of 2 adult zebrafish fin regenerates expect 0 dpa, which required only 1 uninjured zebrafish fin. Fin tissues were then secured with Islet Capture Screens (Seahorse Bioscience). Filled 24-well plates were allowed to equilibrate at 29°C ± 1°C for 30 minutes before being analyzed. After metabolic data had been recorded and corrected for background (blank wells), OCR and ECAR values were averaged for each condition and the ratio of OCR:ECAR was calculated. This ratio was then normalized to 0 dpa such that 0 dpa had a value of 1. OCR:ECAR ratio values greater than 1 signify an oxidative environment and values less than 1 signify a glycolytic environment.

Drug Treatments

Zebrafish embryos and cells were treated with 1 mM *tert*-Butyl hydroperoxide (tBHP, Sigma) in E3 medium or low glucose, serum free DMEM (Life Technologies), respectively (70% solution, 7.26 M stock). Adult zebrafish were treated with 200 μM 4'-hydroxy-3'-methoxyacetophenone (APO, Sigma) in DMSO (200 mM stock), 2 μM diphenyleneiodonium chloride (DPI, Sigma) in DMSO (2 mM stock), 200 μM MCI-186 (MCI, Sigma) in DMSO (200 mM stock), 200 μM N-acetyl-L-cysteine (NAC, Sigma) in DMSO (200 mM stock), 2 μM VAS2870 (VAS, Sigma) in DMSO (2 mM stock), or DMSO (0.1%). Water was exchanged daily.

To detect reactive oxygen species, adult zebrafish and embryos were incubated with 50 μM H_2DCFDA (Life Technologies) in DMSO (50 mM stock) for 2 hours.

Immunostaining

Zebrafish fin immunostaining was performed on whole-mounted fins as previously described (Sousa et al., 2011). Briefly, fin tissue was fixed flat in 4% PFA 1 hour, and then incubated in 80% MeOH, 20% DMSO overnight 4°C. Tissue was rehydrated in 75%, 50%, and finally 25% MeOH in PBS 5 minutes each, permeabilized in acetone 20 minutes -20°C, PBS 5 minutes 2X, 0.5% Triton X-100 in PBS (PBTx) 30 minutes, PBS 5 minutes 3X, serum-free protein block (Dako, Carpinteria, CA) 1 hour, primary antibodies in antibody diluent (Dako) overnight 4°C. Tissue was washed multiple times throughout the day, secondary antibodies in antibody diluent overnight 4°C, PBS 5 minutes 3X, mounted with Vectashield mounting medium with DAPI (Vector Laboratories, Burlingame, CA).

Zebrafish embryo immunostaining was performed on whole-mounted, 1-phenyl 2-thiourea (PTU; Sigma)-treated embryos as previously described (Macdonald, 1999). Briefly, embryos

were fixed in 4% PFA overnight 4°C, washed in PBS 5 minutes 3X, and then storage in MeOH -20°C. Embryos were rehydrated in 75%, 50%, and finally 25% MeOH in PBS 5 minutes each, 0.1% Tween-20 in PBS (PBT) 5 minutes 2X. Only 48 hpf and 72 hpf embryos were washed in ddH_2O 5 minutes, acetone 7 minutes -20°C, rinsed in ddH_2O and then PBT 2X. All embryos were blocked in 10% goat serum in PBT 1-2 hours, primary antibodies in 10% goat serum in PBT overnight 4°C. Tissue was washed in PBT 15 minutes 5X throughout the day, secondary antibodies in 10% goat serum in PBT overnight 4°C, PBT 15 minutes 3X, Hoechst stain in PBS 15 minutes, PBS 5 minutes 2X, mounted in methyl cellulose and then imaged.

Mouse/Zebrafish cell immunostaining: 4% PFA 10 minutes, PBS 5 minutes 3X, 0.3% PBTx 15 minutes, PBS 5 minutes 3X, serum-free protein block (Dako) 1 hour, primary antibodies in antibody diluent (Dako) overnight 4°C, PBS 5 minutes 3X, secondary antibodies in antibody diluent 1 hour, PBS 5 minutes 3X, mounted with Vectashield mounting medium with DAPI (Vector Laboratories, Burlingame, CA).

TUNEL detection was performed using the In Situ Cell Death Detection Kit (Roche, Basel, Switzerland) per the manufacturer's instructions for adherent cells.

The presence of reactive oxygen species in cells was detected using 5 μM CellROX (Life Technologies) for 30 minutes.

Images were quantified in ImageJ. The percent of TUNEL-positive cells was quantified by first counting the number of positive cells and then dividing that count by the number of nuclei in the field counted.

Primary Antibodies

Host Species	Antigen	Company	Cat. No.	Dilution	Application
Rabbit	GFP	Torrey Pines	TP401	1:3000	IHC
Rabbit	p19Arf	Abcam	ab80	1:100	IHC

***In Situ* Hybridization**

Zebrafish embryo mRNA *in situ* hybridization was performed on whole-mounted, PTU-treated embryos as previously described (Chitramuthu and Bennett, 2013). Briefly, embryos were fixed in 4% PFA overnight 4°C, washed in PBS 5 minutes 3X, and then storage in MeOH -20°C. Embryos were rehydrated in 75%, 50%, and finally 25% MeOH in PBS 5 minutes each, 0.1% PBT 5 minutes 3X, incubated in 10 μg/mL proteinase K in PBS 15 minutes (24 hpf), 30 minutes (48 hpf), or 40 minutes (72 hpf). Embryos were fixed in 4% PFA 20 minutes, PBT 5 minutes 3X, incubated in acetylation mixture (125 uL triethanolamine, 27 uL acetic anhydride in 10 mL DEPC H_2O) 10 minutes 2X, PBT 10 minutes, 2X, prehybridized in 200 mL hybridization buffer (50% formamide, 5X SSC, 0.1% Tween-20, 50 ug/mL heparin, 500 ug yeast RNA; pH 6.0 with citric acid) 2-4 hours 70°C. Extra embryos were used to preadsorb the anti-digoxygenin-AP antibody (1:500) in blocking buffer (2% calf serum, 2 mg/mL BSA in PBT) 2-4 hours, and then stored overnight 4°C. After 2-4 hours at 70°C, approximately 200ng probe was added and allowed to hybridize overnight 70°C. Embryos were washed in 100% hybridization buffer, 75%, 50%, 25% with 2x SSC 15 minutes 70°C, 2x SSC 15 minutes 2X 70°C, 0.2x SSC 30 minutes 2X 65°C, 100% 0.2x SSC, 75%, 50%, 25% with PBT 5 minutes, PBT 5 minutes 2X, preincubated in blocking buffer 3-4 hours, incubated with 1:5000 anti-digoxygenin-AP antibody in blocking buffer (1:10 preadsorbed) overnight 4°C. Embryos were washed PBT 15 minutes 6X, NTM (0.1M Tris-HCl pH 9.5, 50mM MgCl2, 0.1M NaCl, 0.1% Tween-20) 15 minutes 2X, incubated with BM Purple supernatant for 0.25-16 hrs (check every 30 min) dark. The reaction was

stopped with stop solution (1 mM EDTA PBT, pH 5.5) 10 minutes 2X, mounted in methyl cellulose and then imaged. The antisense GFP probe was labeled with digoxygenin-11-UTP (Roche) and generated using the following primers: 5'-AAG GGC GAG GAG CTG TTC AC-3' and 5'-GAA CTC CAG CAG GAC CAT GT-3' (MacDonald et al., 2010).

Gene Quantitation

qPCR assays were performed on 100 ng of cDNA using 1 μL of each primer (10 pmol/μL) and iTaq Universal SYBR Green Supermix (Bio-rad) in a 12 μL total reaction volume. The PCR was performed for 40 cycles with annealing temperature of 60°C and 1 minute elongation time. Total RNA was isolated using the RNeasy mini kit (Qiagen) per the manufacturer's instructions. cDNA was prepared from total RNA using random hexamer primers and the SuperScript III First Stand Synthesis System for RT-PCR (Life Technologies) per the manufacturer's instructions.

qPCR Primers

Gene	RefSeq ID	Forward Primer	Reverse Primer
EGFP	JN717244.1	5'-TCG AGC TGG ACG GCG ACG TA-3'	5'-ATG TGG TCG GGG TAG CGC CT-3'
actb2	NM_181601.4	5'-CGA GCA GGA GAT GGG AAC C-3'	5'-CAA CGG AAA CGC TCA TTG C-3'
Arf	JH736019.4	5'-CTG CAA CCA GGT ACG AGA GG-3'	5'-ACC TCG TGC GGG TCT TTA TG-3'

Cell Culture

Primary mouse embryonic fibroblasts (MEFs) were cultured at 37°C, 5% CO_2 in DMEM (Life Technologies) with 10% FBS, 1% L-glutamine, and 1% Pen/Strep. MEFs were isolated as follows. Sleeves of tissue culture (TC) and non-TC dishes as well as a beaker of 70% EtOH were placed in the TC hood. 2 dishes were filled with 70% EtOH and razor blades were placed into 1

of the dishes. The TC hood was then closed and the UV light was turned on. The pregnant mouse was sacrificed and the uterus was dissected, dipped in 70% EtOH, and placed in sterile PBS. Razors and sterile forceps were rinsed in 70% EtOH and then PBS. Embryos were removed from the uterus, washed in separate dishes of PBS, and samples for genotyping were removed and placed into individual tubes. The head of each embryo was removed as well as any red organ (liver). The remaining tissue was then minced in 0.05% Trypsin with EDTA and allowed to incubate for 10 minutes 37°C. Then, 9 mL of culture medium were added, and the tissue was triturated, passed through a 100 μm cell strainer, and then plated.

Primary zebrafish embryonic fibroblasts (ZEFs) were culture at 28°C, 0% CO_2 in L-15 (Life Technologies) with 15% FBS, 1% L-glutamine, 1% Pen/Strep, 10 mg/mL gentamicin, 0.8 mM calcium chloride. ZEFs were isolated as previously described (Choorapoikayil et al., 2013). Briefly, 24 hpf embryos were dechorionated with sterile, EtOH cleaned forceps. Embryos (5 per well of a 6 well plate) were then incubated in 5 mL PBS with 1% Pen/Strep (PBS/PS) 30 minutes, refreshed with PBS/PS, transferred to individual tubes (0.5 mL per tube), and incubated for 20 minutes. Embryos were then incubated in a bleaching solution, 10% bleach in calcium-free Ringer solution (116 mM NaCl, 2.9 mM KCl, 5mM HEPES), 5 minutes, which was replaced with PBS/PS immediately and incubated for 20 minutes. Embryos yolk sacs were removed by trituration with a 200 μL pipette, tissue was then centrifuged for 2 minutes at 1200 g, and the supernatant was carefully discarded. 300 μL TrypLE (Life Technologies) was added to each tube and incubated for 30 minutes 28°C 800 rpm. Tissue was then triturated, centrifuged for 4 minutes at 1200 g, washed with 400 μL PBS, and then resuspended in 400 μL culture medium and plated 5 tubes per well in a 6 well plate.

Results

Evolutionary analysis of Arf in ectothermic and endothermic vertebrates

The Ink4b-Arf-Ink4a locus in the genomes of 11 different vertebrate species including highly regenerative (*Danio rerio, Takifugu rubripes, Xenopus tropicalis,* and *Ambystoma mexicanum*), moderately regenerative (*Anolis carolinensis*), and poorly regenerative (*Alligator mississippiensis, Chrysemys picta bellii, Taeniopygia guttata, Gallus gallus, Mus musculus,* and *Homo sapiens*) vertebrates (Monaghan and Maden, 2013) was analyzed using the Ensembl Genome Brower (Flicek et al., 2014), the UCSC Genome Browser (Karolchik et al., 2014), Genscan (Salzberg et al., 1998, Burge and Karlin, 1997), and Sal-Site (Smith et al., 2005). Protein sequences were then compared using a CLUSTALW multiple sequence alignment tool (GenomeNet, Kyoto University Bioinformatics Center, Kyoto, Japan) (Figure 15, left). The presence of Arf in the genome of each species as well as the method of thermal regulation of each species was assessed and a phylogenic tree was constructed containing all of the species analyzed (Figure 15, right). Actinopterygii is the class of ray-finned fish of which teleosts including *Danio rerio* and *Takifugu rubripes* are a subclass. These fish do not possess Arf in their genomes and they are highly regenerative ectotherms. Amphibia is the class of amphibians to which the orders Anura and Urodela belong. Anura includes frogs such as *Xenopus tropicalis*. This frog does not possess Arf in its genomes, and it is a highly regenerative ectotherm. Urodela is the order of salamanders and newts as such *Ambystoma mexicanum*. This salamander does not possess Arf in their genomes, and it is a highly regenerative ectotherm. Reptilia is the class of reptiles to which the orders Testudomorpha, Lepidosauria, and Crocodilia belong. Testudomorpha is the order of turtles including *Chrysemys picta bellii*. This turtle does not

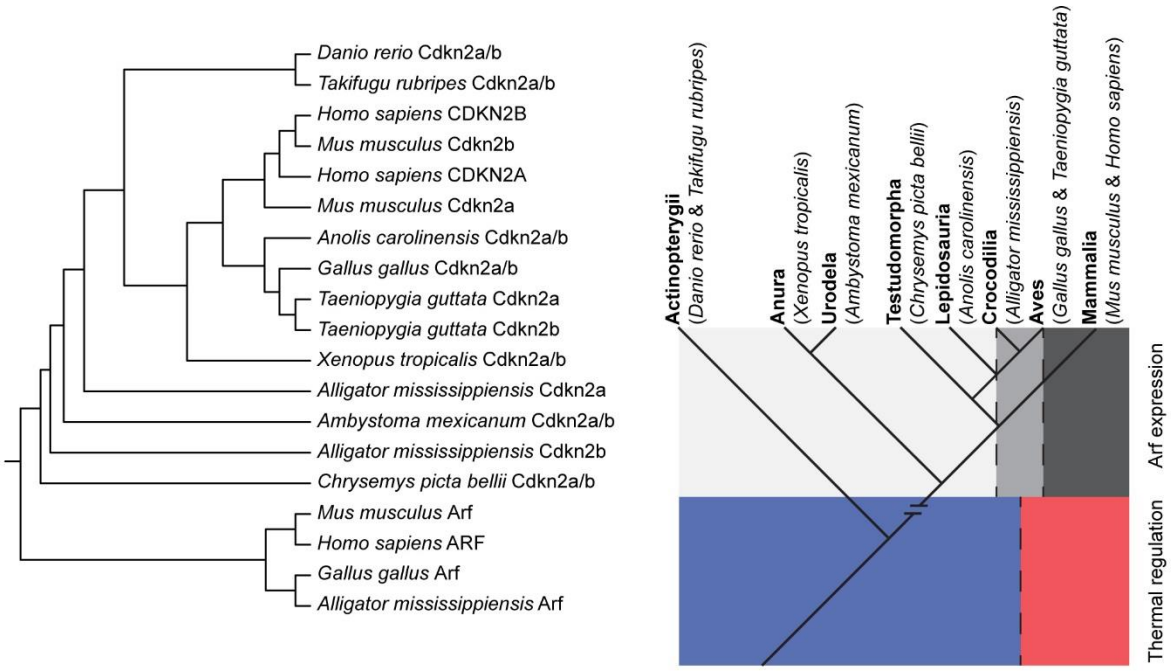

Figure 15. Evolutionary analysis of *Arf* and thermal regulation suggests a direct relationship. Comparison of amino acid sequences of proteins produced by the Cdkn2a/b loci of teleost fish including the zebrafish (*Danio rerio*) and fugu (*Takifugu rubripes*), amphibians including the axolotl (*Ambystoma mexicanum*) and western clawed frog (*Xenopus tropicalis*), reptiles including the Carolina anole (*Anolis carolinensis*), painted turtle (*Chrysemys picta bellii*), and alligator (*Alligator mississippiensis*), birds including the zebra finch (*Taeniopygia guttata*) and chicken (*Gallus gallus*), and mammals including the mouse (*Mus musculus*) and human (*Homo sapiens*) (left). Cladogram comparing the transition from ectothermal (blue) to endothermal (red) regulation and the evolution of *Arf* (grey scale, darker denotes more *Arf*) over evolutionary time (right). While Cdkn2a and Cdkn2b are conserved and encode Ink4 orthologues, Arf evolved recently and orthologues do not exist in highly regenerative, ectothermic vertebrates including teleost fish and urodele amphibians.

possess Arf in its genome, and it is a poor regenerative ectotherm. Lepidosauria includes lizards such as *Anolis carolinensis*. This lizard does not possess Arf in its genome, and it is a moderately regenerative ectotherm. *Anolis carolinensis* is considered moderately regenerative because it is able to partially regenerate its tail when injured. Crocodilia is the order of crocodiles and alligators such as *Alligator mississippiensis*. This alligator possesses Arf in its genome, and it is a poorly regenerative ectotherm. Aves is the class of birds such as *Gallus gallus* and *Taeniopygia guttata*. *Gallus gallus* is an example of a bird that possesses Arf in its genome and is a poorly regenerative endotherm, while *Taeniopygia guttata* is an example of a bird that does not possess Arf in its genome and is a poorly regenerative endotherm. Mammalia is the class of mammals including *Mus musculus* and *Homo sapiens*. Both of these species possess Arf in their genomes and are poorly regenerative endotherms. The results of this analysis elucidate a transitional period with regard to the presence of Arf (Figure 15, right). This period is most likely indicative of when Arf began to evolve because it is a 'grey area' in terms of the correlation of thermal regulation and the presence of Arf; evolution is a slow, gradual process, and transitions are usually marked with species that have pattern-defying characteristics such as ectotherms that express Arf (*Alligator mississippiensis*) and endotherms that do not (*Taeniopygia guttata*). It also coincides with the transition of species from ectothermic to endothermic regulation. The results of this analysis suggest that the evolution of the Ink4b-Arf-Ink4a locus, the loss of regenerative ability over evolutionary time, and the transition from ectothermic to endothermic regulation may be related.

Oxidative stress as a driver for *Arf* evolution

As with most evolutionary hypotheses, it is difficult to directly test the hypothesis that Arf evolved in response to increased mitochondrial activity, reactive oxygen species production, and ultimately oxidative stress as species evolved endothermic regulation. However, it can be postulated that cells of species with Arf expression may be more sensitive to oxidative stress because of the activation of Arf with exposure and subsequent cell cycle arrest or apoptosis to eliminate damaged cells. To test this, primary embryonic mouse fibroblasts (MEFs) and primary embryonic zebrafish fibroblasts (ZEFs) were treated with *tert*-Butyl hydroperoxide (tBHP), a well-known inducer of oxidative stress (Mukaigasa et al., 2012, Faria et al., 2014), and then the incidence of apoptosis and Arf expression were assessed. Zebrafish cells are ectothermic and grow at 30°C. Mouse cells are endothermic, grow at 37°C, and wild-type (*Arf*+/+) MEFs express *Arf*.

When wild-type (*Arf*+/+) MEFs were exposed to either 0 mM tBHP or 1 mM tBHP for two hours, significantly more ROS-positive cells were detected by CellROX staining with 1 mM tBHP, approximately 71% ± 6%, than 0 mM tBHP, approximately 6% ± 0.6% ($N>1000$ cells/condition, $p<0.001$) (Figure 16A). This indicated that 1 mM tBHP was inducing oxidative stress. The percent of Arf-positive cells as assessed by p19Arf staining was also significantly higher with 1 mM tBHP treatment, 23.2% ± 3%, than 0 mM tBHP, 4.6% ± 0.6% ($N>400$ cells/condition, $p<0.001$) (Figure 16B). Additionally, the incidence of apoptosis as assessed by TUNEL staining was significantly elevated from 1.7% ± 1.5% to 19.9% ± 5.5%, a dramatic increase of approximately 1070% ($N>300$, $p<0.01$). However, when MEFs were genetically rendered null for *Arf* (*Arf*-/-), they did not respond to tBHP exposure; the incidence of apoptosis was not significantly elevated ($N>300$, $p>0.05$). ZEFs also did not respond to tBHP exposure.

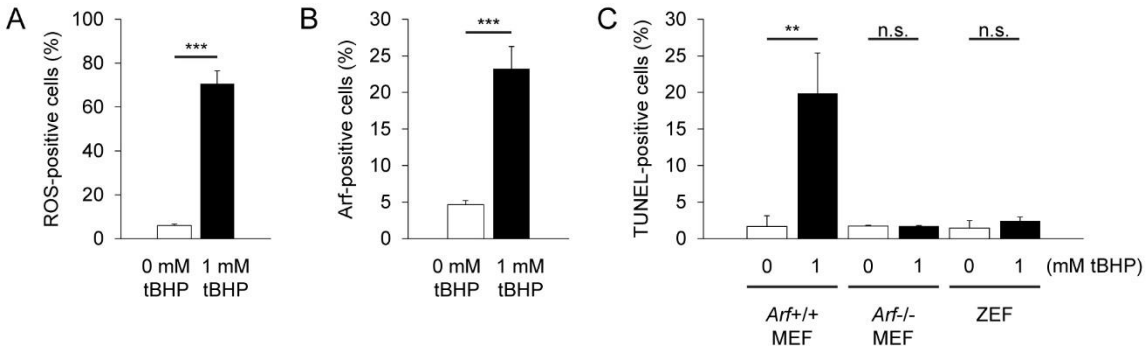

Figure 16. Endothermic cells are more sensitive to oxidative stress than ectothermic cells lacking *Arf*. (A) Quantification of the percent of cells positive for ROS (oxidative stress) as detected by CellROX staining in wild-type (*Arf*+/+) MEFs with or without tBHP treatment (N>1,000 cells/condition, $p<0.001$). (B) Quantification of the percent of cells positive for p19Arf staining in wild-type (*Arf*+/+) MEFs with or without tBHP treatment (N>400 cells/condition, $p<0.001$). (C) Quantification of the percent of cells positive for TUNEL staining in wild-type (*Arf*+/+) MEFs, *Arf*-/- MEFs, and ZEFs with and without tBHP treatment (N>300 cells/condition, $p<0.01$). Oxidative stress induced by tBHP induces Arf-dependent apoptosis. Results are shown as mean ± SD.

The incidence of apoptosis in treated and untreated cells was not significantly different ($N>300$, $p>0.05$), and it was very similar to levels observed in untreated MEFs (Figure 16C).

Oxidative stress is present during zebrafish fin regeneration but not development

While it is known the reactive oxygen species (ROS) are present and seem to be essential for successful zebrafish fin regeneration (Gauron et al., 2013), I confirmed the metabolic state of blastema cells during fin regeneration. Using an XF^e24 Extracellular Flux Analyzer (Seahorse Bioscience) and XF24 Islet Capture Microplates (Seahorse Bioscience), zebrafish fin regenerates were analyzed at 1, 2, 3, and 4 dpa with uninjured fin tissue used as a normalization control. Basal oxygen consumption rate (OCR), a readout for oxidative phosphorylation, and basal extracellular acidification rate (ECAR), a readout for glycolysis, were recorded, and the OCR:ECAR ratio was calculated for each time point and normalized to uninjured fin tissue. When plotted (Figure 17A), it was evident that blastema cells became significantly more oxidative within the first 48 hpa, approximately 200% more oxidative at 24 hpa and 46% more oxidative at 48 hpa, and then activity levels quickly returned to a normalized value. This suggested to us that the mitochondria of cells in the regenerate became significantly more active and that these cells were most likely experiencing a degree of oxidative stress as a result. After amputation, ROS can be detected at the amputation plane as early as 1 hpa up to 24 hpa (Gauron et al., 2013), which is indicative of oxidative stress. However, when the OCR:ECAR ratio of 72 hpf embryos was analyzed using the same methods as above and compared to the OCR:ECAR ratio of uninjured adult zebrafish fins, the OCR:ECAR ratio of 72 hpf embryos was 26% of that observed in uninjured fins (Figure 17B). This result suggests that developing zebrafish are much more glycolytic than adults, and it may indicate that oxidative stress does not normally occur

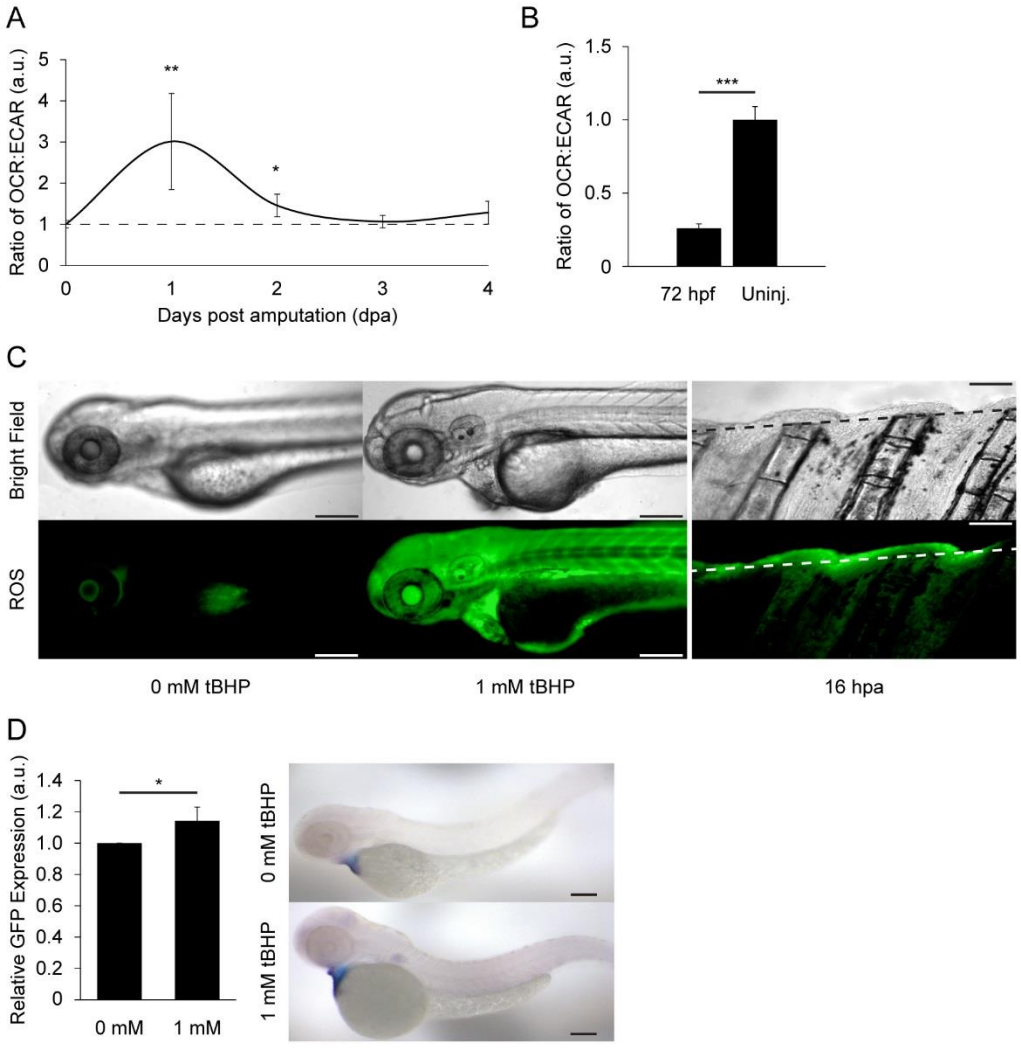

Figure 17. Oxidative stress occurs during zebrafish fin regeneration but not development, and it is capable of activating ARF. (A) Quantification of the ratio of the oxygen consumption rate (OCR) to the extracellular acidification rate (ECAR) of cells in the regenerate at 1, 2, 3, and 4 dpa relative to uninjured fin tissue (0 dpa) plotted as a function of time (N=18, $p<0.01$). The dashed line represents the uninjured baseline. (B) Quantification of the OCR:ECAR ratio of 72 hpf embryos relative to uninjured adult fin tissue (uninj.) (N=18, $p<0.001$). Developing zebrafish are more glycolytic when compared to uninjured adult tissue. (C) Representative images of H_2DCFDA staining to detect ROS production in 72 hpf embryos treated with 0 mM or 1 mM tBHP for 24 hours (left). Representative images of H_2DCFDA staining in 16 hpa adult zebrafish fins (right). ROS levels observed in 72 hpf embryos treated with tBHP are comparable to ROS levels observed during fin regeneration. Scale bars: 200 μm. Dashed lines represent amputation planes. (D) Quantification of GFP expression using qPCR in 72 hpf *ARF*:GFP embryos treated with 0 mM or 1 mM tBHP for 24 hours (left; N=40, $p<0.05$). Values were normalized to β-actin transcripts and then made relative to those of 0 mM tBHP treated embryos. Whole-mount *in situ* hybridization for GFP at 72 hpf in *ARF*:GFP embryos treated with 0 mM or 1 mM tBHP for 24 hours (right). Scale bars: 100 μm. Results are shown as mean ± SD.

during development. It is possible that oxidative stress is essential for blastema formation and ultimately successful regeneration but not successful development.

Oxidative stress activates *ARF*

To determine if *ARF* is activated by oxidative stress similar to that observed during fin regeneration, I used Tg(*ARF*:GFP) transgenic zebrafish as a reporter of *ARF* activation. To simulate oxidative stress conditions, I treated 72 hpf embryos with 1 mM tBHP for 24 hours in the dark. The level of oxidative stress as assessed by H_2DCFDA staining (Figure 17C), was similar between 72 hpf embryos treated with tBHP and 16 hpa adult fin regenerates, which when maximal oxidative stress is observed during fin regeneration (Gauron et al., 2013).

With a model of oxidative stress in zebrafish embryos, I then assessed GFP expression differences with and without tBHP treatment to induce oxidative stress. GFP mRNA transcripts were quantified by qPCR, and the analysis revealed that tBHP treatment significantly increases GFP expression by 14% ($N=40$, $p<0.05$) (Figure 17D, left). Differences in GFP expression were calculated using β-actin transcripts as a reference and values were normalized to untreated 72hpf embryos. *In situ* hybridization was also performed to visualize GFP mRNA transcript accumulation with tBHP treatment. Treated embryos were noticeably more stained than untreated embryos (Figure 17D, right), and the pattern of staining was uniform along the length of the embryos. These results together strongly suggest that *ARF* can be activated by oxidative stress.

Suppression of ROS production inhibits zebrafish fin regeneration and *ARF* activation

To further examine the role of ROS in *ARF* activation, I sought to reduce ROS levels by using several chemical agents to target the NADPH oxidase (NOX) enzyme complex, which is a main source of cellular ROS (Lambeth, 2004, Love et al., 2013). I first tested the effect of 4'-hydroxy-3'-methoxyacetophenone (APO), diphenyleneiodonium chloride (DPI), MCI-186 (MCI), N-acetyl-L-cysteine (NAC), and VAS2870 (VAS) on zebrafish fin regeneration. APO disrupts the assembly of the NOX complex (Love et al., 2013). DPI targets the NOX subunit (Love et al., 2013, Gauron et al., 2013). Both MCI (Love et al., 2013) and NAC (North et al., 2010) are therapeutic anti-oxidants and free radical scavengers. Finally, VAS is a pharmacological inhibitor of NOX (Gauron et al., 2013). After 6 days of continual drug treatment, zebrafish fin regeneration was significantly inhibited in the presence of DPI, MCI, and VAS but not APO or NAC (Figure 18A). DPI reduced the length of the regenerate by 50% ($N=4$, $p<0.01$) and the area of the regenerate by 67% ($N=4$, $p<0.01$). MCI reduced the length of the regenerate by 55% ($N=4$, $p<0.01$) and the area of the regeneration by 58% ($N=4$, $p<0.05$). VAS reduced the length of the regenerate by 54% ($N=4$, $p<0.01$) and the area of the regeneration by 55% ($N=4$, $p<0.05$). While VAS was a potent inhibitor, it was not used in subsequent experiments due to toxicity concerns. These results were potentially confounding because inhibition of fin regeneration alone could potentially inhibit activation of *ARF*; it would not be definitely known that inhibition of ROS production directly inhibited the activation of *ARF* that occurs during fin regeneration. While continual treatment with APO or NAC did not significantly inhibit fin regeneration, I also tested other treatment regimens to determine if they would inhibit ROS production but not fin regeneration. When I treated adult zebrafish with the aforementioned chemical agents for only the first 24 hpa and then assessed fin regeneration at 6

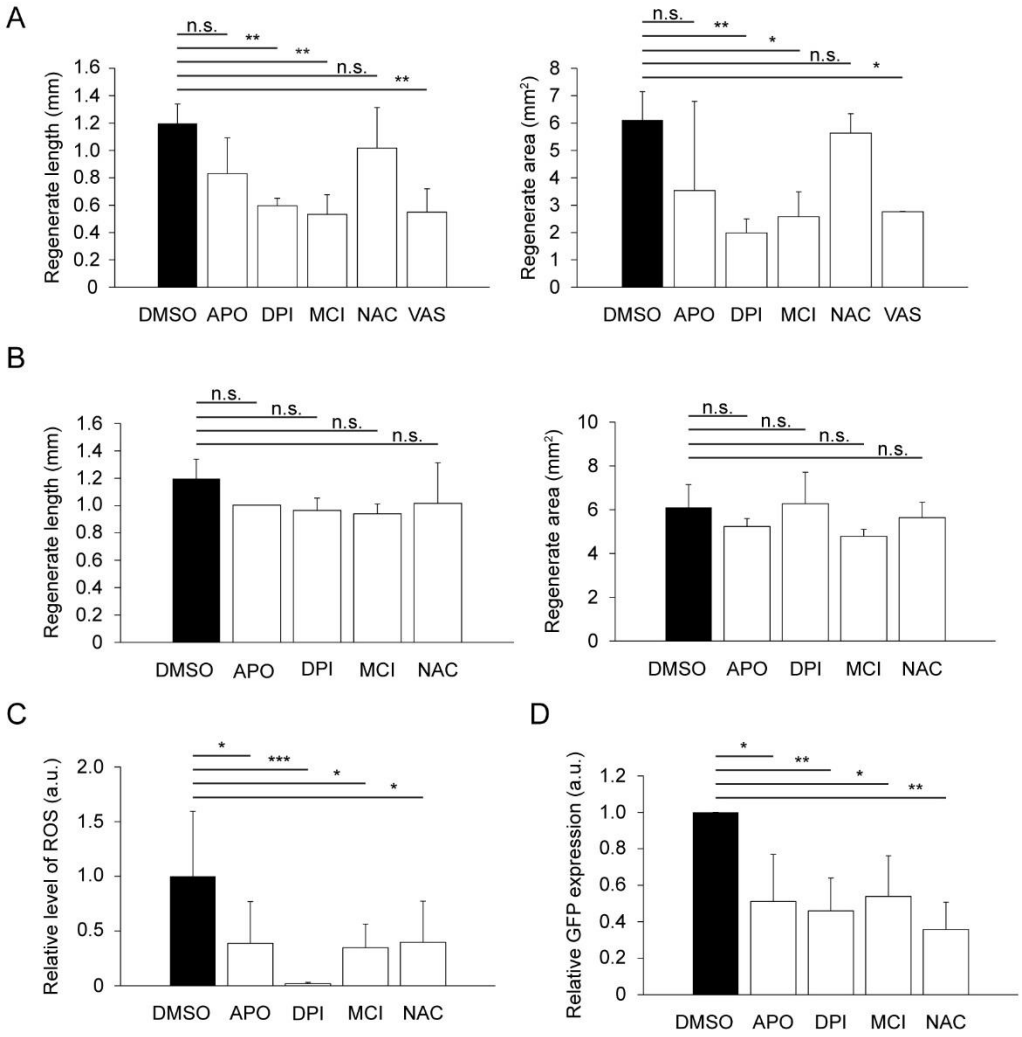

Figure 18. Inhibition of ROS production and signaling inhibits ARF activation with zebrafish fin regeneration. (A) Quantification of regenerate length and area at 6 dpa in zebrafish fins treated continuously with 200 μM APO, 2 μM DPI, 200 μM MCI, 200 μM NAC, or 2 μM VAS (0.1% DMSO). DPI, MCI, and VAS significantly inhibited fin regeneration in both length and area while APO and NAC did not (N=4, $p<0.01$). (B) Quantification of regenerate length and area at 6 dpa in zebrafish fins treated with 200 μM APO, 2 μM DPI, 200 μM MCI, or 200 μM NAC (0.1% DMSO) for the first 24 hpa only. No significant inhibition of fin regeneration was observed (N=4, $p>0.05$). (C) Quantification of H_2DCFDA staining to detect ROS production at 16 hpa in zebrafish fins treated with 200 μM APO, 2 μM DPI, 200 μM MCI, or 200 μM NAC (0.1% DMSO). All agents tested significantly inhibited ROS production (N=8, $p<0.05$). ROS levels were made relative to those observed in fins treated with the carrier, DMSO. (D) Quantification of GFP expression using qPCR at 2 dpa in *ARF*:GFP transgenic zebrafish fins treated continuously with 200 μM APO or 200 μM NAC or only for the first 24 hpa with 2 μM DPI or 200 μM MCI (0.1% DMSO). All agents tested significantly inhibited *ARF* activation (N=5, $p<0.05$). Values were normalized to β-actin transcripts and then made relative to those detected in fins treated with the carrier, DMSO. Results are shown as mean ± SD.

dpa, all of the agents tested did not significantly inhibit fin regeneration (Figure 18B). I chose to treat for the first 24 hpa only because ROS is observed only during the first 24 hpa (Gauron et al., 2013).

To confirm that the chemical agents tested were effective at reducing oxidative stress and ROS production, I amputated zebrafish fins, incubated the fish with APO, DPI, MCI, or NAC, and then assessed ROS levels with H_2DCFDA at 16 hpa. It was determined that all chemical agents tested significantly inhibited ROS production at 16 hpa (Figure 18C). APO inhibited ROS production by 62% ($N=8$, $p<0.05$). DPI inhibited ROS production by 98% ($N=8$, $p<0.001$). MCI inhibited ROS production by 65% ($N=8$, $p<0.05$), and NAC inhibited ROS production by 60% ($N=8$, $p<0.05$).

With the knowledge that ROS production is significantly inhibited when zebrafish are treated with all of the tested chemical agents, I sought to determine whether these agents could influence *ARF* activation during zebrafish fin regeneration. I amputated Tg(*ARF*:GFP) transgenic zebrafish fins and treated the fish with DMSO, APO, or NAC continuously for two days. Fish were also treated with DPI or MCI for the first 24 hpa only and then DMSO for the remainder of the experiment. Fin regenerates were harvested at 2 dpa, the time point at which GFP is most highly expressed, and GFP expression was analyzed by qPCR normalized to β-actin expression. All four of the chemical agents tested significantly reduced GFP expression at 2 dpa when compared to DMSO treated fins (Figure 18D). APO reduced GFP expression by 49% ($N=5$, $p<0.05$). DPI reduced GFP expression by 54% ($N=5$, $p<0.01$). MCI reduced GFP expression by 46% ($N=5$, $p<0.05$), and NAC reduced GFP expression by 64% ($N=5$, $p<0.01$).

Since NAC was able to significantly inhibit ROS production at 16 hpa and *ARF* activation during fin regeneration but not fin regeneration itself, I sought to determine if NAC

could dampen the effect of ARF on fin regeneration. Using the Tg(*ARF*:ARF) transgenic zebrafish line, I amputated fins and treated zebrafish with either DMSO or NAC continuously for six days. At 6 dpa, fin regenerate length and area were assessed, and it was determined that NAC treatment can significantly counteract the regeneration inhibition phenotype of *ARF*:ARF transgenic zebrafish (N=8, $p<0.01$) (Figure 19). Without NAC treatment, *ARF*:ARF fin regenerates were 0.69 mm ± 0.24 mm long and 2.85 mm^2 ± 1.29 mm^2 in area while NAC treated fins were 1.0 mm ± 0.16 mm long and 4.88 mm^2 ± 0.92 mm^2 in area, which constitutes an increase in length of approximately 45% and an increase in area of 71%.

The experiments included in this chapter, while ranging in focus from the evolutionary transition from ectothermy to endothermy to the role of oxidative stress in *ARF* activation during zebrafish fin regeneration, all shed light on the validity of a common hypothesis that *Arf* evolved to counteract the negative effects of a more metabolically active intracellular environment. The results of these experiments suggest that *Arf* evolved around the same as time as the transition from ectothermic to endothermic regulation. The results also indicate that oxidative stress and ROS activate *ARF* specifically. In all, the validity of my hypothesis seems sound.

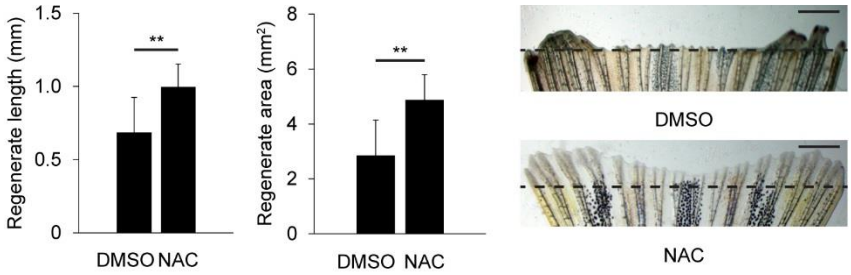

Figure 19. Treatment with N-acetyl-L-cysteine (NAC) suppresses *ARF* activation and rescues zebrafish fin regeneration. Quantification of regenerate length and area at 6 dpa in *ARF*:ARF fins treated with DMSO (0.1%) or 200 μM NAC (left; N=8 fins/condition, $p<0.01$). Representative images of fin regeneration at 6 dpa in *ARF*:ARF fins treated with DMSO (0.1%) or 200 μM NAC (right). Scale bars: 1 mm. Results are shown as mean ± SD.

Discussion

The results of the experiments included in this chapter provided some very interesting insights into potential pressures driving Arf evolution. My evolutionary analysis, while purely correlative, demonstrates that the transition of species from ectothermic and endothermic regulation overlaps very well with not only the presence of *Arf* in that species' genome, but also the relative regenerative ability of that species. Ectotherms tend to be more regenerative that endotherms, and ectotherms tend to lack *Arf* while endotherms do not. My cell culture experiments with mouse and zebrafish cells reinforce these observations. Mouse cells are endothermic and are highly sensitive to oxidative stress as demonstrated by the increased incidence of apoptosis and Arf expression with tBHP treatment. Zebrafish cells, however, are ectothermic, do not express Arf, and are not sensitive to oxidative stress. My experiments with *Arf*-/- cells demonstrate that *Arf* plays a large role in oxidative stress induced apoptosis, and suggests that endotherms may be more sensitive to oxidative because of *Arf*. The higher sensitivity of endotherms to oxidative stress agrees with my hypothesis that endotherms possess a more sensitive p53 axis due to the inclusion of *Arf*. The enhanced sensitivity of this axis is essential as it responds to and tightly controls potentially genotoxic oxidative stress in the form of excess ROS of which more is present due to the higher mitochondrial activity of endotherms.

With the knowledge that oxidative stress is essential for zebrafish fin regeneration (Gauron et al., 2013) and that oxidative stress may be a potential driver of Arf evolution, I investigated the role of ROS and oxidative stress in the activation of *ARF* during fin regeneration. I first sought to confirm the metabolic state of blastema cells. I expected blastema cells to be glycolytic because of their high rates of proliferation, which is reminiscent of cancer growth (Jones and Thompson, 2009). However, I was surprised to discover that blastema cells

are very oxidative during the first two days of regeneration and then quickly return to baseline. This peak in oxidative activity overlaps very well with the timing of blastema formation during zebrafish fin regeneration (Poss et al., 2003, Jones and Thompson, 2009). It is possible that ROS signaling is essential for blastema formation. The mechanism underlying ROS signaling is one of redox chemistry rather than protein interactions to cause post translational modifications (D'Autreaux and Toledano, 2007). It has been discovered that ROS can activate p38 mitogen-activated protein kinase (MAPK) (Finkel, 2011, D'Autreaux and Toledano, 2007), which can then activate a cascade of signaling ending with Rb pathway inhibition, E2f release, and potentially Arf activation.

The next set of experiments was focused on investigating whether oxidative stress and ROS signaling were capable of activating *ARF*. To induce oxidative stress in embryonic zebrafish, I treated 48 hpf Tg(*ARF*:GFP) embryos with 1 mM tBHP for 24 hours in the dark and assessed ROS production and gene expression changes at 72 hpf. I decided to use an embryonic model because I was concerned about the toxic effects of tBHP treatment on adult zebrafish and using embryos allowed us to keep the tBHP treatment regimen consistent between *in vivo* and *in vitro* experiments. After 24 hours of treatment, ROS was clearly detected in 72 hpf embryos, and ROS levels were comparable to those observed at 16 hpa during fin regeneration. When GFP expression was analyzed, significantly more GFP was detected with tBHP treatment. These results demonstrate that *ARF* activity is induced by oxidative stress.

I next used chemical agents to determine whether inhibition of ROS production or signaling can inhibit *ARF* activation with fin regeneration. I first tested the effect of continuous use of 4'-hydroxy-3'-methoxyacetophenone (APO), diphenyleneiodonium chloride (DPI), MCI-186 (MCI), N-acetyl-L-cysteine (NAC), or VAS2870 (VAS) on zebrafish fin regeneration and

discovered that DPI, MCI, and VAS significantly inhibited fin regeneration while APO and NAC did not. Since inhibition of fin regeneration is potentially confounding for the detection of inhibition of *ARF* activation with fin regeneration, I eliminated continuous use of DPI, MCI, or VAS as candidates that could conclusively answer whether inhibition of ROS production or signaling could inhibit *ARF* activation. Additionally, I eliminated VAS due to toxicity concerns. I also tested other treatment regimens, and treatment with DPI or MCI for the first 24 hpa only did not affect fin regeneration. I continued with this treatment regimen for DPI and MCI. I next tested the inhibitory ability of APO, DPI, MCI, and NAC on ROS levels during fin regeneration, and I observed that all of the candidates significantly reduced ROS levels at 16 hpa. Finally, I treated the ability of continuous use of APO or NAC or initial use of DPI or MCI to inhibit GFP expression during fin regeneration in Tg(*ARF*:GFP) transgenic zebrafish. All candidates tested significantly reduced GFP expression, but the one that stood out the most was NAC.

NAC had the smallest effect on fin regeneration, significantly reduced ROS levels at 16 hpa, and had the largest effect on GFP expression. It may seem counterintuitive that NAC can inhibit ROS and *ARF* activation but not fin regeneration since oxidative stress and ROS production are essential for fin regeneration (Gauron et al., 2013), but NAC is a ROS scavenger and acts to mop up excess ROS (North et al., 2010) instead of directly inhibiting the NOX complex like APO, DPI, or VAS (Gauron et al., 2013, Love et al., 2013). However, the mechanism of action for NAC must be unique because MCI is also a ROS scavenger (Love et al., 2013), but it inhibits fin regeneration when used continuously. NAC is a thiol and acts to reduce extracellular cystine to cysteine and as a source of SH metabolites (Kelly, 1998). It is theorized that the ability of NAC to act as a source of SH groups is the basis of its ability to act directly on ROS and inhibit any downstream signaling (De Vries and De Flora, 1993). In the

clinic, NAC is used widely as an antioxidant in the contexts of HIV infection, cancer, heart disease, cigarette smoking, acetaminophen-induced hepatotoxicity, and as a prophylactic chelating agent when radiocontrast agents must be used (Kelly, 1998). As my experiments with *ARF*:ARF transgenic zebrafish showed, NAC can also counteract the inhibitory effect of ARF on zebrafish fin regeneration. This result is exciting for a number of reasons. It could shed light on the differences in signaling present during development and regeneration for one. *ARF* is not active during development, but it is during regeneration. Oxidative stress is not present during development, but it is during regeneration (Gauron et al., 2013). It is possible that oxidative stress and ROS signaling represents a boost in signaling necessary for *ARF* activation, and the inhibition of oxidative stress, ROS signaling, and *ARF* activation by NAC suggest that this may be the case. The inhibition of *ARF* activation by NAC may also elucidate the signaling threshold for *ARF* activation. By reducing ROS signaling, NAC was able to bypass *ARF* surveillance. I have also observed that in *ARF*:ARF transgenic zebrafish the dorsal lobe of the caudal fin is more affected than the ventral lobe. The dorsal lobe is slight longer than the ventral lobe, and when cut at the same plane, the dorsal lobe most likely experiences a more intense regenerative response because more tissue needs to be replaced (Lee et al., 2005). This difference in fin length could equate to the difference in signaling required to surpass the signaling threshold of *ARF*, and future experiments should be focused on determining this activation threshold. Another future experiment worth pursuing is determining if NAC treatment can exasperate tumorigenesis. If *ARF* activation is inhibited by NAC treatment, then it can be predicted that *ARF* would be less able to prevent or counteract cancer progression, for instance, in a zebrafish tumor model of hepatocellular carcinoma.

The experiments included in this chapter validate my hypothesis that *Arf* evolved to counteract the negative effects of a more metabolically active intracellular environment. My evolutionary analysis suggests that the evolution of *Arf* and the transition from ectothermic to endothermic regulation occurred around the same time. My zebrafish experiments also confirm that oxidative stress is present during regeneration but not development, and they further indicate that *ARF* is specifically activated by oxidative stress and ROS signaling. In all, the evolution of *Arf* strengthened the p53 axis of regulation to counteract cellular insults be they internal or external.

Discussion

In this dissertation I investigated the role of Arf in zebrafish epimorphic fin regeneration, the role of Arf in a mammalian model of epimorphic regeneration, the role of the Rb pathway in the maintenance of the differentiated state in the context of zebrafish epimorphic fin regeneration, and finally potential evolutionary pressures driving the evolution of *Arf*.

With regards to the role of Arf in zebrafish epimorphic fin regeneration, I have experimentally tested the hypothesis that tumor suppressor evolution may impact regenerative capacity. I found that the core mammalian tumor suppressor *ARF* senses regeneration signals and specifically responds to negatively alter the proliferative balance in the zebrafish blastema, greatly perturbing regeneration. My findings provide the first *in vivo* experimental evidence that evolution of tumor suppressors can negatively impact solid tissue regeneration potential.

Although the core tumor suppressors as a whole support regenerative processes, the properties of *ARF* identified in this study are at odds with epimorphic regeneration. This new example of antagonistic pleiotropy adds to previously recognized trade-off characteristics of tumor suppressor genes affecting mammalian stem cell function, reviewed in (Pardal et al., 2005, Greaves, 2007, Pomerantz and Blau, 2013, Rodier et al., 2007) and shows that *ARF* antagonistic properties also manifest in the context of the blastema. The evidence that ARF is a critical tumor suppressor in mammals (Sherr, 2006, Sharpless, 2005) but opposes regeneration functions (Sharpless and DePinho, 2007), this study) suggests that the selective pressure that has driven the evolution of ARF has primarily enhanced tumor suppression either at the expense of or in the absence of regeneration pressures. Although my experiments and those of others (Gemberling et al., 2013, Poss et al., 2003) show that the regenerative capacity of zebrafish is vulnerable to single gene alterations, whether altering function of a single gene in mammals would induce the

emergence of robust epimorphic regenerative capacity is a much more complex issue. Indeed, the multifactorial genetic differences of highly and less regenerative vertebrates make it unlikely that manipulation of a single gene could enable regeneration. It is notable, however, that *Cdkn1a* (*p21*) knockout mice do possess a somewhat enhanced ability to regenerate solid structures (Heber-Katz et al., 2013, Clark et al., 1998) such as pinnae, which lack the complex tissue structure of a digit, but nonetheless, demonstrate that alteration of cellular growth control mechanisms can impact regeneration. Moreover, the importance of active repression of ARF to maintain stem cell function (Molofsky et al., 2005), and of ARF reduction to facilitate dedifferentiation (Pajcini et al., 2010) have been documented.

Among the core tumor suppressor genes that are frequently inactivated in mammalian tumors, *ARF* is unique in that it does not have orthologues represented in most vertebrates including highly regenerative species. By contrast, *Tp53*, *Pten*, and *Ink4a* have distant orthologues, being present in invertebrates and vertebrates alike. The transgenesis approach I used to study ARF in fin regeneration made it possible for us to study ARF with its human regulatory components but without increasing *CDKN2A* CKI gene dosage which could have been a complicating factor in a transgenic harboring the entire *CDKN2A (INK4A/ARF)* locus. This study extends our group's previous observations (Pajcini et al., 2010) that ARF prevents dedifferentiation in muscle cells in culture and provides new evidence that ARF functions *in vivo* to oppose tissue regeneration. Future experiments will determine whether ARF prevents dedifferentiation *in vivo*, such as the dedifferentiation of osteoblasts in regenerating fins, or whether it acts on proliferating blastema cells after they have dedifferentiated. Combined, my findings suggest that zebrafish cells are more promiscuous in terms of tolerance to high levels of mitogenic activity, thus permitting the cellular processes required for epimorphic regeneration. It

follows that regenerating cells in organisms that have an *ARF* gene would need to prevent ARF activation or would be inherently more restricted in these activities.

I found that ARF recapitulates its core mammalian mechanistic functions in zebrafish cells and tissues. As in mammals, when ARF is overexpressed in zebrafish cells, it associates with Mdm2, stabilizes Tp53, and induces cell cycle arrest or apoptosis. This functional conservation over an evolutionary distance demonstrates that cross-species genetic variations can be experimentally examined in the study of regeneration. When ARF expression is driven by its endogenous human promoter in zebrafish cells, activation of the p53 axis occurs specifically in the blastema-regeneration scenario. In the developing or adult uninjured state, E2f1 is sequestered and inhibited by Rb1, and *ARF* is inactive. However, during blastema formation and regeneration, Rb1 hyperphosphorylation is associated with sufficient free E2f1 to activate *ARF*, which inhibits fin regeneration via a Tp53-dependent mechanism. My findings and model are in agreement with the recent proposal that in salamanders the absence of ARF permits downregulation of Tp53 during blastema formation (Yun et al., 2013). The responsiveness of *ARF* to the Rb pathway proliferative signaling characteristic of zebrafish fin regeneration implies that similar mitogenic signaling occurring in a mammalian context would be detected as aberrant, activate ARF-MDM2-TP53 tumor suppressor mechanisms, and oppose regeneration. My findings are compatible with previous mouse studies showing that ARF is a potent tumor suppressor that is dispensable for normal development (Serrano et al., 1996, Kamijo et al., 1997). Although the majority of tumor suppressors probably function in regeneration as they do in normal development, the findings of the present study indicate that *ARF* represents an unusual departure from that paradigm in that the properties that cause it to respond specifically to tumorigenesis also cause it to distinguish regeneration contexts from developmental ones.

I also found that ARF recapitulates its core mammalian mechanistic functions in the context of tumorigenesis and adds to the tumor suppressor repertoire of transgenic zebrafish. Using a zebrafish model of hepatocellular carcinoma (HCC) that specifically expresses constitutively active β-catenin in the liver (Evason et al., 2015), I discovered that *ARF* not only detected oncogenic signaling, but also responded to it to prevent histological anomalies and reduce tumor burden. While ARF did not prevent all signs of disease, it was effective in an objectively severe model of HCC (Evason et al., 2015). This line of experimentation confirms that while ARF may serve as a regeneration suppressor in the context of zebrafish fin regeneration, its function as a tumor suppressor is conserved.

With regards to the role of Arf in a mammalian model of epimorphic regeneration, the critical limit for successful regeneration after digit tip amputation seems to lie distal to the nail bed, distal to the distal interphalangeal joint. The location of this critical limit is most likely due to stem cells in the nail bed matrix (Takeo et al., 2013, Rinkevich et al., 2011, Zhao and Neufeld, 1995). These epithelial stem cells require Wnt activation, which also assists in the attraction of nerves to promote mesenchymal blastema formation and growth leading to the regeneration of the digit tip (Takeo et al., 2013). If the activation of the nail bed stem cell pool is the predominant driving force behind digit tip regeneration, then my observations of regenerative failure proximal to this pool are in agreement with and lend credence to the literature. Most epithelial stem cells expresses Bmi1, a member of the Polycomb Repressive Complex (Pietersen et al., 2008, Tanaka et al., 2013, Tian et al., 2011), so it would not be very surprising if nail bed stem cells express Bmi1 as well. Bmi1 is a known negative regulator of the *Cdkn2a* locus (Molofsky et al., 2005), so it is possible that the lack of *Arf* or *Cdkn2a* in my experiments would

not promote regeneration in a context in which it is normally transcriptionally repressed i.e. the nail bed.

Amputations made proximal to the nail bed seem to default to a wounding healing response rather than a regenerative one. It is possible that Wnt signaling and subsequent nerve attraction influence the fate of cells responding to the injury as well as the surrounding mesenchyme. It has recently been identified that macrophages are essential for limb regeneration in salamanders (Godwin et al., 2013) and fin regeneration in zebrafish (Petrie et al., 2014). Ablation of macrophages caused dysregulation of blastema markers, stunted activation of MMP9 and MMP3, and a lack of matrix remodeling (Godwin et al., 2013), which is necessary for successful limb regeneration (Vinarsky et al., 2005). Macrophage matrix metalloprotease genes are implicated with successful limb regeneration, and their expression is sensitive to denervation (Yang et al., 1999). If nerves are recruited by Wnt signaling or the paracrine factor(s) secreted from Wnt-activated cells in the nail bed (Takeo et al., 2013), then that could explain why a presumed blastema forms there and not at locations proximal to the nail bed. Nerves are essential for regeneration and their recruitment seems to be an initiator of blastema formation (Mullen et al., 1996); the exact mechanism responsible for nerve-dependent promotion of blastema formation remains an open and actively investigated issue in regeneration biology.

With regards to blastema formation and the mesenchyme that contributes to it, there has been a fair amount of debate whether or not the cell mass that gives rise to the mammalian digit tip regenerate is analogous to blastemas observed during urodele amphibian and teleost fish regeneration and can be called a true blastema. Blastema formation in urodele amphibians and teleost fish involves the process of dedifferentiation (Han et al., 2005), which is the term ascribed to mature, post-mitotic cells at the site of injury reverting to a more proliferative, but still fate-

restricted, state. Since digit tip regeneration proceeds from stem or progenitor cells in the nail bed instead of dedifferentiation, many groups consider mammal regeneration to be devoid of a true blastema (Muneoka et al., 2008, Agrawal et al., 2010, Brockes and Kumar, 2005, Rinkevich et al., 2011, Reginelli et al., 1995). Other groups disagree and consider the mass of proliferative cells at the digit tip a blastema regardless of cellular origin (Fernando et al., 2011, Han et al., 2008).

It is likely that proximal amputations default to a wound healing response because the lack of signaling essential for nerve recruitment and matrix remodeling renders the injury site non-permissive for a blastema-like structure to form regardless of *Arf* or *Cdkn2a* dosage. Lack of *Arf* or *Cdkn2a* may expedite proliferative events, but regeneration requires more than proliferation to be successful. The first step to successful regeneration is the assembly of a permissive niche. Since this presumably does not occur at proximal amputation sites, cells that would contribute to the regenerate are not activated nor aggregated. The lack of *Arf* or *Cdkn2a* does not promote regeneration in contexts where it does not normally occur because the proliferative advantage of *Arf* or *Cdkn2a* loss is never realized; a blastema-like structure is never formed at proximal amputation planes.

Additionally, lack of key regulators of the differentiated state such as *Arf* or *Cdkn2a* could conceivably be detrimental to regeneration. Regeneration requires a permissive niche, proliferative ability, and tight developmental regulation in order to reproduce near identical copies of lost structures. This tight regulation is essential for cellular differentiation at the end of successful regeneration, and it would most likely be disrupted in the context of *Arf* or *Cdkn2a* loss.

While out of the scope of this dissertation, an interesting and relatively unexplored area of regeneration regards the mechanisms by which mammals can regenerate solid organs such as the liver in the presence of *Arf*. In keeping with my hypothesis that *Arf* plays a large role in regenerative success, I hypothesize that *Arf* is somehow being inhibited during liver regeneration. Several groups have reported that hepatocyte proliferation drives liver regeneration (Michalopoulos, 2007, Mitchell and Willenbring, 2008) and that microRNAs control hepatocyte proliferation (Song et al., 2010). It has also been reported that *Arf* is targeted and inhibited by a number of microRNAs (Mudhasani et al., 2008) including miR-24 (To et al., 2012) and miR-125b (Amir et al., 2013). However, microRNAs can also support the differentiation-promoting activities of *Arf* depending on cellular contexts including miR-34a (Iqbal et al., 2014) and even miR-125b (Liang et al., 2010). Long non-coding RNAs could also play a role in *Arf* inhibition, particularly the long non-coding RNA ANRIL, which is a product of the INK4 locus (Pasmant et al., 2011, Wan et al., 2013). ANRIL has been shown to directly bind the *CDKN2B* transcript and is capable of recruiting the Polycomb Repressor Complex (PRC) to inhibit expression from the INK4 locus (Kotake et al., 2011, Yap et al., 2010). With all of this in mind, it seems likely that *Arf* and other Ink4 products could be inhibited during liver regeneration.

With regards to the role of the Rb pathway in the maintenance of the differentiated state in the context of zebrafish epimorphic fin regeneration, knockdown of *rb1* with a Morpholino oligomer (MO) injected and electroporated into fin blastemas was surprisingly effective. I had anticipated that the other Rb family members, *rbl1* and *rbl2*, would compensate for the loss of *rb1*. The effect size of the *rb1* knockdown suggests that *rbl1* and *rbl2* are not major players and are incapable of compensating for an acute loss of *rb1*. One limitation of the MO knockdown experiments was that only already formed blastemas could be injected. I attempted to inject

uninjured fin tissue to determine if *rb1* loss could promote the initial phases of regeneration, particularly dedifferentiation, but it proved to be too technically difficult. Another limitation is that MOs are only effective for 48 hours post injection and electroporation (Thummel et al., 2006). The efficiency of MO incorporation is another thing to consider because the technical process of injecting the blastemas and then electroporating the fin tissue can lead to variability in observed phenotypes.

Even with these limitations, the experiments strongly suggested a role for Rb1 during the redifferentiation and outgrowth phase of zebrafish fin regeneration. With *rb1* knockdown, proliferation increased, bone development was reduced, and the incidence of apoptosis remained constant. These results signify that without Rb1, osteoblasts are not able to redifferentiate, which could lead to the observed inhibition of regeneration because there is no new tissue on which to grow. Regeneration is highly controlled not only so that cells can proliferate and contribute to the blastema without causing cancer, but also so that cells can appropriately differentiate to form the stable, mature regenerate. As zebrafish regeneration proceeds, the tailing edge of the proximal blastema begins to differentiate, thus providing the blastema with tissue on which to grow (Poss et al., 2003). This appropriately timed differentiation promotes outgrowth of the regenerate, and disruption of this process will predictably lead to regenerative failure.

The creation of and experiments with the *hs*:Rb1 transgenic zebrafish line did not produce the desired effect on differentiation reinforcement, but they did teach us about the cellular plasticity of zebrafish cells dedifferentiating to contribute to the blastema. Even though Rb1 was overexpressed with heat shock in this line, it was not enough to prevent dedifferentiation. This result, while negative, is telling. It suggests that zebrafish cells are incredibly plastic. The amount of signaling leading to Rb1 inhibition is so great that it can

overcome an excess of Rb1. While there must be a saturation point for the cyclin-dependent kinases that inhibit Rb1, the limit seems to be very high.

The Tg(*bglap*:CreER^{T2}) transgenic zebrafish line that I created was not an effective conditional, inducible Cre line. However, I do not believe that the problem lies with the transgene construct. The promoter sequences were subcloned from an existing transgene (Singh et al., 2012), and the CreER^{T2} cassette was subcloned from another functional plasmid. I think that *bglap* is the best promoter to use since it is active in only mature osteoblasts. However, other osteoblast-specific Cre lines do exist and have been published. One example is the Tg(*osterix*:mTagBFP-2A-CreER)^{pd45} transgenic line (Singh et al., 2012), which uses the intermediate osteoblast promoter *osterix* (*sp7*) to drive CreER expression.

I was successful in using the CRISPR/Cas9 system to mutate the first intron of zebrafish *rb1* to insert a silent gene trap with the intension of creating a nonsense allele with Cre-mediated recombination. However, the gene trap was too silent; when gene trap containing embryos were injected with Cre mRNA, no recombination was detected in the form of blue fluorescence from the included mTagBFP2 tag. I believe that the failure of the gene trap can be attributed to the included splice acceptor. I do not think that the gene trap splice acceptor was strong enough to outcompete the splice acceptor of the second exon of *rb1*.

I used a two-step mutation/insertion strategy to insert the gene trap into the first intron of *rb1* because, at the time, only short sequences had been reported to have been successfully inserted into particular genetic loci with a reasonable degree of efficiency. However, that is no longer the case. Several groups have used homologous recombination-like techniques to insert whole reporter genes or promoter regions to create knock-in transgenic zebrafish (Auer et al., 2014, Kimura et al., 2014).

With regards to potential evolutionary pressures driving the evolution of *Arf*, my evolutionary analysis, while purely correlative, demonstrates that the transition of species from ectothermic and endothermic regulation overlaps very well with not only the presence of *Arf* in that species' genome, but also the relative regenerative ability of that species. Ectotherms tend to be more regenerative that endotherms, and ectotherms tend to lack *Arf* while endotherms do not. My cell culture experiments with mouse and zebrafish cells reinforce these observations. Mouse cells are endothermic and are highly sensitive to oxidative stress as demonstrated by the increased incidence of apoptosis and Arf expression with tBHP treatment. Zebrafish cells, however, are ectothermic, do not express Arf, and are not sensitive to oxidative stress. My experiments with *Arf*-/- cells demonstrate that *Arf* plays a large role in oxidative stress induced apoptosis, and suggests that endotherms may be more sensitive to oxidative because of *Arf*. The higher sensitivity of endotherms to oxidative stress agrees with my hypothesis that endotherms possess a more sensitive p53 axis due to the inclusion of *Arf*. The enhanced sensitivity of this axis is essential as it responds to and tightly controls potentially genotoxic oxidative stress in the form of excess ROS of which more is present due to the higher mitochondrial activity of endotherms.

With the knowledge that oxidative stress is essential for zebrafish fin regeneration (Gauron et al., 2013) and that oxidative stress may be a potential driver of Arf evolution, I investigated the role of ROS and oxidative stress in the activation of *ARF* during fin regeneration. I first sought to confirm the metabolic state of blastema cells. I expected blastema cells to be glycolytic because of their high rates of proliferation, which is reminiscent of cancer growth (Jones and Thompson, 2009). However, I was surprised to discover that blastema cells are very oxidative during the first two days of regeneration and then quickly return to baseline.

This peak in oxidative activity overlaps very well with the timing of blastema formation during zebrafish fin regeneration (Poss et al., 2003, Jones and Thompson, 2009). It is possible that ROS signaling is essential for blastema formation. The mechanism underlying ROS signaling is one of redox chemistry rather than protein interactions to cause post translational modifications (D'Autreaux and Toledano, 2007). It has been discovered that ROS can activate p38 mitogen-activated protein kinase (MAPK) (Finkel, 2011, D'Autreaux and Toledano, 2007), which can then activate a cascade of signaling ending with Rb pathway inhibition, E2f release, and potentially Arf activation.

The next set of experiments was focused on investigating whether oxidative stress and ROS signaling were capable of activating *ARF*. To induce oxidative stress in embryonic zebrafish, I treated 48 hpf Tg(*ARF*:GFP) embryos with 1 mM tBHP for 24 hours in the dark and assessed ROS production and gene expression changes at 72 hpf. I decided to use an embryonic model because I was concerned about the toxic effects of tBHP treatment on adult zebrafish and using embryos allowed us to keep the tBHP treatment regimen consistent between *in vivo* and *in vitro* experiments. After 24 hours of treatment, ROS was clearly detected in 72 hpf embryos, and ROS levels were comparable to those observed at 16 hpa during fin regeneration. When GFP expression was analyzed, significantly more GFP was detected with tBHP treatment. These results demonstrate that *ARF* activity is induced by oxidative stress.

I next used chemical agents to determine whether inhibition of ROS production or signaling can inhibit *ARF* activation with fin regeneration. I first tested the effect of continuous use of 4'-hydroxy-3'-methoxyacetophenone (APO), diphenyleneiodonium chloride (DPI), MCI-186 (MCI), N-acetyl-L-cysteine (NAC), or VAS2870 (VAS) on zebrafish fin regeneration and discovered that DPI, MCI, and VAS significantly inhibited fin regeneration while APO and NAC

did not. Since inhibition of fin regeneration is potentially confounding for the detection of inhibition of *ARF* activation with fin regeneration, I eliminated continuous use of DPI, MCI, or VAS as candidates that could conclusively answer whether inhibition of ROS production or signaling could inhibit *ARF* activation. Additionally, I eliminated VAS due to toxicity concerns. I also tested other treatment regimens, and treatment with DPI or MCI for the first 24 hpa only did not affect fin regeneration. I continued with this treatment regimen for DPI and MCI. I next tested the inhibitory ability of APO, DPI, MCI, and NAC on ROS levels during fin regeneration, and I observed that all of the candidates significantly reduced ROS levels at 16 hpa. Finally, I treated the ability of continuous use of APO or NAC or initial use of DPI or MCI to inhibit GFP expression during fin regeneration in Tg(*ARF*:GFP) transgenic zebrafish. All candidates tested significantly reduced GFP expression, but the one that stood out the most was NAC.

NAC had the smallest effect on fin regeneration, significantly reduced ROS levels at 16 hpa, and had the largest effect on GFP expression. It may seem counterintuitive that NAC can inhibit ROS and *ARF* activation but not fin regeneration since oxidative stress and ROS production are essential for fin regeneration (Gauron et al., 2013), but NAC is a ROS scavenger and acts to mop up excess ROS (North et al., 2010) instead of directly inhibiting the NOX complex like APO, DPI, or VAS (Gauron et al., 2013, Love et al., 2013). However, the mechanism of action for NAC must be unique because MCI is also a ROS scavenger (Love et al., 2013), but it inhibits fin regeneration when used continuously. NAC is a thiol and acts to reduce extracellular cystine to cysteine and as a source of SH metabolites (Kelly, 1998). It is theorized that the ability of NAC to act as a source of SH groups is the basis of its ability to act directly on ROS and inhibit any downstream signaling (De Vries and De Flora, 1993). In the clinic, NAC is used widely as an antioxidant in the contexts of HIV infection, cancer, heart

disease, cigarette smoking, acetaminophen-induced hepatotoxicity, and as a prophylactic chelating agent when radiocontrast agents must be used (Kelly, 1998). As my experiments with *ARF*:ARF transgenic zebrafish showed, NAC can also counteract the inhibitory effect of ARF on zebrafish fin regeneration. This result is exciting for a number of reasons. It could shed light on the differences in signaling present during development and regeneration for one. *ARF* is not active during development, but it is during regeneration. Oxidative stress is not present during development, but it is during regeneration (Gauron et al., 2013). Is possible that oxidative stress and ROS signaling represents a boost in signaling necessary for *ARF* activation, and the inhibition of oxidative stress, ROS signaling, and *ARF* activation by NAC suggest that this may be the case. The inhibition of *ARF* activation by NAC may also elucidate the signaling threshold for *ARF* activation. By reducing ROS signaling, NAC was able to bypass *ARF* surveillance.

Arf may have evolved to protect cells from potentially harmful factors like ROS, but its evolution was a double edged sword. *Arf* functions to prevent cancer, but it surveils proliferative activity so finely that it can negatively affect stem cell function and may cause aging as a result (Sharpless and DePinho, 2007, He et al., 2009). Tumor suppressors are essential for genomic integrity of stem cells, and they help to balance factors promoting self-renewal to prevent tumorigenesis. However, with age, expression of p16Ink4a and Arf increases and reduces stem and progenitor cell frequency and function in a variety of tissues (He et al., 2009). Increased expression of these proteins has also been associated with senescence, a G0 cellular growth state where the cell can never reenter the cell cycle. Senescence is thought to be a cancer prevention mechanism, but it is also associated with aging (Sharpless and DePinho, 2007). It seems as *Arf* dosage increases, stem cell function decreases, which agrees with my observation that Arf is a regeneration suppressor. Cells with *Arf*, such as mammalian cells, are less plastic and less

capable of regeneration, which is most likely a result of decreased stem and progenitor cell function.

In this dissertation, I showed how examination of zebrafish that are humanized with respect to candidate regeneration modifiers is informative for understanding disparate regenerative capacities. Such an approach should prove useful for examining other candidate genes and pathways of interest. My findings with respect to ARF strongly suggest that it is a barrier to mammalian epimorphic regeneration because it interprets the regeneration context as similar to tumorigenesis. It follows conceptually that approaches to induce epimorphic regeneration clinically would need to disrupt ARF-MDM2-TP53 axis activation. I also showed that genetic disruption of *Arf* in the context of mammalian digit tip regeneration does not produce a more highly regenerative situation; mammalian regeneration does not proceed most likely because a true blastema does not form. I identified roles for Rb1 during zebrafish fin regeneration. It is essential during the redifferentiation and outgrowth phase of regeneration, and it may have a deeply involved role in dedifferentiation as well. Additionally, the evolutionary and zebrafish fin regeneration experiments included here validate my hypothesis that *Arf* evolved to counteract the negative effects of a more metabolically active intracellular environment. My evolutionary analysis suggests that the evolution of *Arf* and the transition from ectothermic to endothermic regulation occurred around the same time. My zebrafish experiments also confirm that oxidative stress is present during regeneration but not development, and they further indicate that *ARF* is specifically activated by oxidative stress and ROS signaling. In all, ARF is a double edged sword. It is essential for cancer prevention, but it prevents epimorphic regeneration as well.

References

AGRAWAL, V., JOHNSON, S. A., REING, J., ZHANG, L., TOTTEY, S., WANG, G., HIRSCHI, K. K., BRAUNHUT, S., GUDAS, L. J. & BADYLAK, S. F. 2010. Epimorphic regeneration approach to tissue replacement in adult mammals. *Proc Natl Acad Sci U S A,* 107**,** 3351-5.

AMIR, S., MA, A. H., SHI, X. B., XUE, L., KUNG, H. J. & DEVERE WHITE, R. W. 2013. Oncomir miR-125b suppresses p14(ARF) to modulate p53-dependent and p53-independent apoptosis in prostate cancer. *PLoS One,* 8**,** e61064.

AUER, T. O., DUROURE, K., DE CIAN, A., CONCORDET, J. P. & DEL BENE, F. 2014. Highly efficient CRISPR/Cas9-mediated knock-in in zebrafish by homology-independent DNA repair. *Genome Res,* 24**,** 142-53.

BELYI, V. A., AK, P., MARKERT, E., WANG, H., HU, W., PUZIO-KUTER, A. & LEVINE, A. J. 2010. The origins and evolution of the p53 family of genes. *Cold Spring Harb Perspect Biol,* 2**,** a001198.

BERGHMANS, S., MURPHEY, R. D., WIENHOLDS, E., NEUBERG, D., KUTOK, J. L., FLETCHER, C. D., MORRIS, J. P., LIU, T. X., SCHULTE-MERKER, S., KANKI, J. P., PLASTERK, R., ZON, L. I. & LOOK, A. T. 2005. tp53 mutant zebrafish develop malignant peripheral nerve sheath tumors. *Proc Natl Acad Sci U S A,* 102**,** 407-12.

BERKERS, C. R., MADDOCKS, O. D., CHEUNG, E. C., MOR, I. & VOUSDEN, K. H. 2013. Metabolic regulation by p53 family members. *Cell Metab,* 18**,** 617-33.

BERMAN, S. D., YUAN, T. L., MILLER, E. S., LEE, E. Y., CARON, A. & LEES, J. A. 2008. The retinoblastoma protein tumor suppressor is important for appropriate osteoblast differentiation and bone development. *Mol Cancer Res,* 6**,** 1440-51.

BERTRAND, J. Y., CHI, N. C., SANTOSO, B., TENG, S., STAINIER, D. Y. & TRAVER, D. 2010. Haematopoietic stem cells derive directly from aortic endothelium during development. *Nature,* 464**,** 108-11.

BORGENS, R. B. 1982. Mice regrow the tips of their foretoes. *Science,* 217**,** 747-50.

BROCKES, J. P. & KUMAR, A. 2002. Plasticity and reprogramming of differentiated cells in amphibian regeneration. *Nat Rev Mol Cell Biol,* 3**,** 566-74.

BROCKES, J. P. & KUMAR, A. 2005. Appendage regeneration in adult vertebrates and implications for regenerative medicine. *Science,* 310**,** 1919-23.

BROCKES, J. P. & KUMAR, A. 2008. Comparative aspects of animal regeneration. *Annu Rev Cell Dev Biol,* 24**,** 525-49.

BURGE, C. & KARLIN, S. 1997. Prediction of complete gene structures in human genomic DNA. *J Mol Biol,* 268**,** 78-94.

CHARGE, S. B. & RUDNICKI, M. A. 2004. Cellular and molecular regulation of muscle regeneration. *Physiol Rev,* 84**,** 209-38.

CHIN, L., POMERANTZ, J. & DEPINHO, R. A. 1998. The INK4a/ARF tumor suppressor: one gene--two products--two pathways. *Trends Biochem Sci,* 23**,** 291-6.

CHITRAMUTHU, B. P. & BENNETT, H. P. 2013. High resolution whole mount in situ hybridization within zebrafish embryos to study gene expression and function. *J Vis Exp***,** e50644.

CHOORAPOIKAYIL, S., OVERVOORDE, J. & DEN HERTOG, J. 2013. Deriving cell lines from zebrafish embryos and tumors. *Zebrafish,* 10**,** 316-25.

CLARK, L. D., CLARK, R. K. & HEBER-KATZ, E. 1998. A new murine model for mammalian wound repair and regeneration. *Clin Immunol Immunopathol,* 88**,** 35-45.

D'AUTREAUX, B. & TOLEDANO, M. B. 2007. ROS as signalling molecules: mechanisms that generate specificity in ROS homeostasis. *Nat Rev Mol Cell Biol,* 8**,** 813-24.

DAMALAS, A., VELIMEZI, G., KALAITZAKIS, A., LIONTOS, M., PAPAVASSILIOU, A. G., GORGOULIS, V. & ANGELIDIS, C. 2011. Loss of p14(ARF) confers resistance to heat shock- and oxidative stress-mediated cell death by upregulating beta-catenin. *Int J Cancer,* 128**,** 1989-95.

DE VRIES, N. & DE FLORA, S. 1993. N-acetyl-l-cysteine. *J Cell Biochem Suppl,* 17F**,** 270-7.

DEL ARROYO, A. G., EL MESSAOUDI, S., CLARK, P. A., JAMES, M., STOTT, F., BRACKEN, A., HELIN, K. & PETERS, G. 2007. E2F-dependent induction of p14ARF during cell cycle re-entry in human T cells. *Cell Cycle,* 6**,** 2697-705.

DINSMORE, C. E. & AMERICAN SOCIETY OF ZOOLOGISTS. 1991. *A History of regeneration research : milestones in the evolution of a science,* Cambridge England ; New York, Cambridge University Press.

EVASON, K. J., FRANCISCO, M. T., JURIC, V., BALAKRISHNAN, S., LOPEZ PAZMINO, M. P., GORDAN, J. D. K., S., SPITSBERGEN, J., GOGA, A. & STAINIER, D. Y. R. 2015. Identification of Chemical Inhibitors of beta-Catenin-Driven Liver Tumorigenesis in Zebrafish. *PLoS Genet*.

FARIA, M., NAVAS, J. M., SOARES, A. M. & BARATA, C. 2014. Oxidative stress effects of titanium dioxide nanoparticle aggregates in zebrafish embryos. *Sci Total Environ,* 470-471**,** 379-89.

FERNANDO, W. A., LEININGER, E., SIMKIN, J., LI, N., MALCOM, C. A., SATHYAMOORTHI, S., HAN, M. & MUNEOKA, K. 2011. Wound healing and blastema formation in regenerating digit tips of adult mice. *Dev Biol,* 350**,** 301-10.

FINKEL, T. 2011. Signal transduction by reactive oxygen species. *J Cell Biol,* 194**,** 7-15.

FLICEK, P., AMODE, M. R., BARRELL, D., BEAL, K., BILLIS, K., BRENT, S., CARVALHO-SILVA, D., CLAPHAM, P., COATES, G., FITZGERALD, S., GIL, L., GIRON, C. G., GORDON, L., HOURLIER, T., HUNT, S., JOHNSON, N., JUETTEMANN, T., KAHARI, A. K., KEENAN, S., KULESHA, E., MARTIN, F. J., MAUREL, T., MCLAREN, W. M., MURPHY, D. N., NAG, R., OVERDUIN, B., PIGNATELLI, M., PRITCHARD, B., PRITCHARD, E., RIAT, H. S., RUFFIER, M., SHEPPARD, D., TAYLOR, K., THORMANN, A., TREVANION, S. J., VULLO, A., WILDER, S. P., WILSON, M., ZADISSA, A., AKEN, B. L., BIRNEY, E., CUNNINGHAM, F., HARROW, J., HERRERO, J., HUBBARD, T. J., KINSELLA, R., MUFFATO, M., PARKER, A., SPUDICH, G., YATES, A., ZERBINO, D. R. & SEARLE, S. M. 2014. Ensembl 2014. *Nucleic Acids Res,* 42**,** D749-55.

GAURON, C., RAMPON, C., BOUZAFFOUR, M., IPENDEY, E., TEILLON, J., VOLOVITCH, M. & VRIZ, S. 2013. Sustained production of ROS triggers compensatory proliferation and is required for regeneration to proceed. *Sci Rep,* 3**,** 2084.

GEMBERLING, M., BAILEY, T. J., HYDE, D. R. & POSS, K. D. 2013. The zebrafish as a model for complex tissue regeneration. *Trends Genet,* 29**,** 611-20.

GIL, J. & PETERS, G. 2006. Regulation of the INK4b-ARF-INK4a tumour suppressor locus: all for one or one for all. *Nat Rev Mol Cell Biol,* 7**,** 667-77.

GILLEY, J. & FRIED, M. 2001. One INK4 gene and no ARF at the Fugu equivalent of the human INK4A/ARF/INK4B tumour suppressor locus. *Oncogene,* 20**,** 7447-52.

GODWIN, J. W., PINTO, A. R. & ROSENTHAL, N. A. 2013. Macrophages are required for adult salamander limb regeneration. *Proc Natl Acad Sci U S A,* 110**,** 9415-20.

GREAVES, M. 2007. Darwinian medicine: a case for cancer. *Nat Rev Cancer,* 7**,** 213-21.

HALLORAN, M. C., SATO-MAEDA, M., WARREN, J. T., SU, F., LELE, Z., KRONE, P. H., KUWADA, J. Y. & SHOJI, W. 2000. Laser-induced gene expression in specific cells of transgenic zebrafish. *Development,* 127**,** 1953-60.

HAN, M., YANG, X., LEE, J., ALLAN, C. H. & MUNEOKA, K. 2008. Development and regeneration of the neonatal digit tip in mice. *Dev Biol,* 315**,** 125-35.

HAN, M., YANG, X., TAYLOR, G., BURDSAL, C. A., ANDERSON, R. A. & MUNEOKA, K. 2005. Limb regeneration in higher vertebrates: developing a roadmap. *Anat Rec B New Anat,* 287**,** 14-24.

HE, S., NAKADA, D. & MORRISON, S. J. 2009. Mechanisms of stem cell self-renewal. *Annu Rev Cell Dev Biol,* 25**,** 377-406.

HEBER-KATZ, E., ZHANG, Y., BEDELBAEVA, K., SONG, F., CHEN, X. & STOCUM, D. L. 2013. Cell cycle regulation and regeneration. *Curr Top Microbiol Immunol,* 367**,** 253-76.

HUH, M. S., PARKER, M. H., SCIME, A., PARKS, R. & RUDNICKI, M. A. 2004. Rb is required for progression through myogenic differentiation but not maintenance of terminal differentiation. *J Cell Biol,* 166**,** 865-76.

HULBERT, A. J. & ELSE, P. L. 1989. Evolution of mammalian endothermic metabolism: mitochondrial activity and cell composition. *Am J Physiol,* 256**,** R63-9.

HWANG, W. Y., FU, Y., REYON, D., MAEDER, M. L., TSAI, S. Q., SANDER, J. D., PETERSON, R. T., YEH, J. R. & JOUNG, J. K. 2013. Efficient genome editing in zebrafish using a CRISPR-Cas system. *Nat Biotechnol,* 31**,** 227-9.

HYDE, D. R., GODWIN, A. R. & THUMMEL, R. 2012. In vivo electroporation of morpholinos into the regenerating adult zebrafish tail fin. *J Vis Exp*.

HYUN, J. S., CHUNG, M. T., WONG, V. W., MONTORO, D., LONGAKER, M. T. & WAN, D. C. 2012. Rethinking the blastema. *Plast Reconstr Surg,* 129**,** 1097-103.

IQBAL, N., MEI, J., LIU, J. & SKAPEK, S. X. 2014. miR-34a is essential for p19(Arf)-driven cell cycle arrest. *Cell Cycle,* 13**,** 792-800.

JACKS, T., FAZELI, A., SCHMITT, E. M., BRONSON, R. T., GOODELL, M. A. & WEINBERG, R. A. 1992. Effects of an Rb mutation in the mouse. *Nature,* 359**,** 295-300.

JONES, R. G. & THOMPSON, C. B. 2009. Tumor suppressors and cell metabolism: a recipe for cancer growth. *Genes Dev,* 23**,** 537-48.

JOPLING, C., SLEEP, E., RAYA, M., MARTI, M., RAYA, A. & IZPISUA BELMONTE, J. C. 2010. Zebrafish heart regeneration occurs by cardiomyocyte dedifferentiation and proliferation. *Nature,* 464**,** 606-9.

KAMIJO, T., ZINDY, F., ROUSSEL, M. F., QUELLE, D. E., DOWNING, J. R., ASHMUN, R. A., GROSVELD, G. & SHERR, C. J. 1997. Tumor suppression at the mouse INK4a locus mediated by the alternative reading frame product p19ARF. *Cell,* 91**,** 649-59.

KAROLCHIK, D., BARBER, G. P., CASPER, J., CLAWSON, H., CLINE, M. S., DIEKHANS, M., DRESZER, T. R., FUJITA, P. A., GURUVADOO, L., HAEUSSLER, M., HARTE, R. A., HEITNER, S., HINRICHS, A. S., LEARNED, K., LEE, B. T., LI, C. H., RANEY, B. J., RHEAD, B., ROSENBLOOM, K. R., SLOAN, C. A., SPEIR, M. L., ZWEIG, A. S., HAUSSLER, D., KUHN, R. M. & KENT, W. J. 2014. The UCSC Genome Browser database: 2014 update. *Nucleic Acids Res,* 42**,** D764-70.

KELLY, G. S. 1998. Clinical applications of N-acetylcysteine. *Altern Med Rev,* 3**,** 114-27.

KIKUCHI, K., HOLDWAY, J. E., WERDICH, A. A., ANDERSON, R. M., FANG, Y., EGNACZYK, G. F., EVANS, T., MACRAE, C. A., STAINIER, D. Y. & POSS, K. D. 2010. Primary contribution to zebrafish heart regeneration by gata4(+) cardiomyocytes. *Nature,* 464**,** 601-5.

KIM, S. H., MITCHELL, M., FUJII, H., LLANOS, S. & PETERS, G. 2003. Absence of p16INK4a and truncation of ARF tumor suppressors in chickens. *Proc Natl Acad Sci U S A,* 100**,** 211-6.

KIMURA, Y., HISANO, Y., KAWAHARA, A. & HIGASHIJIMA, S. 2014. Efficient generation of knock-in transgenic zebrafish carrying reporter/driver genes by CRISPR/Cas9-mediated genome engineering. *Sci Rep,* 4**,** 6545.

KNOPF, F., HAMMOND, C., CHEKURU, A., KURTH, T., HANS, S., WEBER, C. W., MAHATMA, G., FISHER, S., BRAND, M., SCHULTE-MERKER, S. & WEIDINGER, G. 2011. Bone regenerates via dedifferentiation of osteoblasts in the zebrafish fin. *Dev Cell,* 20**,** 713-24.

KOMAROV, P. G., KOMAROVA, E. A., KONDRATOV, R. V., CHRISTOV-TSELKOV, K., COON, J. S., CHERNOV, M. V. & GUDKOV, A. V. 1999. A chemical inhibitor of p53 that protects mice from the side effects of cancer therapy. *Science,* 285**,** 1733-7.

KOMORI, T. 2006. Regulation of osteoblast differentiation by transcription factors. *J Cell Biochem,* 99**,** 1233-9.

KOTAKE, Y., NAKAGAWA, T., KITAGAWA, K., SUZUKI, S., LIU, N., KITAGAWA, M. & XIONG, Y. 2011. Long non-coding RNA ANRIL is required for the PRC2 recruitment to and silencing of p15(INK4B) tumor suppressor gene. *Oncogene,* 30**,** 1956-62.

KWAN, K. M., FUJIMOTO, E., GRABHER, C., MANGUM, B. D., HARDY, M. E., CAMPBELL, D. S., PARANT, J. M., YOST, H. J., KANKI, J. P. & CHIEN, C. B. 2007. The Tol2kit: a multisite gateway-based construction kit for Tol2 transposon transgenesis constructs. *Dev Dyn,* 236**,** 3088-99.

LAMBETH, J. D. 2004. NOX enzymes and the biology of reactive oxygen. *Nat Rev Immunol,* 4**,** 181-9.

LEE, Y., GRILL, S., SANCHEZ, A., MURPHY-RYAN, M. & POSS, K. D. 2005. Fgf signaling instructs position-dependent growth rate during zebrafish fin regeneration. *Development,* 132**,** 5173-83.

LIANG, L., WONG, C. M., YING, Q., FAN, D. N., HUANG, S., DING, J., YAO, J., YAN, M., LI, J., YAO, M., NG, I. O. & HE, X. 2010. MicroRNA-125b suppressesed human liver cancer cell proliferation and metastasis by directly targeting oncogene LIN28B2. *Hepatology,* 52**,** 1731-40.

LOVE, N. R., CHEN, Y., ISHIBASHI, S., KRITSILIGKOU, P., LEA, R., KOH, Y., GALLOP, J. L., DOREY, K. & AMAYA, E. 2013. Amputation-induced reactive oxygen species are required for successful Xenopus tadpole tail regeneration. *Nat Cell Biol,* 15**,** 222-8.

LOWE, S. W. & SHERR, C. J. 2003. Tumor suppression by Ink4a-Arf: progress and puzzles. *Curr Opin Genet Dev,* 13**,** 77-83.

MACDONALD, R. 1999. Zebrafish Immunohistochemistry. *In:* GUILLE, M. (ed.) *Molecular Methods in Developmental Biology.* Humana Press.

MACDONALD, R. B., DEBIAIS-THIBAUD, M., TALBOT, J. C. & EKKER, M. 2010. The relationship between dlx and gad1 expression indicates highly conserved genetic pathways in the zebrafish forebrain. *Dev Dyn,* 239**,** 2298-306.

MADDOCKS, O. D. & VOUSDEN, K. H. 2011. Metabolic regulation by p53. *J Mol Med (Berl),* 89**,** 237-45.

MANZINI, P., MARCUCCIO, R. & BIBLIOTECA ANTONIO PANIZZI. *Catalogo dei manoscritti di Lazzaro Spallanzani nella Biblioteca Panizzi di Reggio Emilia. Quarto supplemento, Carteggi*.

MENENDEZ, S., KHAN, Z., COOMBER, D. W., LANE, D. P., HIGGINS, M., KOUFALI, M. M. & LAIN, S. 2003. Oligomerization of the human ARF tumor suppressor and its response to oxidative stress. *J Biol Chem,* 278**,** 18720-9.

MEUWISSEN, R., LINN, S. C., LINNOILA, R. I., ZEVENHOVEN, J., MOOI, W. J. & BERNS, A. 2003. Induction of small cell lung cancer by somatic inactivation of both Trp53 and Rb1 in a conditional mouse model. *Cancer Cell,* 4**,** 181-9.

MICHALOPOULOS, G. K. 2007. Liver regeneration. *J Cell Physiol,* 213**,** 286-300.

MITCHELL, C. & WILLENBRING, H. 2008. A reproducible and well-tolerated method for 2/3 partial hepatectomy in mice. *Nat Protoc,* 3**,** 1167-70.

MOLOFSKY, A. V., HE, S., BYDON, M., MORRISON, S. J. & PARDAL, R. 2005. Bmi-1 promotes neural stem cell self-renewal and neural development but not mouse growth and survival by repressing the p16Ink4a and p19Arf senescence pathways. *Genes Dev,* 19**,** 1432-7.

MONAGHAN, J. R. & MADEN, M. 2013. Cellular plasticity during vertebrate appendage regeneration. *Curr Top Microbiol Immunol,* 367**,** 53-74.

MORGAN, T. H. 1901. Regeneration and Liability to Injury. *Science,* 14**,** 235-48.

MOULIN, S., LLANOS, S., KIM, S. H. & PETERS, G. 2008. Binding to nucleophosmin determines the localization of human and chicken ARF but not its impact on p53. *Oncogene,* 27**,** 2382-9.

MUDHASANI, R., ZHU, Z., HUTVAGNER, G., EISCHEN, C. M., LYLE, S., HALL, L. L., LAWRENCE, J. B., IMBALZANO, A. N. & JONES, S. N. 2008. Loss of miRNA biogenesis induces p19Arf-p53 signaling and senescence in primary cells. *J Cell Biol,* 181**,** 1055-63.

MUKAIGASA, K., NGUYEN, L. T., LI, L., NAKAJIMA, H., YAMAMOTO, M. & KOBAYASHI, M. 2012. Genetic evidence of an evolutionarily conserved role for Nrf2 in the protection against oxidative stress. *Mol Cell Biol,* 32**,** 4455-61.

MULLEN, L. M., BRYANT, S. V., TOROK, M. A., BLUMBERG, B. & GARDINER, D. M. 1996. Nerve dependency of regeneration: the role of Distal-less and FGF signaling in amphibian limb regeneration. *Development,* 122**,** 3487-97.

MULLER, T. L., NGO-MULLER, V., REGINELLI, A., TAYLOR, G., ANDERSON, R. & MUNEOKA, K. 1999. Regeneration in higher vertebrates: limb buds and digit tips. *Semin Cell Dev Biol,* 10**,** 405-13.

MUNEOKA, K., ALLAN, C. H., YANG, X., LEE, J. & HAN, M. 2008. Mammalian regeneration and regenerative medicine. *Birth Defects Res C Embryo Today,* 84**,** 265-80.

NACU, E. & TANAKA, E. M. 2011. Limb regeneration: a new development? *Annu Rev Cell Dev Biol,* 27**,** 409-40.

NEUFELD, D. A. & ZHAO, W. 1993. Phalangeal regrowth in rodents: postamputational bone regrowth depends upon the level of amputation. *Prog Clin Biol Res,* 383A**,** 243-52.

NEUFELD, D. A. & ZHAO, W. 1995. Bone regrowth after digit tip amputation in mice is equivalent in adults and neonates. *Wound Repair Regen,* 3**,** 461-6.

NORTH, T. E., BABU, I. R., VEDDER, L. M., LORD, A. M., WISHNOK, J. S., TANNENBAUM, S. R., ZON, L. I. & GOESSLING, W. 2010. PGE2-regulated wnt signaling and N-acetylcysteine are synergistically hepatoprotective in zebrafish acetaminophen injury. *Proc Natl Acad Sci U S A,* 107**,** 17315-20.

OBERPRILLER, J. O. & OBERPRILLER, J. C. 1974. Response of the adult newt ventricle to injury. *J Exp Zool,* 187**,** 249-53.

PAJCINI, K. V., CORBEL, S. Y., SAGE, J., POMERANTZ, J. H. & BLAU, H. M. 2010. Transient inactivation of Rb and ARF yields regenerative cells from postmitotic mammalian muscle. *Cell Stem Cell,* 7**,** 198-213.

PARDAL, R., MOLOFSKY, A. V., HE, S. & MORRISON, S. J. 2005. Stem cell self-renewal and cancer cell proliferation are regulated by common networks that balance the activation of proto-oncogenes and tumor suppressors. *Cold Spring Harb Symp Quant Biol,* 70**,** 177-85.

PASMANT, E., SABBAGH, A., VIDAUD, M. & BIECHE, I. 2011. ANRIL, a long, noncoding RNA, is an unexpected major hotspot in GWAS. *FASEB J,* 25**,** 444-8.

PEARSON, B. J. & SANCHEZ ALVARADO, A. 2008. Regeneration, stem cells, and the evolution of tumor suppression. *Cold Spring Harb Symp Quant Biol,* 73**,** 565-72.

PETRIE, T. A., STRAND, N. S., YANG, C. T., RABINOWITZ, J. S. & MOON, R. T. 2014. Macrophages modulate adult zebrafish tail fin regeneration. *Development,* 141**,** 2581-91.

PIETERSEN, A. M., EVERS, B., PRASAD, A. A., TANGER, E., CORNELISSEN-STEIJGER, P., JONKERS, J. & VAN LOHUIZEN, M. 2008. Bmi1 regulates stem cells and proliferation and differentiation of committed cells in mammary epithelium. *Curr Biol,* 18**,** 1094-9.

POMERANTZ, J., SCHREIBER-AGUS, N., LIEGEOIS, N. J., SILVERMAN, A., ALLAND, L., CHIN, L., POTES, J., CHEN, K., ORLOW, I., LEE, H. W., CORDON-CARDO, C. & DEPINHO, R. A. 1998. The Ink4a tumor suppressor gene product, p19Arf, interacts with MDM2 and neutralizes MDM2's inhibition of p53. *Cell,* 92**,** 713-23.

POMERANTZ, J. H. & BLAU, H. M. 2013. Tumor suppressors: enhancers or suppressors of regeneration? *Development,* 140**,** 2502-12.

POSS, K. D. 2010. Advances in understanding tissue regenerative capacity and mechanisms in animals. *Nat Rev Genet,* 11**,** 710-22.

POSS, K. D., KEATING, M. T. & NECHIPORUK, A. 2003. Tales of regeneration in zebrafish. *Dev Dyn,* 226**,** 202-10.

REGINELLI, A. D., WANG, Y. Q., SASSOON, D. & MUNEOKA, K. 1995. Digit tip regeneration correlates with regions of Msx1 (Hox 7) expression in fetal and newborn mice. *Development,* 121**,** 1065-76.

RINKEVICH, Y., LINDAU, P., UENO, H., LONGAKER, M. T. & WEISSMAN, I. L. 2011. Germ-layer and lineage-restricted stem/progenitors regenerate the mouse digit tip. *Nature,* 476**,** 409-13.

ROBERTSON, K. D. & JONES, P. A. 1998. The human ARF cell cycle regulatory gene promoter is a CpG island which can be silenced by DNA methylation and down-regulated by wild-type p53. *Mol Cell Biol,* 18**,** 6457-73.

RODIER, F., CAMPISI, J. & BHAUMIK, D. 2007. Two faces of p53: aging and tumor suppression. *Nucleic Acids Res,* 35**,** 7475-84.

ROSENTHAL, L. J., REINER, M. A. & BLEICHER, M. A. 1979. Nonoperative management of distal fingertip amputations in children. *Pediatrics,* 64**,** 1-3.

SALZBERG, S. L., SEARLS, D. B. & KASIF, S. 1998. *Computational methods in molecular biology,* Amsterdam ; New York, Elsevier.

SERRANO, M., LEE, H., CHIN, L., CORDON-CARDO, C., BEACH, D. & DEPINHO, R. A. 1996. Role of the INK4a locus in tumor suppression and cell mortality. *Cell,* 85**,** 27-37.

SHARPLESS, N. E. 2005. INK4a/ARF: a multifunctional tumor suppressor locus. *Mutat Res,* 576**,** 22-38.

SHARPLESS, N. E. & DEPINHO, R. A. 2007. How stem cells age and why this makes us grow old. *Nat Rev Mol Cell Biol,* 8**,** 703-13.

SHERR, C. J. 2006. Divorcing ARF and p53: an unsettled case. *Nat Rev Cancer,* 6**,** 663-73.

SINGH, S. P., HOLDWAY, J. E. & POSS, K. D. 2012. Regeneration of amputated zebrafish fin rays from de novo osteoblasts. *Dev Cell,* 22**,** 879-86.

SMITH, J. J., PUTTA, S., WALKER, J. A., KUMP, D. K., SAMUELS, A. K., MONAGHAN, J. R., WEISROCK, D. W., STABEN, C. & VOSS, S. R. 2005. Sal-Site: integrating new and existing ambystomatid salamander research and informational resources. *BMC Genomics,* 6**,** 181.

SONG, G., SHARMA, A. D., ROLL, G. R., NG, R., LEE, A. Y., BLELLOCH, R. H., FRANDSEN, N. M. & WILLENBRING, H. 2010. MicroRNAs control hepatocyte proliferation during liver regeneration. *Hepatology,* 51**,** 1735-43.

SOUSA, S., AFONSO, N., BENSIMON-BRITO, A., FONSECA, M., SIMOES, M., LEON, J., ROEHL, H., CANCELA, M. L. & JACINTO, A. 2011. Differentiated skeletal cells contribute to blastema formation during zebrafish fin regeneration. *Development,* 138**,** 3897-905.

STACHURA, D. L., REYES, J. R., BARTUNEK, P., PAW, B. H., ZON, L. I. & TRAVER, D. 2009. Zebrafish kidney stromal cell lines support multilineage hematopoiesis. *Blood,* 114**,** 279-89.

STEWART, S. & STANKUNAS, K. 2012. Limited dedifferentiation provides replacement tissue during zebrafish fin regeneration. *Dev Biol,* 365**,** 339-49.

STOCUM, D. L. & CAMERON, J. A. 2011. Looking proximally and distally: 100 years of limb regeneration and beyond. *Dev Dyn,* 240**,** 943-68.

STOICK-COOPER, C. L., MOON, R. T. & WEIDINGER, G. 2007. Advances in signaling in vertebrate regeneration as a prelude to regenerative medicine. *Genes Dev,* 21**,** 1292-315.

STRAUBE, W. L. & TANAKA, E. M. 2006. Reversibility of the differentiated state: regeneration in amphibians. *Artif Organs,* 30**,** 743-55.

TAKEO, M., CHOU, W. C., SUN, Q., LEE, W., RABBANI, P., LOOMIS, C., TAKETO, M. M. & ITO, M. 2013. Wnt activation in nail epithelium couples nail growth to digit regeneration. *Nature,* 499**,** 228-32.

TANAKA, E. M., GANN, A. A., GATES, P. B. & BROCKES, J. P. 1997. Newt myotubes reenter the cell cycle by phosphorylation of the retinoblastoma protein. *J Cell Biol,* 136**,** 155-65.

TANAKA, E. M. & REDDIEN, P. W. 2011. The cellular basis for animal regeneration. *Dev Cell,* 21**,** 172-85.

TANAKA, T., KOMAI, Y., TOKUYAMA, Y., YANAI, H., OHE, S., OKAZAKI, K. & UENO, H. 2013. Identification of stem cells that maintain and regenerate lingual keratinized epithelial cells. *Nat Cell Biol,* 15**,** 511-8.

TAUB, R. 2004. Liver regeneration: from myth to mechanism. *Nat Rev Mol Cell Biol,* 5**,** 836-47.

THUMMEL, R., BAI, S., SARRAS, M. P., JR., SONG, P., MCDERMOTT, J., BREWER, J., PERRY, M., ZHANG, X., HYDE, D. R. & GODWIN, A. R. 2006. Inhibition of zebrafish fin regeneration using in vivo electroporation of morpholinos against fgfr1 and msxb. *Dev Dyn,* 235**,** 336-46.

TIAN, H., BIEHS, B., WARMING, S., LEONG, K. G., RANGELL, L., KLEIN, O. D. & DE SAUVAGE, F. J. 2011. A reserve stem cell population in small intestine renders Lgr5-positive cells dispensable. *Nature,* 478**,** 255-9.

TO, K. H., PAJOVIC, S., GALLIE, B. L. & THERIAULT, B. L. 2012. Regulation of p14ARF expression by miR-24: a potential mechanism compromising the p53 response during retinoblastoma development. *BMC Cancer,* 12**,** 69.

TSONIS, P. A. 1996. *Limb regeneration,* Cambridge England ; New York, NY, USA, Cambridge University Press.

TSONIS, P. A., MADHAVAN, M., TANCOUS, E. E. & DEL RIO-TSONIS, K. 2004. A newt's eye view of lens regeneration. *Int J Dev Biol,* 48**,** 975-80.

TU, S. & JOHNSON, S. L. 2011. Fate restriction in the growing and regenerating zebrafish fin. *Dev Cell,* 20**,** 725-32.

VASSILEV, L. T., VU, B. T., GRAVES, B., CARVAJAL, D., PODLASKI, F., FILIPOVIC, Z., KONG, N., KAMMLOTT, U., LUKACS, C., KLEIN, C., FOTOUHI, N. & LIU, E. A. 2004. In vivo activation of the p53 pathway by small-molecule antagonists of MDM2. *Science,* 303**,** 844-8.

VIDAL, P. & DICKSON, M. G. 1993. Regeneration of the distal phalanx. A case report. *J Hand Surg Br,* 18**,** 230-3.

VINARSKY, V., ATKINSON, D. L., STEVENSON, T. J., KEATING, M. T. & ODELBERG, S. J. 2005. Normal newt limb regeneration requires matrix metalloproteinase function. *Dev Biol,* 279**,** 86-98.

WALSH, K. & PERLMAN, H. 1997. Cell cycle exit upon myogenic differentiation. *Curr Opin Genet Dev,* 7**,** 597-602.

WAN, G., MATHUR, R., HU, X., LIU, Y., ZHANG, X., PENG, G. & LU, X. 2013. Long non-coding RNA ANRIL (CDKN2B-AS) is induced by the ATM-E2F1 signaling pathway. *Cell Signal,* 25**,** 1086-95.

WEBER, J. D., JEFFERS, J. R., REHG, J. E., RANDLE, D. H., LOZANO, G., ROUSSEL, M. F., SHERR, C. J. & ZAMBETTI, G. P. 2000. p53-independent functions of the p19(ARF) tumor suppressor. *Genes Dev,* 14**,** 2358-65.

WEBER, J. D., TAYLOR, L. J., ROUSSEL, M. F., SHERR, C. J. & BAR-SAGI, D. 1999. Nucleolar Arf sequesters Mdm2 and activates p53. *Nat Cell Biol,* 1**,** 20-6.

WEHNER, D., CIZELSKY, W., VASUDEVARO, M. D., OZHAN, G., HAASE, C., KAGERMEIER-SCHENK, B., RODER, A., DORSKY, R. I., MORO, E., ARGENTON, F., KUHL, M. & WEIDINGER, G. 2014. Wnt/beta-catenin signaling defines organizing centers that orchestrate growth and differentiation of the regenerating zebrafish caudal fin. *Cell Rep,* 6**,** 467-81.

WELLS, J., GRAVEEL, C. R., BARTLEY, S. M., MADORE, S. J. & FARNHAM, P. J. 2002. The identification of E2F1-specific target genes. *Proc Natl Acad Sci U S A,* 99**,** 3890-5.

YANG, E. V., GARDINER, D. M., CARLSON, M. R., NUGAS, C. A. & BRYANT, S. V. 1999. Expression of Mmp-9 and related matrix metalloproteinase genes during axolotl limb regeneration. *Dev Dyn,* 216**,** 2-9.

YANG, H., WANG, H., SHIVALILA, C. S., CHENG, A. W., SHI, L. & JAENISCH, R. 2013. One-step generation of mice carrying reporter and conditional alleles by CRISPR/Cas-mediated genome engineering. *Cell,* 154**,** 1370-9.

YAP, K. L., LI, S., MUNOZ-CABELLO, A. M., RAGUZ, S., ZENG, L., MUJTABA, S., GIL, J., WALSH, M. J. & ZHOU, M. M. 2010. Molecular interplay of the noncoding RNA ANRIL and methylated histone H3 lysine 27 by polycomb CBX7 in transcriptional silencing of INK4a. *Mol Cell,* 38**,** 662-74.

YUN, M. H., GATES, P. B. & BROCKES, J. P. 2013. Regulation of p53 is critical for vertebrate limb regeneration. *Proc Natl Acad Sci U S A,* 110**,** 17392-7.

ZHAO, W. & NEUFELD, D. A. 1995. Bone regrowth in young mice stimulated by nail organ. *J Exp Zool,* 271**,** 155-9.

ZINDY, F., WILLIAMS, R. T., BAUDINO, T. A., REHG, J. E., SKAPEK, S. X., CLEVELAND, J. L., ROUSSEL, M. F. & SHERR, C. J. 2003. Arf tumor suppressor promoter monitors latent oncogenic signals in vivo. *Proc Natl Acad Sci U S A,* 100**,** 15930-5.

Publishing Agreement

It is the policy of the University to encourage the distribution of all theses, dissertations, and manuscripts. Copies of all UCSF theses, dissertations, and manuscripts will be routed to the library via the Graduate Division. The library will make all theses, dissertations, and manuscripts accessible to the public and will preserve these to the best of their abilities, in perpetuity.

Please sign the following statement:

I hereby grant permission to the Graduate Division of the University of California, San Francisco to release copies of my thesis, dissertation, or manuscript to the Campus Library to provide access and preservation, in whole or in part, in perpetuity.

Author Signature

6/12/15

Date